Pathophysiology of EHD1-related hearing impairment

DISSERTATION ZUR ERLANGUNG DES DOKTORGRADES DER NATURWISSENSCHAFTEN (DR. RER. NAT.) DER FAKULTÄT FÜR BIOLOGIE UND VORKLINISCHE MEDIZIN DER UNIVERSITÄT REGENSBURG

Vorgelegt von

Katrin Jordan, geb. Imminger

Aus

Memmingen

Im Jahr

2024

Pathophysiology of EHD1-related hearing impairment

DISSERTATION ZUR ERLANGUNG DES DOKTORGRADES DER NATURWISSENSCHAFTEN (DR. RER. NAT.) DER FAKULTÄT FÜR BIOLOGIE UND VORKLINISCHE MEDIZIN DER UNIVERSITÄT REGENSBURG

Vorgelegt von

Katrin Jordan, geb. Imminger

Aus

Memmingen

Im Jahr

2024

Das Promotionsgesuch wurde eingereicht am:

11.06.2024

Die Arbeit wurde angeleitet von:

Prof. Dr. med. Richard Warth

Unterschrift:

Acknowledgements

An dieser Stelle möchte ich allen beteiligten Personen danken, die mich bei meiner Dissertation unterstützt haben.

Mein besonderer Dank gilt Herrn Prof. Dr. med. Warth für die Ermöglichung der Promotion und der Unterstützung bei der Umsetzung der gesamten Arbeit.

Vielen Dank auch an Dr. rer. nat. Olaf Wendler und Elisabeth Sterna der HNO-Klinik Erlangen für die unglaublich bedeutende Einarbeitung in die Cochlea-Präparation. Ohne euch wäre dieses Projekt in dieser Form nicht möglich gewesen!

Danke auch an Dr. rer. nat. Tziridis für die Bereitstellung der Gerätschaften und Räumlichkeiten für die f-ABR Messungen, sowie die vielen Ratschläge und fachlichen Einschätzungen der erhobenen Daten.

Vielen Dank an Helga für die zahlreichen Stunden am Elektronenmikroskop und all die Arbeit, die du in mein Projekt gesteckt hast, um mir eine morphologische Beurteilung der Cochlea zu ermöglichen.

Außerdem möchte ich der gesamten Arbeitsgruppe Warth für die schöne Zeit danken, die vielen lustigen Momente, den wissenschaftlichen und freundschaftlichen Austausch.

Ganz besonders danke ich Ines für ihre tatkräftige Unterstützung im Labor während meiner Schwangerschaft. Du hast mir so oft den Rücken freigehalten, hattest immer ein offenes Ohr und warst mir wirklich eine riesige Hilfe.

Anna-Lena, vielen Dank für deine riesengroße Unterstützung während meiner ganzen Doktorandenzeit. Es war so wertvoll, dich als inoffizielle Ansprechpartnerin zu haben – egal ob es um wissenschaftlichen Austausch, die Etablierung von Methoden oder

die Durchsicht meiner Dissertation ging. Danke für dein offenes Ohr und die vielen Ratschläge. Danke auch, dass du während meiner Schwangerschaft so viel für mich übernommen hast. Ohne dich hätte ich viele Experimente nicht fertigstellen können.

Sascha, du warst seit Beginn meines Studiums ein Mentor für mich und ich bin so froh, dass ich vor so langer Zeit die Möglichkeit hatte, als studentische Hilfskraft für dich zu arbeiten. Ich konnte sehr viel von dir lernen und werde nicht nur den wissenschaftlichen Austausch mit dir vermissen, sondern auch die vielen persönlichen Gespräche.

Allen, thank you so much for all the hours you spent helping me tinkering with new methods and for all the fun in the lab and during lunch hours.

Markus, danke für die Schreibtisch-Nachbarschaft, die vielen lustigen Momente und deinen wissenschaftlichen Input, wenn ich ihn gebraucht habe. Ich werde deine Tee-Trink-Geräusche und unsere Gespräche sehr vermissen!

Mark – thank you for being the wise owl that you are. I'm immensely grateful for your friendship, our silly conversations as well as the scientific ones.

Ein großer Dank geht auch an meine Eltern und meine Schwester. Danke, dass ihr mich immer unterstützt in dem, was ich tue, mir zuhört und immer für mich da seid.

Timo, danke dass du immer mein Fels in der Brandung bist. Du hältst mir so oft den Rücken frei, hörst mir immer zu, sagst mir ehrlich deine Meinung und unterstützt mich bedingungslos. Danke, dass du mein Partner auf Augenhöhe bist, immer für mich da bist und mich erdest.

Für Charlie, weil du mir die Welt bedeutest.

Abstract

EHD1 is a member of four Eps15 homology domain proteins and has been shown to be part of the endocytic recycling machinery and ciliogenesis. It is involved in the recycling of several receptors, such as transferrin I, glucose transporter type 4 (GLUT4), and insulin-like growth factor 1 receptor (IGFR1) and has been implicated in the remodelling of connexin 43 gap junctions in the heart. A founder mutation in EHD1 presenting with sensorineural hearing loss in patients indicates a role of EHD1 in the process of hearing and its consideration as a novel hearing loss gene. This study aimed to identify the role of EHD1 in the process of hearing in mice and the pathophysiology of EHD1-related hearing impairment. Therefore, the localisation as well as underlying mechanisms of hearing loss due to the inactivation of EHD1 were examined in an EHD1$^{-/-}$ mouse model. Frequency-dependent auditory brainstem response (F-ABR) measurements revealed hearing loss of EHD1$^{-/-}$ mice and histological analysis of murine cochleae showed Ehd1 to be localised within the stria vascularis. No alterations in expression levels or localisation of essential transporters were observed due to the loss of Ehd1. However, degeneration of marginal and intermediate cells of the stria vascularis was observed via transmission electron micrographs of EHD1$^{-/-}$ striae. In addition, alterations in gene expression patterns indicated an ongoing inflammatory response within the stria vascularis. Proteome and transcriptome analyses of murine stria vascularis pointed towards the disruption of pericytes in EHD1$^{-/-}$ animals with significantly upregulated proteins typically found in this cell type. Proteome analysis also revealed the significant upregulation of connexin 43 in Ehd1-deficient striae. In the stria vascularis, connexin 43 is important for the generation of the endolymphatic potential (EP) and its absence is known to cause hearing loss. In addition, pericytes are known to form gap junctions with endothelial cells consisting of connexin 43. Taken together, the results obtained from morphological and functional studies suggest the degeneration of the stria vascularis with a possible disturbance of connexin 43 gap junctions and strial pericyte dysfunction. Further studies are required to determine the chain of events. Whether a dysfunction of pericytes, a disruption of gap junction remodelling processes or another underlying condition is responsible for the phenotype observed in this study remains to be investigated.

Table of contents

List of abbreviations

Abbreviation	Meaning
CHL	congenital hearing loss
EE	early endosome
EHD	Eps15 homology domain
Ehd1$^{-/-}$	Ehd1 knockout mouse
Ehd1$^{+/+}$	Ehd1 wildtype mouse
Ehd1he	heterozygous EHD1R398W mouse (R398/R398W)
Ehd1^{R398W}	mouse carrying the mutation R398W (R398W/R398W)
EP	endolymphatic potential
ER	endoplasmic reticulum
ERC	endocytic recycling compartment
F-ABR	frequency-dependent auditory brainstem response
FFPE	formalin-fixed paraffin embedded
HC	hair cells
HL	hearing loss
IF	immunofluorescence
IHC	inner hair cells
IS	intrastrial space
LE	late endosome
NSHL	non-syndromic hearing loss
OHC	outer hair cells
PVM	perivascular macrophage
SHL	syndromic hearing loss
SNHL	sensorineural hearing loss

Introduction

According to the World Health Organisation, over 5 % of the world's population suffers from disabling hearing loss, which can result in a variety of functional, social, and economic obstacles for patients, depending on their access to medical care and social background. [1] Besides sight, balance, smell, taste and touch, hearing is one of our sensory systems and very important in gathering information about the various sounds surrounding us. The range of hearing differs across different species, with humans perceiving sound from 20 Hz to 20 kHz while mice, for instance, can sense sound from 1 to 90 kHz. [2, 3] In humans, hearing loss (HL) is categorised in mild (25 – 40 dB), moderate (41 – 55 dB), moderate severe (56 – 70 dB), severe (71 – 90 dB) and profound (> 90 dB). [1] HL can either be conductive – relating to problems in transferring sound along the outer or middle ear – or sensorineural. Sensorineural hearing loss (SNHL) refers to hearing loss caused within the cochlea, auditory nerve or central nervous system and is the most common type of HL. [4] In order to understand the causes of SNHL, however, one must first understand the physiological properties of hearing.

The physiology of hearing

In mammals, the ear is partitioned into outer, middle, and inner ear. Sound is funneled into the ear by the pinna, where it hits the tympanic membrane (eardrum) via the external acoustic meatus (**Figure 1**). There, vibrations of the tympanic membrane caused by the soundwaves are transmitted to the inner ear via the three ear ossicles. As part of the middle ear, the malleus, incus, and stapes are responsible for setting the fluids within the inner ear into motion. The malleus is connected to the tympanic membrane and therefore is brought to motion according to its vibrations which are then

transferred to the incus and stapes. The stapes ultimately transmits the vibrations of the tympanic membrane to the oval window (fenestra ovalis) where it is located (**Figure 1**). As a result, the oval window vibrates and transmits the initially airborne soundwaves into movements of fluid within the inner ear.

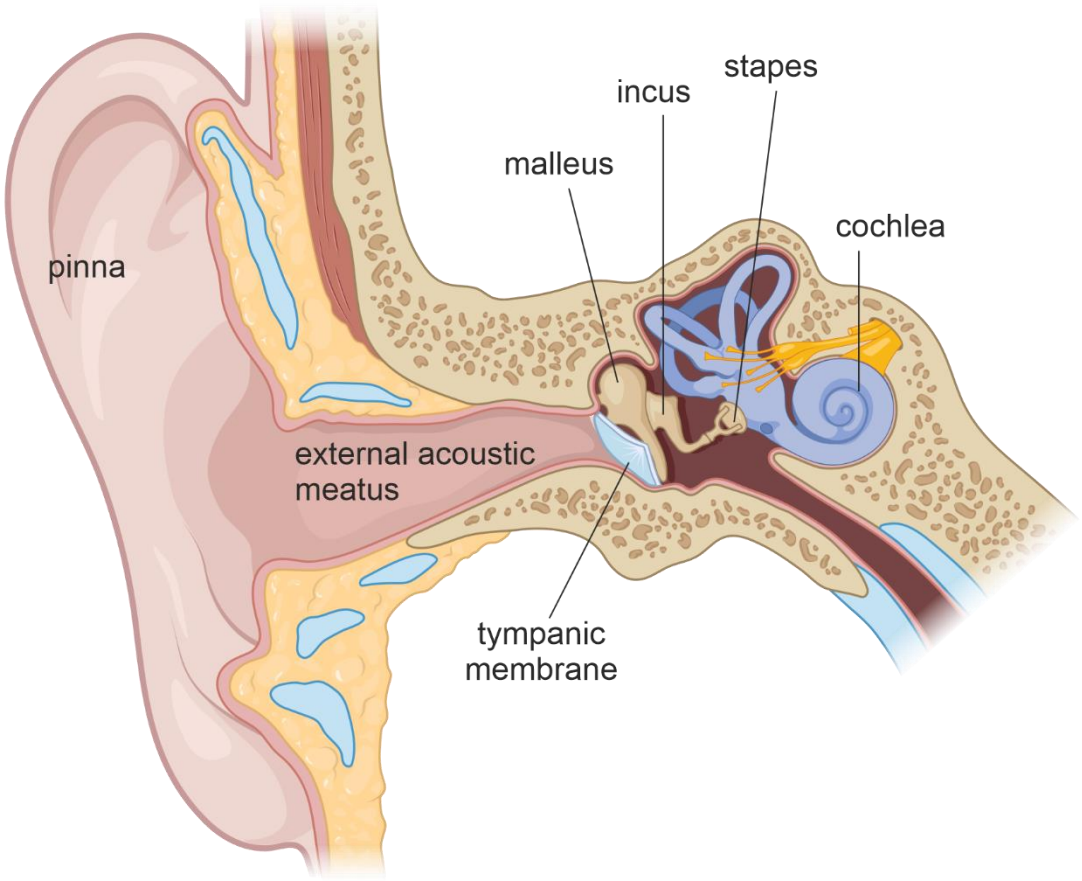

Figure 1 **Properties of the outer, middle, and inner ear.** Sound travels from the outer ear via the external acoustic meatus to the tympanic membrane. From here, the malleus, incus and stapes of the middle ear contribute to the transformation of airborne soundwaves into motion of fluids within the inner ear (cochlea). Created with BioRender.com

The inner ear

The cochlea consists of a bony structure coiled around a central axis called modiulus as well as the membranous structures within the coil. The stapedial footplate sits at the oval window, which itself marks the basal end of the cochlea (**Figure 2**). Here, stapedial motion leads to vibrations of the oval window which, in turn, causes the fluids within the inner ear to move. Thus, the soundwaves initially funnelled by the outer ear are being translated into movement of fluid within the membranous structures of the cochlea. The cochlea is characterised by three fluid-filled chambers. The scala vestibuli directly communicates with the oval window at the base of the cochlea and winds its way up to the apex. From here, the fluid called perilymph travels back to the round window within the scala tympani. Both outer chambers are connected via a small opening known as the helicotrema at the apex of the cochlea (**Figure 2**). The secondary tympanic membranes covering both the round and oval window mark the borders between middle and inner ear and facilitate movement of the fluid within the cochlea as they vibrate in opposite phase ensuring hair cell stimulation. The inner chamber is called scala media (cochlear duct) and contains endolymph - a fluid very rich in K^+ and low in Na^+ and Ca^{2+}. [5, 6] Scala tympani and scala media are separated by the basilar membrane on which the Organ of Corti is located. In addition, the Reissner's membrane separates the scalae vestibuli and media (**Figure 3**). As the stapedial movements lead to vibrations of the oval window, the perilymph within the outer scalae is set to motion correspondently. As a result, the basilar membrane moves up and down in response to the soundwaves, ultimately causing hair cell stimulation and the following excitation of auditory nerve fibres, leading to the interpretation of sound in the brain. Most importantly, the width and stiffness of the basilar membrane varies across its length. At the base of the cochlea, the basilar membrane is narrower

and stiffer than at the apex which marks the groundwork of our ability to distinguish between different frequencies - tonotopy. Due to the non-uniformity in stiffness and width of the basilar membrane, the wave of motion rippling along its length peaks at different places depending on the sound frequency, with high frequencies being registered near the base and low frequencies peaking near the apex of the cochlea.[7, 8]

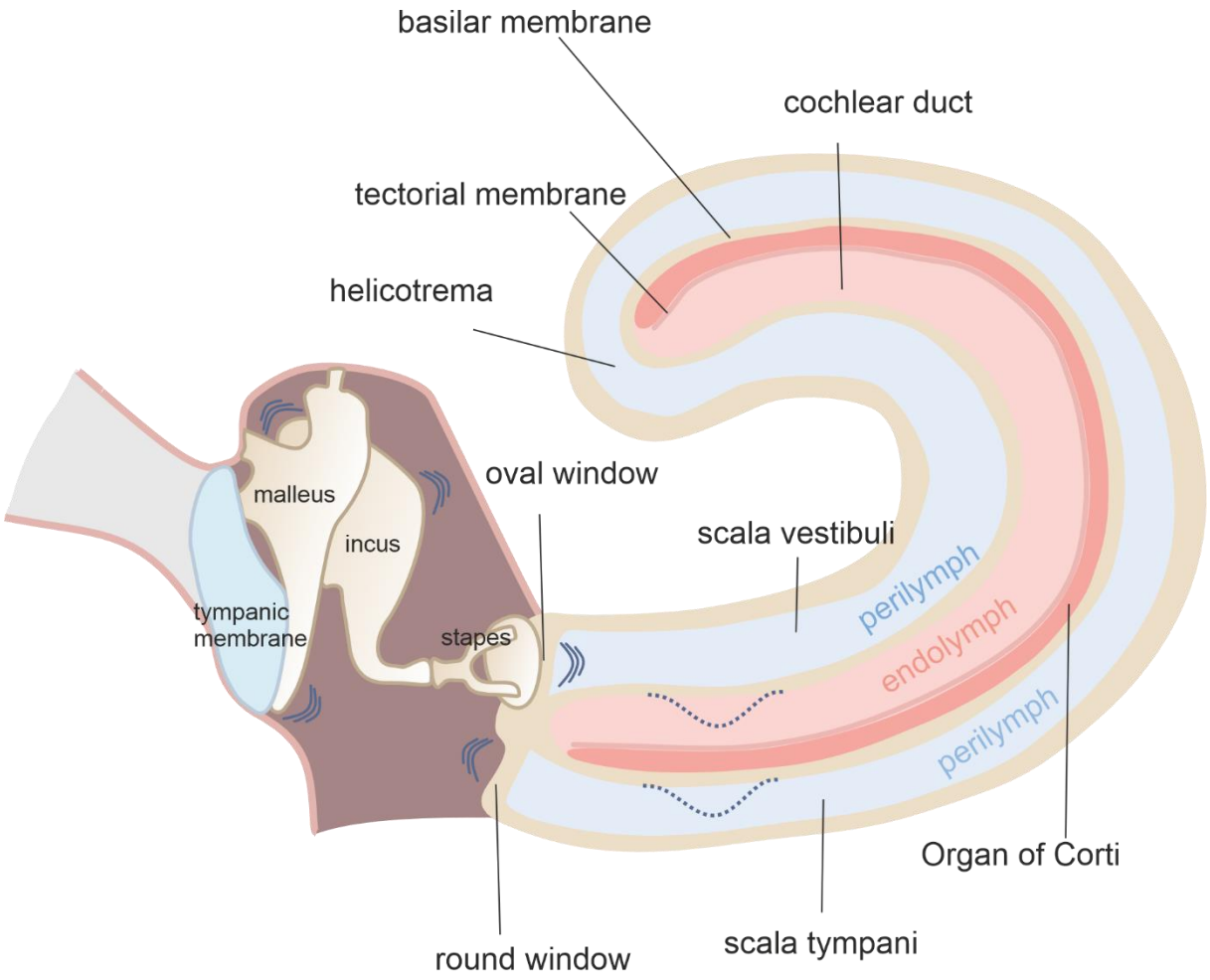

Figure 2 **Features of the middle and inner ear.** Malleus, incus, and stapes transfer soundwaves onto the oval window which sets cochlear fluids into motion. Perilymphatic spaces scala vestibuli and scala tympani are connected by the helicotrema at the apex. The cochlear duct is filled with endolymph. Adapted from Brooks/Cole – Thomson Learning

The cochlear duct

The cochlear duct, or scala media, is the endolymph-filled chamber sandwiched between the scalae vestibuli and tympani and comprises the Organ of Corti as well as the stria vascularis (**Figure 3**). As mentioned above, both outer scalae are filled with perilymph, which is similarly composed to extracellular fluid. In contrast, the scala media contains the endolymph, a fluid very rich in K^+ and low in Na^+ and features a very high endocochlear potential (EP). [6] The EP, alongside high potassium concentrations, is crucial for proper hair cell functioning. [9-11] Situated on the basilar membrane, the Organ of Corti contains the sensory hair cells (HC). They are embedded in a variety of supporting cells and sandwiched between the basilar membrane and the acellular tectorial membrane (**Figure 3**). One row of inner hair cells (IHC) is responsible for the transduction of sound while three rows of outer hair cells (OHC) are thought to act mainly as a cochlear amplifier. [3, 12, 13] Each hair cell contains stereocilia on their apical membrane which are mechanically linked via tip links and present in a staircase formation as stereociliary hair bundles. Upon sound vibrations, the hair bundles bend against the tectorial membrane. This, in turn, activates mechanoelectrical transduction (MET) ion channels located at the very tip of the stereocilia which leads to the influx of K^+ and therefore depolarises the hair cell. [3, 14, 15] Due to depolarisation, voltage gated Ca^{2+} channels lead to Ca^{2+} influx which triggers the release of glutamate and the conveyance of action potentials along the auditory nerve to the brain.[13, 16]

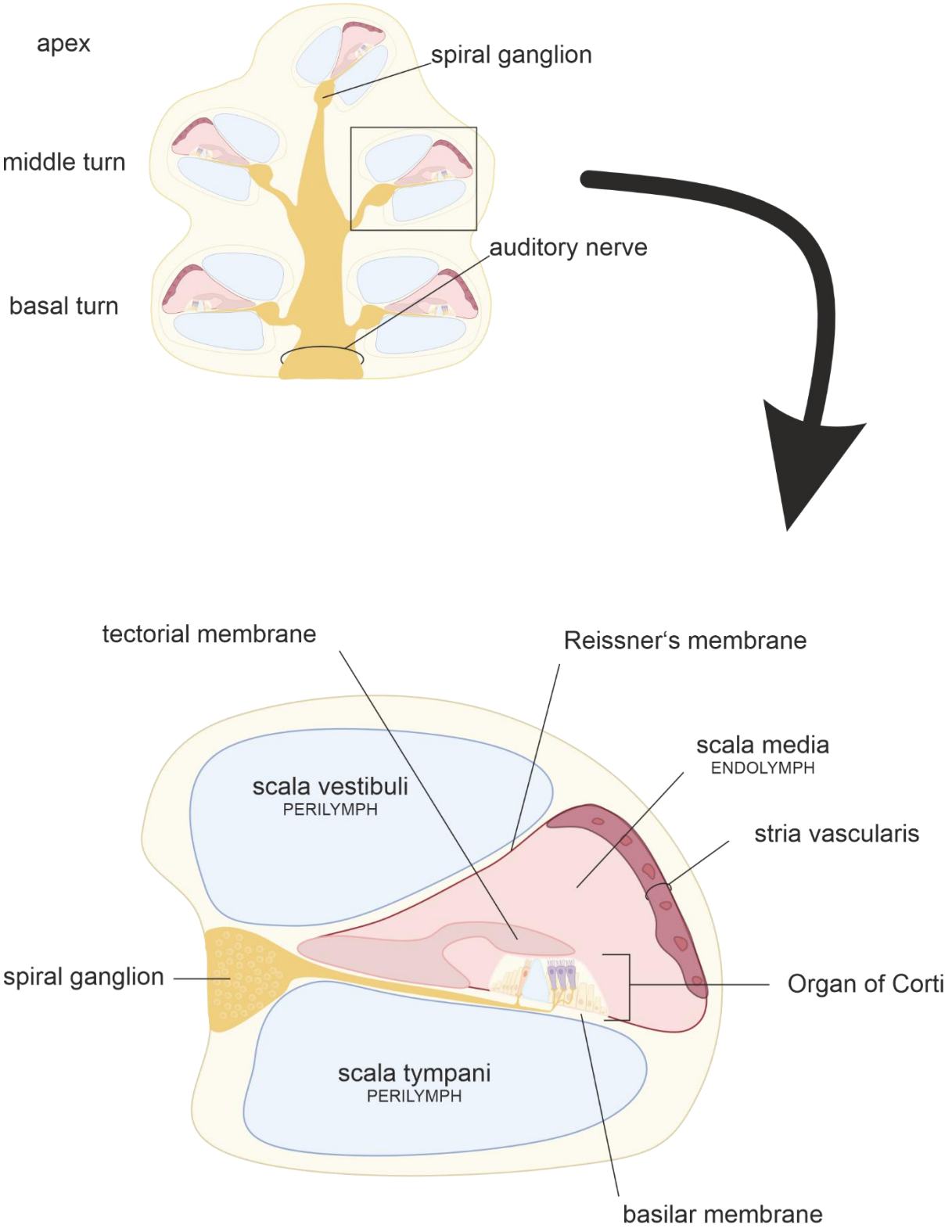

Figure 3 **Cross section of a cochlear turn.** The endolymph-filled scala media contains the Organ of Corti with sensory hair cells as well as the stria vascularis and tectorial membrane. The Reissner's membrane borders the perilymph-filled scala vestibuli while the basilar membrane borders the scala tympani. Created with BioRender.com. Adapted from [9]

The stria vascularis

As part of the lateral wall, the stria vascularis presents as a highly vascularised epithelium which main task is thought to be to produce the unique endolymph and uphold the EP. [9, 17] The stria vascularis mainly consists of marginal, intermediate, and basal cells. [18, 19] In addition, perivascular macrophages (PVM) as well as pericytes reside near the many blood vessels (**Figure 4**). [20-23] Apically, a monolayer of marginal cells rich in mitochondria directly borders the endolymph-filled cochlear duct. On the other side, the basal cells face the fibrocytes of the spiral ligament which lies beneath the stria vascularis. In between, the intermediate cells as well as numerous capillaries can be found in a space called the intrastrial space (IS). The basolateral membranes of marginal cells form extensive interdigitations with apical membranes of intermediate cells with the very narrow IS measuring only 15 nm in between. [2] An extensive network of tight junctions ensures the upholding of the electrochemical properties within the stria vascularis. Luminally, tight junctions between marginal cells form a continuous barrier between the stria vascularis and the endolymph while tight junctions between basal cells ensure a tight boundary to the neighbouring perilymph (**Figure 4**). The insulation of the stria vascularis is completed by a network of tight junctions between endothelial cells, thus ensuring the formation of the blood-strial barrier. [19, 24] Pericytes as well as PVMs are thought to complement the blood-strial barrier via gap junctions connecting them to endothelial cells, and therefore also contribute to the composition of the endolymph and the upholding of the EP. [19, 22] Gap junctions consist of connexins. The proteins form hexameric hemichannels [25] and can either act as functional channels by themselves or form a complete gap junction by connecting to a partner hemichannel from an adjacent cell. [26] Of the many different connexin genes, four have well known

associations with SNHL (*GJB2*, *GJB3*, *GJB4*, *GJB6*) [27-29] and are expressed in the inner ear with possible links to potassium cycling. [30, 31] In addition, the interaction of different connexins within the cochlea is indicated by the variety of phenotypes observed in patients carrying one or several mutations in *GJB6* or *GJB3* in addition to *GJB2*. [25]

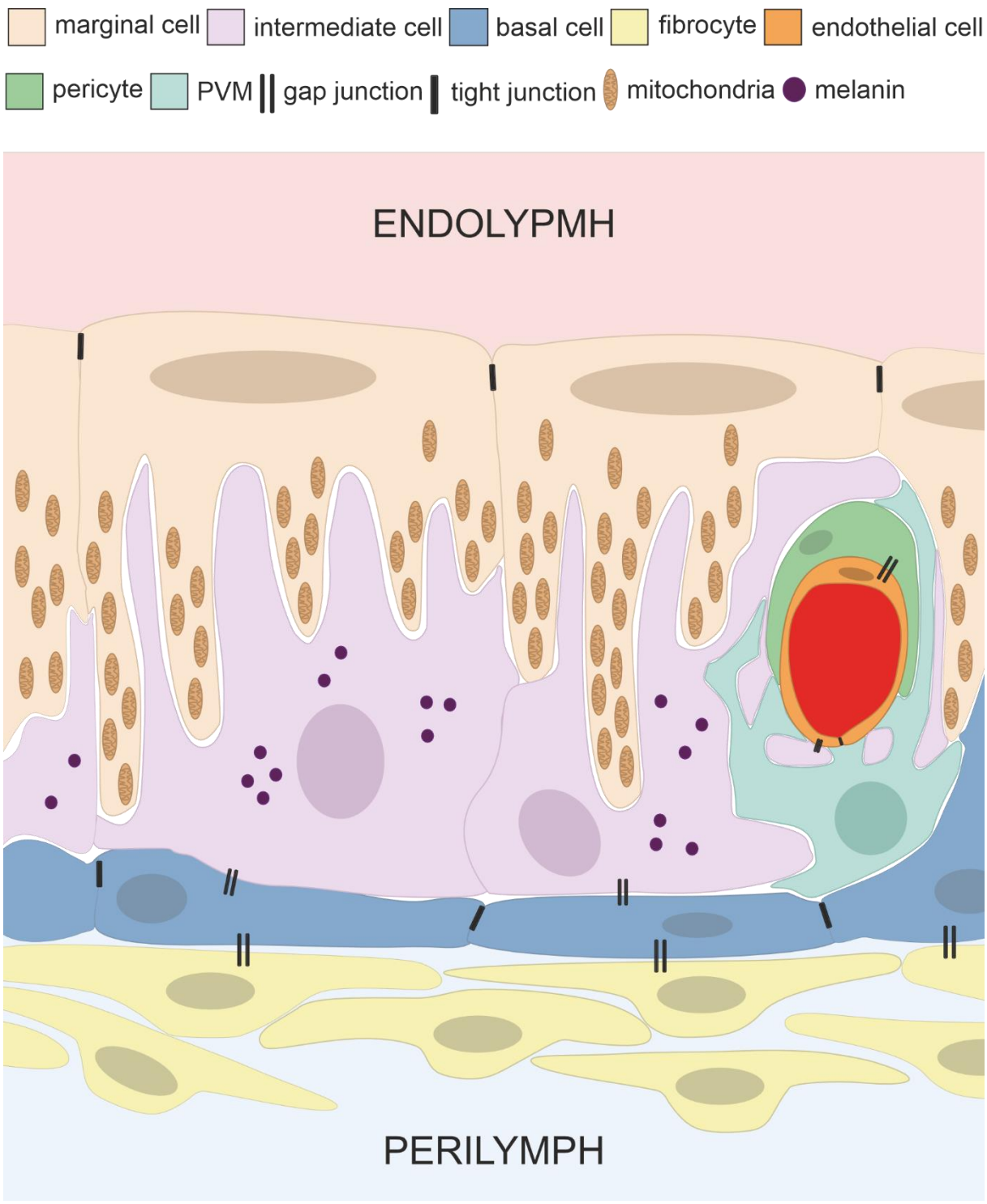

***Figure 4* Components of the stria vascularis.** Marginal, intermediate, and basal cells as well as numerous capillaries form the stria vascularis. Perivascular macrophages (PVM) as well as pericytes complete the blood-strial barrier formed by endothelial cells. Adapted from [32, 33]

As mentioned above, the composition of the endolymph is unique and crucial for mechanoelectrical transduction within the inner ear. As **Table 1** shows, high K^+ concentrations of roughly 150 mM as well as low Ca^{2+} and Na^+ concentrations are the

main feature of this fluid. [6] In addition, the endolymphatic space harbours a very high potential of +80 mV relative to perilymph and blood plasma, known as the EP. [6, 34] The EP is crucial for the process of hearing as it generates a large driving force and therefore increases K^+ and Ca^{2+} influx into the sensory hair cells of the Organ of Corti.

Table 1
Ionic composition of mammalian perilymph and endolymph.

Ion concentration[mmol/l]	Endolymph	Perilymph
Na^+	1.3	148
K^+	157	4
Ca^{2+}	0.02	1.3
Mg^{2+}	0.01	0.7

Data obtained from [6, 35, 36].

The stria vascularis is responsible for the generation of the EP as well as the maintenance of the endolymph. Due to the gap junctional network between fibrocytes of the spiral ligament as well as basal cells and intermediate cells of the stria vascularis, they are believed to share electrochemical properties and can be considered one layer called epithelial syncytium. [18, 37, 38] The marginal-cell layer, on the other hand, forms a separate entity within the lateral wall. Both layers are separated by the IS, which forms an electrically isolated space with a potential of +90 mV. [39] It is this electrically isolated space alongside two K^+ diffusion potentials which are critical for EP generation. After entering the sensory hair cells via MET channels and basally leaving them, K^+ ions are thought to be recycled back to the stria vascularis via the perilymph or a network of supporting cells and the spiral ligament. [18, 40-43] Fibrocytes of the spiral ligament take up K^+ ions via Na^+, K^+-ATPase and Na^+, K^+, $2Cl^-$-cotransporter NKCC. [44-50] K^+ diffuses to the apical membrane of intermediate cells via a network of gap junctions between fibrocytes, basal cells, and the basolateral membrane of intermediate cells to then enter the IS via inward rectifier K^+ channel Kir4.1 located at the apical membrane of intermediate cells (**Figure 5**). [51-54] To uphold the high

potential within the IS, Na^+, K^+-ATPase as well as NKCC at the basolateral membrane of the marginal cells take up K^+ ions. Cl^- channel CLCNK/Barttin at the basolateral membrane of marginal cells ensures proper functioning of NKCC by recycling Cl^- ions back to the intrastrial space. [11, 18, 55-60] Finally, K^+ is excreted into the endolymphatic space via KCNQ1/KCNE1 situated in the apical membrane of marginal cells (**Figure 5**). [18, 61-64] The high potential within the IS is crucial for the generation of the EP and is believed to be upheld via NKCC and Na^+, K^+-ATPase activity in the basolateral membrane of marginal cells. Thus, the K^+ concentration within the IS is kept low (1 – 2 mM) and ensures the generation of the high potential due to K^+ efflux via Kir4.1. [18] Tight junctions between basal cells, marginal cells and endothelial cells ensure insulation from the perilymphatic and endolymphatic space, respectively, and are therefore crucial for the generation of the IS potential and EP. In addition, gap junctional networks within the stria vascularis are known to play an important role in K^+ cycling and the generation of the EP as well as the composition of the endolymph (**Figure 4**). Mutations in several genes involved in K^+ cycling have been identified to cause hearing impairment. In Kir4.1-deficient mice, for example, a complete loss of EP has been observed while in humans, mutations in Kir4.1 cause sensorineural hearing loss. [10, 65-67] The elimination of the EP can also be observed in mice lacking Claudin-11, which is part of the tight junctional network of basal cells in the stria vascularis. [68-70] In addition, a disruption of the gap junctional network in mice (connexins 30 and 26) led to the loss of the EP. [37, 71, 72]

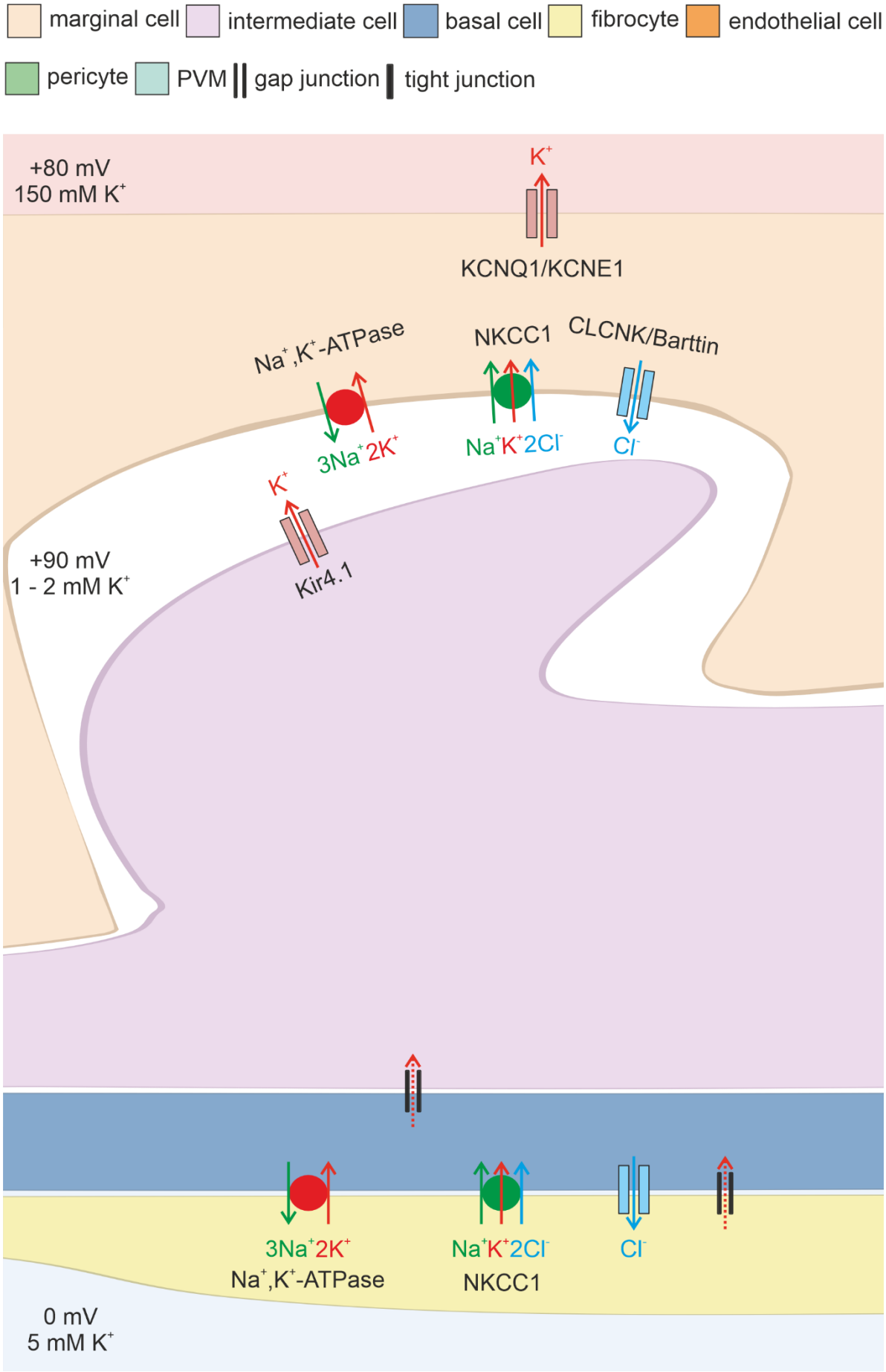
marginal cell
intermediate cell
basal cell
fibrocyte
endothelial cell
pericyte
PVM
gap junction
tight junction
+80 mV
150 mM K+
K+
KCNQ1/KCNE1
Na+,K+-ATPase
3Na+2K+
NKCC1
Na+K+2Cl-
CLCNK/Barttin
Cl-
K+
Kir4.1
+90 mV
1 - 2 mM K+
3Na+2K+
Na+,K+-ATPase
Na+K+2Cl-
NKCC1
Cl-
0 mV
5 mM K+

***Figure 5* K^+ cycling in the stria vascularis.** Na^+,K^+-ATPase and $Na^+,K^+,2Cl^-$ cotransporter (NKCC1) in fibrocytes take up K^+ ions from the spiral ligament. K^+ travels via gap junctions to the apical membrane of intermediate cells where it is released into the intrastrial space via inward rectifier K^+ channel Kir4.1. Na^+,K^+-ATPase and NKCC1 are responsible for K^+ uptake into marginal cells from where it is excreted into the endolymph via K^+ channel KCNQ1/KCNE1. CLCNK/Barttin is involved the polarisation of the membrane and the recycling of Cl^- ions into the intrastrial space. Adapted from [9, 18]

Sensorineural hearing loss

As mentioned above, SNHL is the most common form of HL. A variety of causes can lead to SNHL. While presbycusis (age-related HL), noise-induced HL and ototoxicity (drug-induced HL) may be acquired over time, congenital hearing loss (CHL) describes hearing loss present at or shortly after birth. [1, 4] While environmental causes of CHL include prenatal infections and maternal drug abuse during pregnancy, CHL is thought to be mostly caused by genetic factors and is further divided into syndromic (SHL) and non-syndromic hearing loss (NSHL). [73] Syndromic forms of HL contribute to a third of cases and include syndromes such as Pendred syndrome, Stickler syndrome and Waardenburg syndrome. [74-82] Most genetic defects are, however, non-syndromic and mostly inherited in an autosomal-recessive manner. [83] Over 150 genes have been associated with NSHL so far, such as gap junction protein connexin 26 (*GJB2)* [83, 84], but also genes encoding for key player proteins such as *SLC12A2* (NKCC1) [85], and *BSND* (Barttin) [86] and genes encoding for myosin proteins such as *MYO3A* [87] and *MYO15A* [88]. A full list of all genes associated with hereditary HL can be found in the

Supplements (**Table 9**) as well as on https://hereditaryhearingloss.org.[74] Interestingly, the kidney shares quite a few features with the cochlea. It doesn't come as a surprise, therefore, that several disorders are known to present with both SNHL and kidney manifestations.[89, 90] In addition to the equivalent expression of several ion channels, collagen IV is part of both of their membrane network. [89, 91] Thus, patients with Alport syndrome present with high frequency HL as well as proteinuria and a decline in glomerular filtration rate as this syndrome is caused by mutations in type IV collagen *COL4A3*, *COL4A4* and *COL4A5*. [92-94] Another example are MYH9-related disorders, in which mutations in *MYH9* (non-muscle myosin IIA) lead to varying degrees of hearing loss and chronic kidney disease. [95] Another prominent syndrome is Bartter syndrome, which can affect ion transport mechanisms present in both the loop of Henle of the kidney and the stria vascularis. Mutations in *BSND* (Barttin) as well as *CLCNKA* and *CLCNKB* lead to severe salt-losing nephropathy as well as sensorineural deafness. [56, 59, 60, 96] Mutations in potassium channel Kir4.1 encoding gene *KCNJ10* also present with renal and cochlear phenotypes in form of the EAST syndrome. As Kir4.1 is expressed in the distal nephron, its loss leads to hypokalaemia and metabolic alkalosis but also to sensorineural hearing loss, as it's involved in the generation of the endolymph and the EP within the stria vascularis. [66, 67, 90, 97]

EHD1 - functions and properties

A recent study found EHD1 to be involved in both kidney and inner ear function. [98] As a member of the family of four dynamin-like C-terminal Eps15 homology domain (EHD) proteins, EHD1 is known to play an important role in endocytic recycling. [99, 100] Like other EHD proteins, EHD1 is found to be expressed in a broad range of tissues, including the cochlea. [101-103] The exact role of EHD1 in the inner ear, however, is yet to be uncovered. EHDs present with very similar molecular structures and have been shown to be involved in several processes involving membrane remodelling. [99] When it comes to endocytic recycling, EHD1 is the most studied of the EHD proteins. The endocytic recycling machinery ensures the sorting and re-exporting of internalised membrane components. Once cargo has been internalised from the plasma membrane, it is transported to the early endosome – a group of tubules and vesicles dedicated to the sorting of cargo for their downstream destination. From there, most ligands undergo degradation via late endosomes and lysosomes, while their receptors can return to the plasma membrane or be degraded, too. For recycling, cargo is either directly transported back to the plasma membrane from the early endosome (fast recycling) or via the endocytic recycling compartment (slow recycling). Back at the plasma membrane, receptors are then able to repeat another cycle of ligand-binding and internalisation. Endocytic recycling is tightly regulated by several proteins, with members of the Rab family of small GTPases playing a central role. Rab proteins are known to recruit a number of effector proteins for various functions such as coating proteins, transporting vesicles and mediating fusion with the target membrane. [104] A schematic overview of the properties of the endocytic recycling machinery can be seen in **Figure 6**. Several effectors of Rab proteins have been discovered to interact with EHDs, while EHD1 has been shown to co-localise with

Rab8, Rab11 and MICAL-L1 in cultured cells – all three of whom are known markers of the endocytic recycling compartment. [105-107] In addition, the recycling of several receptors such as transferrin I, GLUT4, IGFR1, integrin as well as MHC II molecules has been shown to be delayed in the absence of EHD1. [108-112] Interestingly, EHD1 has also been shown to regulate the endocytic trafficking of gap junction protein connexin 43 with alterations in the gap junctional network of cardiomyocytes being associated to heart failure in human and mouse. [113] Studies also demonstrated an involvement of EHD1 in retrograde trafficking which is regulated by the retromer complex. [99, 114] There, an interaction between EHD1 and SNX1 as well as Rab5 effector Rank 5 has been reported. [115, 116] In addition, SNX17, a sorting nexin involved in the regulation of receptor recycling has been shown to interact with EHD1. [117]

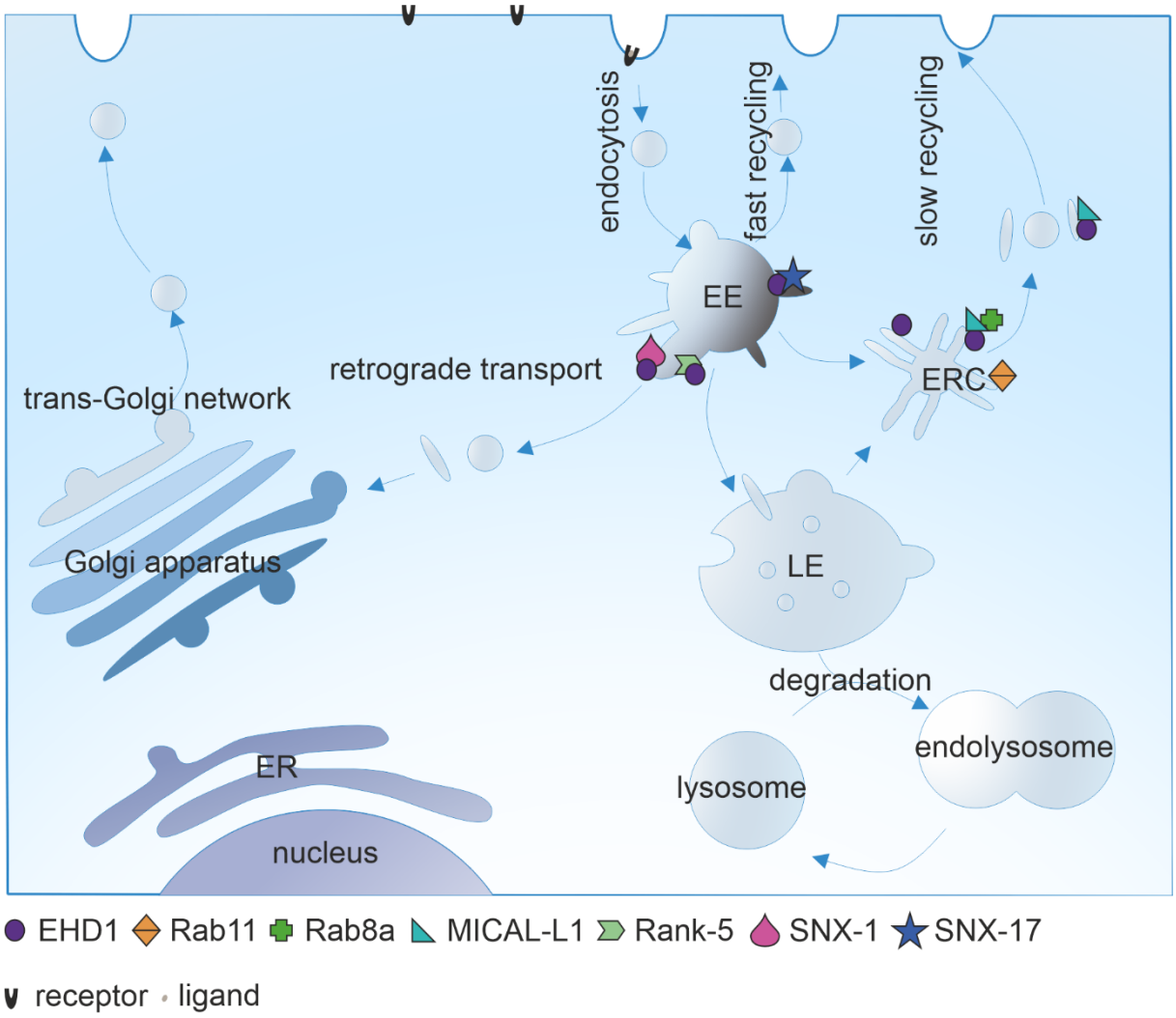

***Figure 6* Regulation of endocytic transport by EHD1 and interacting proteins.** Internalised cargo is sorted at the early endosome. Receptors destined for recycling are then directly transported back to the plasma membrane (fast recycling) or transit through the endocytic recycling compartment (slow recycling). Recycling back to the plasma membrane can also occur via retrograde transport through the trans-Golgi network while cargo destined for degradation is processed at the late endosome. EE = early endosome, ERC = endocytic recycling compartment, LE = late endosome, ER = endoplasmic reticulum. Figure modified from [100, 118].

However, EHD1's functions don't seem to be restricted to receptor recycling and endocytosis. The protein and its family members have also been linked to several aspects of muscle development. [99] During myogenesis as well as regeneration of adult muscle tissue, precursor myoblasts fuse into myotubes. While EHD2 has been linked to plasma membrane transport of Myoferlin [119], EHD1 and EHD2 have been

shown to interact with Fer1L5, which, like Myoferlin, is involved in myoblast fusion. [120] In addition, EHD1 null mice have been found to have smaller muscles. [121] Another aspect of EHD1's involvement in muscle development concerns T tubules of mature skeletal muscle. At these characteristic invaginations of plasma membrane, several ion channels involved in muscle contraction are expressed. Interestingly, EHD1 has been demonstrated to localise to T-tubules and seems to be involved in their formation although its exact role is unknown. [99, 121, 122] Another feature of EHD1 within muscle function seems to involve repairing of injuries occurring during muscle contraction. There, EHD1 has been shown to be present alongside other proteins such as dysferlin, BIN1, MG53 as well as EHD2. [123] In addition to endocytic recycling and muscle development, EHD1 also plays a role in ciliogenesis. [99] Ciliogenesis describes the formation of primary and motile cilia and is involved in the regulation of various signaling pathways. [124] Interestingly, embryonic lethality has been reported for certain EHD1 knockout mice caused by defects in ciliogenesis. [125] Mutated EHD1, as described in *EHD1 mutation R398W*, has been shown to disrupt spermiogenesis in mice – a process highly dependent on ciliary formation. [126] In addition, EHD1 and EHD3 recruitment to certain vesicles during intracellular ciliary formation seems to depend on MICAL L1 as well as SNARE protein SNAP29. [127, 128] The exact role of EHD proteins in the process of ciliogenesis, however, remains unclear. Another aspect of EHD function seems to involve the maintenance of caveolae. [99] These protein-coated membrane invaginations function in mechano-transduction, membrane repair as well as endocytosis. Caevolin and cavin proteins are principal components forming the caveolae membrane, but other proteins including EHD2 have been shown to be present, too. [129, 130] In vitro studies demonstrated the recruitment of EHD1, 2 and 4 to caveolae and cells lacking EHDs have been shown to lose the ability to assemble characteristic caveolar clusters. In addition, cells lacking

EHDs also proved to be less resilient to mechanical stress due to destabilised caveolae. [131]

EHD1 mutation R398W

Robert Kleta and collaborators at the Royal Free Hospital, Centre for Nephrology in London examined six patients of four families with tubular proteinuria and sensorineural hearing loss in the high frequency range (> 2000 Hz) (**Figure 7**). Via linkage analysis, DNA sequencing and haplotype reconstruction, a mutation in the gene encoding for EHD1 was identified to be responsible for the phenotype described above. The mutated EHD1 is inherited in an autosomal recessive manner and results in the substitution of the amino acid arginine by tryptophan at the position 398 (*EHD1*^{R398W}). [98, 132] Similar to the patients, mice carrying the mutation also presented with compromised receptor-mediated endocytosis in proximal tubules as well as hearing impairment in the high frequency range.[98] These findings lay the groundwork for this doctorate to answer questions concerning the role of EHD1 in the process of hearing.

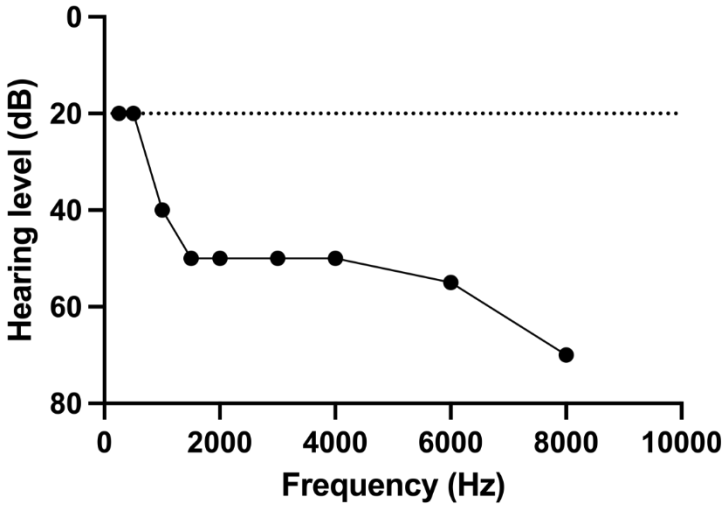

Figure 7 **Representative audiogram from one patient carrying the *EHD1*^{R398W} mutation.** Dashed line represents normal hearing, solid line represents the hearing ability of one of the patients. Figure adapted from [98].

Aims

Patients carrying the mutation R398W indicate a possible role of EHD1 in the process of hearing and its identification as a candidate for SNHL – especially in combination with renal abnormalities. This doctorate aims to characterise the role of EHD1 within the inner ear. Therefore, different methods and approaches came to use. The localisation of EHD1 within the inner ear was observed via different protein staining methods in murine cochleae. An *Ehd1* knockout mouse-model was used to assess hearing capabilities of mice in the presence and absence of EHD1. Further studies of EHD1 within murine cochleae were conducted via immuno-fluorescence staining methods, electron microscopy as well as transcriptome and proteome analysis.

Materials

Expendable materials

Substance	**Manufacturer**
0.9 % NaCl isotonic solution	B. Braun Melsungen AG, Melsungen, Germany
2-Methylbutane	Carl Roth GmbH + Co. KG, Karlsruhe, Germany
Acetic acid (glacial)	Merck, Darmstadt, Germany
Acetone	Sigma, Taufkirchen, Germany
Agarose	AppliChem, Darmstadt, Germany
Ammonium acetate	Sigma, Taufkirchen, Germany
Bovine serum albumin (BSA)	Sigma, Taufkirchen, Germany
$CaCl_2$	Carl Roth GmbH + Co. KG, Karlsruhe, Germany
Citric acid monohydrate	Sigma, Taufkirchen, Germany
DePeX mounting medium	Serva Electrophoresis GmbH, Heidelberg, Germany
D-Mannitol	Fluka Chemie GmbH, Buchs, Switzerland
DNA gel loading dye 6x	Thermo Scientific, Vilnius, Lithuania
EDTA	Sigma, Taufkirchen, Germany
EGTA	Sigma, Taufkirchen, Germany
Eosin Y	Abcam, Cambridge, United Kingdom
Epoxy embedding medium	Sigma, Taufkirchen, Germany

Ethanol	J. T. Baker, Deventer, Netherlands
GeneRuler™ DNA ladder (50 bp, 100 bp, 1 kb)	MBI Fermentas GmbH, St. Leon-Rot, Germany
Glucose	Merck, Darmstadt, Germany
Glutaraldehyde	Sigma, Taufkirchen, Germany
Glycerol	Sigma, Taufkirchen, Germany
Glycine	Merck, Darmstadt, Germany
Heparin (Liquemin N 25000, 5 mL)	Roche, Mannheim, Germany
HEPES	AppliChem, Darmstadt, Germany
Isoflurane	Baxter Deutschland GmbH, Unterschleissheim, Germany
Isopropanol	Merck, Darmstadt, Germany
K_2HPO_4	Merck, Darmstadt, Germany
$K_3[Fe(CN)_6]$	Merck, Darmstadt, Germany
$K_4[Fe(CN)_6]$	Sigma, Taufkirchen, Germany
KCl	Merck, Darmstadt, Germany
Ketamine 100 mg/mL	Sigma, Taufkirchen, Germany
KH_2PO_4	Merck, Darmstadt, Germany
Mayer’s hemalum solution	Carl Roth GmbH + Co. KG, Karlsruhe, Germany
MEM medium	Thermo Fisher Scientific, Dreieich, Germany
Methanol	Merck, Darmstadt, Germany
MgCl	Merck, Darmstadt, Germany

MIDORY green DNA/RNA stain	NIPPON Genetics Europe GmbH, Düren, Germany
Na_2HPO_4	Merck, Darmstadt, Germany
NaCl	Merck, Darmstadt, Germany
Non-fluorescent glycergel mounting medium	DakoCytomation, Dakato North America Inc., Carpinteria, USA
OsO_4	Sigma, Taufkirchen, Germany
Osteosoft®	Merck, Darmstadt, Germany
Paraffin	Paraplast-Plus Paraffin, Sherwood, St. Louis, USA
Paraformaldehyde	Merck, Darmstadt, Germany
Sodium cacodylate trihydrate	Sigma, Taufkirchen, Germany
Sodium citrate-dihydrate	Merck, Darmstadt, Germany
Sodium deoxycholate	Sigma, Taufkirchen, Germany
Sodium dodecyl sulfate (SDS)	Merck, Darmstadt, Germany
Sucrose	Merck, Darmstadt, Germany
TAE buffer 50x	AppliChem, Darmstadt, Germany
Tissue-Tek® O.C.T. Compound	Sakura Finetek USA Inc., Torrance, USA
Triton X-100	Sigma, Taufkirchen, Germany
X-Gal (5-Bromo-4-chloro-3-indolyl ß-D-galactopyranoside)	Sigma, Taufkirchen, Germany
Xylol	Merck, Darmstadt, Germany
β_2-microglobulin, human, recombinant, E.coli	Merck Millipore, Darmstadt, Germany
β-Mercaptoethanol	Merck, Darmstadt, Germany

Equipment

Equipment	**Manufacturer**
Adhesion slides Superfrost® Plus	Gebhard Menzel B.V. & Co. KG, Braunschweig, Germany
CED 3505 programmable attenuator	Cambridge Electronic Division Limited, Cambridge, United Kingdom
CED micro 1401 data acquisition unit	Cambridge Electronic Divison Limited, Cambridge, United Kingdom
Confococal Microscope LSM 710	Zeiss, Jena, Germany
Coverslips	A. Hartenstein GmbH, Würzburg, Germany
CryoStar NX70	Thermo Fisher Scientific, Dreieich, Germany
Eppendorf tubes (0.2 mL, 0.5 mL, 1.5 mL, 2 mL)	Eppendorf AG, Hamburg, Germany
Falcon tubes (15 mL, 50 mL)	Greiner bio-one, Frickenhausen, Germany
Gas mixer for isoflorane vaporiser	MFI Föhr Medical Instruments GmbH, Seeheim, Germany
Light-Cycler LC480	Roche, Mannheim, Germany
Microcentrifuge	Hettich, Tuttlingen, Germany
Microcentrifuge ThermoScientific™ Fresco™ 21	Thermo Fisher Scientific, Dreieich, Germany
Micropipettes (2.5 µL, 10 µL, 100 µL, 1000 µL)	Brand, Wertheim, Germany

Nanodrop 2000c Spectrophotometer	Thermo Fisher Scientific, Dreieich, Germany
Nanodrop 3000 Fluorospectrometer	Thermo Fisher Scientific, Dreieich, Germany
Paraffin incubator	Modell 300, Memmert, Schwabach, Germany
Pasteur pipettes	Brand, Wertheim, Germany
PCR cycler (genotyp. PCR)	
Perfusor Precidor 902681	Infors AG, Bottmingen, Switzerland
pH/mV meter inoLab® pH720	Xylem Analytics, WTW, Weilheim, Germany
Pipette controller accu-jet® pro	Brand, Wertheim, Germany
Pipette tips (10 µL, 100 µL, 1000 µL)	Sarstedt, Nürmbrecht, Germany
Scale EK-600	A&D Instruments Ltd, Tokyo, Japan
Serological pipettes	Nerbe Plus GmbH, Winsen/Luhe, Germany
Sound-attenuated chamber	Industrial Acoustics, Niederkürchten, Germany
Speaker SinusLive neo 25S	Pro hifi, Kaltenkirchen, Germany
Surgery instruments	FST, Bad Oeynhausen, Germany
Thermomixer 5436	Eppendorf GmbH, Hamburg, Germany
Transmission electron microscope EM902	Zeiss, Oberkochen, Germany
Ultramicrotome Leica EM UC6	Leica Mikrosysteme, Vienne, Austria

Warm plate HI 1220 (for paraffin sections)	Leica, Wetzlar, Germany
Warm plate (surgeries)	Dr. J. Barhanin, Nice, France
Water bath W13	Haake, Karlsruhe, Germany

Kits and enzymes

Kit/Enzyme	**Manufacturer**
Alexa Fluor® 546 protein labeling kit	Thermo Fisher Scientific, Dreieich, Germany
DNase I (Rnase-free DNase set)	Quiagen, Hilden, Germany
dNTP-Mix	MBI Fermentas GmbH, St. Leon-Rot, Germany
HiYield® Clean-up/Gel extraction kit	Süd-Laborbedarf GmbH, Gauting, Germany
M-MLV Reverse Transcriptase	Promega, Madison, Wisconsin, USA
M-MLV Reverse Transcriptase Buffer (5x)	Promega, Madison, Wisconsin, USA
Protease	Sigma, Taufkirchen, Germany
Proteinase K	Carl Roth GmbH + Co. KG, Karlsruhe, Germany
Random Hexamer Primer (100 µM)	MBI Fermentas GmbH, St. Leon-Rot, Germany
Rneasy® Mini Kit	Quiagen, Hilden, Germany
SYBR® Green PCR Kit	Roche, Mannheim, Germany

Buffer solutions

	Substance	**Amount**
Antibody solution	BSA	0.5 %
	Triton X-100	0.04 %
	in PBS buffer	

	Substance	**Amount**
Blocking solution	BSA	5 %
	Triton X-100	0.04 %
	in PBS buffer	

	Substance	**Amount**
Citrate buffer, pH 6	Sodium citrate – dihydrate	2.059 g
	Citric acid – monohydrate	0.317 g
	in distilled water	to 1000 mL

	Substance	**Amount**
Endolymph solution, pH 7.4	NaCl	1 mM
	KCl	140 mM
	$CaCl_2$	0.025 mM
	$MgCl_2$	0.025 mM
	KH_2PO_4	1.4 mM
	K_2HPO_4	1.8 mM
	HEPES	5 mM

	Mannitol	25 mM
	in distilled water	

	Substance	**Amount**
Fixation solution, pH 7.4	EGTA	1 mM
	K_2HPO_4	15 mM
	$MgCl_2$	2 mM
	NaCl	90 mM
	Paraformaldehyde	3 %
	Sucrose	100 mM
	in distilled water	

	Substance	**Amount**
glutaraldehyde solution, pH 7.4	Glutaraldehyde	2 %
	Sodium cacodylate	0.1 M
	in distilled water	

	Substance	**Amount**
OsO_4 solution, pH 7.4	OsO_4	1 %
	Sodium cacodylate	0.1 M
	in distilled water	

Phosphate Buffered Saline (PBS), pH 7.4	**Substance**	**Amount**
	KH_2PO_4	1.8 mM

	Na_2HPO_4	10.3 mM
	NaCl	137 mM
	in distilled water	

	Substance	**Amount**
Postfixation solution	PBS	13.32 mL
	Sucrose	3.20 g
	Fixation solution	20 mL

	Substance	**Amount**
Ringer solution, pH 7.4	HEPES	5 mM
	NaCl	145 mM
	K_2HPO_4	1.6 mM
	KH_2PO_4	0.4 mM
	Glucose	5 mM
	$MgCl_2$	1 mM
	$CaCl_2$	1 mM
	in distilled water	

	Substance	**Amount**
Tail buffer, pH 8	EDTA	0.1 M
	SDS	0.5 %
	Tris-HCl	50 mM
	in distilled water	

	Substance	Amount
TE buffer, pH 7.4	EDTA	1 mM
	Tris	10 mM
	in distilled water	

	Substance	Amount
Xgal buffer, pH 7.4	Sodium deoxycholate	1 mg/mL
	IGEPAL CA-630	2 mg/mL
	EGTA	5 mM
	$MgCl_2$	2 mM
	K_2HPO_4	100 mM
	in distilled water	

	Substance	Amount
Xgal working solution	X-Gal	0.5 mg/mL
	$K_3[Fe(CN)_6]$	10 mM
	$K_4[Fe(CN)_6]$	10 mM
	in Xgal buffer	

Software

Software	**Developer**
Adobe Photoshop CS4	Adobe Inc., San José, USA
BioRender	BioRender, Toronto, Ontario
Clone Manager Professional 9	Sci Ed Software LCC, Westminster, USA
Corel Draw Graphics Suite X7	Corel Corporation, Ottawa, Canada
EndNote X7	Clarivate Analytics, London, United Kingdom
GraphPad Prism 9	GraphPad Software, San Diego, USA
Light Cycler software	Roche, Mannheim, Germany
Microsoft Office	Microsoft, Redmond, USA
Spike2	CED, custom made
Zen Pro V2.3	Zeiss, Jena, Germany

Antibodies

Primary antibodies

Antibody	**Catalogue number**	**Manufacturer**	**Dilution**
anti-ATP1A1	ab7671	Abcam	1:100
anti-Bgal	Z378A	Promega	1:100
Anti-BSND	ab242408	Abcam	1:100
Anti-EHD1	ab109311	Abcam	1:50 / 1:100
Anti-KCNQ1	sc-20816	Santa Cruz Biotechnology	1:100

Anti-Kir4.1	APC-035	Alomone Labs	1:100
Anti-NKCC1	ab59791	Abcam	1:100
Anti-Phalloidin-iFluor488	ab176753	Abcam	1:1000

Secondary antibodies and nuclear staining

Antibody	**Catalogue number**	**Manufacturer**	**Dilution**
Alexa Fluor® 488 donkey anti-rabbit	A-21206	Thermo Fisher Scientific, Dreieich, Germany	1:400
Alexa Fluor® 555 donkey anti-rabbit	A-31572	Thermo Fisher Scientific, Dreieich, Germany	1:400
Alexa Fluor® 647 donkey anti-goat	A-21447	Thermo Fisher Scientific, Dreieich, Germany	1:400
Alexa Fluor® 647 donkey anti-mouse	A-31571	Thermo Fisher Scientific, Dreieich, Germany	1:400
HOE33342	H3569	Invitrogen, Karlsruhe, Germany	1:400

Oligonucleotides

All oligonucleotides were purchased from Invitrogen, Karlsruhe, Germany.

Primers for genotyping

gene	**Sequence [5'→3']**	**Amplicon length [bp]**	
LacZ reverse	TCGTGGTATCGTTATGCGCC	102	
Ehd1 forward	CACTTATGGTCAGCGGATGG		456
Ehd1 reverse	CCCTCTGGACAAATGAACTGG		
Ehd1R398W forward	ACTCCCCTGCTTGGATAGTCT	480	
Ehd1R398W reverse	CCTTGTCCACATCTGCCAAC		

Primers for qPCR

Primers were designed using the software Clone Manager, NCBI Splign and NCBI Blast function and purchased from Invitrogen, Karlsruhe, Germany.

gene	**Annealing temperature [°C]**	**Sequence 5'→3'**	**Amplicon length [bp]**
Atp1a1 forward	58	TTGAGCCGAGGATTAACACC	106
Atp1a1 reverse	58	GGCAGAATTTCACCCATTCG	
Bsnd forward	61	CTCAGAGCAGCCCTTCAGTG	124
Bsnd reverse	61	TGTGGCTCATCCCTGTTGG	
Ehd1 forward	58	CAGCCGAGGTTATGACTTTG	99
Ehd1 reverse	58	TCTGAGATGTCCAGCTTGTG	
Kcnj10 forward	58	ACCTTCGAGCCAAGATGAC	150
Kcnj10 reverse	58	CAGCAATGTGCTCCATTCTC	
Kcnq1 forward	57	CTTCACCGTCTTCCTCATTG	110
Kcnq1 reverse	57	GGACAATCTCCATCCAGAAG	
Slc12a2 forward	61	GTGGGAAGCAAAGGCTCAG	102
Slc12a2 reverse	61	TTGGGCTTCTTGCTCTCCAG	

Methods

Mouse models

To analyse the role of EHD1 within the inner ear, a mouse model allowing cre-mediated deletion of exon 2 of *Ehd1* was generated by the Sanger Institute in C57BL6/6N embryonic stem cells as described previously. [133] Previous to this doctorate, the mouse was bred with a global 129/Sv Cre Recombinase pCX-NLS Cre mouse. [132] Repeated backcrossing of at least six times of said offspring resulted in *Ehd1*$^{-/-}$ animals of 129/SV background presenting with a global deletion of exon 2 after Cre Recombinase reaction. Due to the presence of the lacZ promoter upstream of the deleted region, β-galactosidase activity and presence could be measured in *Ehd1*$^{-/-}$ animals. In addition, a mouse lineage carrying the mutation R398W was used. Therefore, C57BL/6NTac-Ehd1$^{m1a1(EUCOMM)Wtsi/WtsiBiat}$ mice were crossed with pCX-Cre before this doctorate.

Isolation of genomic DNA from mouse ear snips

To identify the genotype of *Ehd1*$^{-/-}$, *Ehd1*$^{+/+}$ as well as *Ehd1*^{R398W} animals, ear snips were digested with Proteinase K in Tail Buffer at 55°C at 500 rpm overnight. This was followed by the precipitation of genomic DNA. Therefore, 7.5 M ammonium acetate and 99% isopropanol were added to each sample, vortexed and incubated at -20°C for 30 minutes. Samples were centrifuged for 15 minutes at 13,000 rpm and the supernatant was discarded. The pellet was washed with 70% ethanol and centrifuged for 10 minutes at 13,000 rpm. After carefully removing any remaining ethanol, the pellet was air-dried for 5 minutes, dissolved in 50 µL TE buffer and vortexed. To ensure that the DNA pellets had dissolved completely, the samples were incubated at 55°C;

500 rpm for 5 hours. A diagnostic 0.7% agarose gel was run to verify good quality of the genomic DNA before continuing with the genotyping PCR.

Genotyping of *Ehd1*$^{-/-}$, *Ehd1*$^{+/+}$ and *Ehd1*$^{+/-}$ animals

To identify the genotype of *Ehd1*$^{-/-}$, *Ehd1*$^{+/+}$ and *Ehd1*$^{+/-}$ animals, 0.5 µL genomic DNA was mixed with 10 µL SYBR Green mix, 1 µL forward primer (10 µm), 1 µL reverse primer (10 µm) and 7 µL PCR grade H_2O. Primers were designed to identify exon 2 of wildtype *Ehd1* or the lacZ region added at exon 2 of *Ehd1*, respectively. Primer sequences are listed in *Oligonucleotides*. The following PCR program was run with both primer pair samples:

94°C	3 min	
94°C	30 s	30 cycles
55°C	30 s	
72°C	30 s	
72°C	5 min	
4°C	continuous	

After the PCR, a 3% agarose gel confirmed the respective genotype of each animal.

Genotyping of *Ehd1*^{R398W}, *Ehd1* and *Ehd1he* animals

To identify the genotype of *Ehd1*$^{R398W/R398W}$ (*Ehd1*^{R398W}), *Ehd1*$^{R398/R398}$ (*Ehd1*) and *Ehd1*$^{R398/R398W}$ (*Ehd1he*) animals, specific DNA fragments were amplified from genomic DNA. Therefore, 1 µL of genomic DNA was mixed with 10 µL SYBR Green Mix, 1 µL forward primer 5256 (10 µM), 1 µL reverse primer 5257 (10 µM) and 7 µL PCR grade H_2O. The following PCR program was used:

94°C	10 min	
94°C	1 min	32 cycles
55°C	1 min	
72°C	30 s	
72°C	2 min	
4°C	continuous	

A diagnostic 2% agarose gel was run to check on amplicon size and quality. Subsequently, the PCR samples were purified using the HiYield® Clean-up/Gel Extraction Kit and the DNA was eluted in 20 µL PCR grade H_2O. Purified DNA was mixed with 2 µL forward primer 5256 (10 µM) and 8 µL of PCR grade H_2O and sent for sequencing to Microsynth Seqlab GmbH. All primer sequences are listed in *Oligonucleotides*.

Auditory brainstem response measurements

To assess the hearing capability of *Ehd1*$^{-/-}$ mice compared to their wildtype litter mates, frequency-dependent auditory brainstem response (f-ABR) measurements were performed in collaboration with Prof. Dr. Holger Schulze and Dr. Konstantin Tziridis, Department of Otorhinolaryngology – Head and Neck Surgery, University Hospital Erlangen. Therefore, 7 *Ehd1*$^{-/-}$ and 8 *Ehd1*$^{+/+}$ mice aged 8 weeks were anaesthetised with a mixture of ketamine (96 mg/kg) and xylazine (4 mg/kg) in 0.9% sodium chloride. The mixture was applied via intraperitoneal injection at 10 µL per gram bodyweight.

The measurements were done following the protocol and equipment as previously described [134]. Thus, anaesthetised animals were equipped with subcutaneously placed thin silver wire electrodes (0.25 mm in diameter) and placed within a sound-attenuated chamber. F-ABR of the left ear was measured free-field at a 3 cm distance from the animal's pinna using a CED micro 1401 data acquisition unit with a CED 3505 programmable attenuator via a custom-made program. The presented stimuli were pure tones (6 ms duration including 2 ms cosine-squared rise and fall times) at 4, 8, 16 and 32 kHz. During each measurement, 150 stimuli were presented with alternating inverted phase with a repetition rate of 4 Hz. Stimulation was presented pseudorandomised starting at the highest attenuation of 10 dB SPL and ending at the lowest attenuation of 95 dB SPL in 5 dB steps.

Dissection of cochleae

Mice were euthanised in a euthanasia chamber using isoflurane followed by cervical dislocation and decapitation. The skull was freed from fur and skin and a midsagittal bisection was performed. While dissecting one half, the other half of the skull was stored in ice-cold 1xRinger solution. After the removal of brain tissue, the otic capsule was identified. The encapsulated cochleae were dislodged via the predetermined breaking point behind the petrous bone. For further dissection, a stereo microscope came to use while the cochlear tissue was kept in ice-cold 1xRinger solution throughout the following procedure. Firstly, the cochleae were exposed by carefully breaking down and removing the bulla tympanica. The cochleae were freed from any remaining surrounding tissue and a hole was drilled near the cochlear apex to either ensure thorough flushing with fixation solution or as a point of entry for further dissection.

Formalin-fixed paraffin embedded (FFPE) cochleae

For formalin-fixed paraffin-embedded (FFPE) tissue, the dissection of the cochlea was followed by careful application of fixation solution through the round window using an insulin syringe. For further fixation, the tissue was incubated in fixation solution for 1.5 hours, washed with 1xPBS and decalcified in Osteosoft® solution for four days at 4°C. To ensure adequate supply with EDTA, fresh Osteosoft® solution was added after two days. The post-fixation procedure consisted of the incubation with postfixation solution containing 1 % formaldehyde, followed by treatment with 50 mM HEPES buffer (pH 8) with increasing sucrose concentrations of 10 and 15 %, respectively. The tissue underwent a commonly applied dehydration process of incubation in methanol of increasing concentration (70, 80, 90 and 100 % methanol) and 99 % isopropanol for 20 minutes each. This was followed by the infiltration with wax at 60°C, starting with a 50 % dilution of paraffin in isopropanol for 1 hour and undiluted paraffin incubation overnight. To ensure complete clearance of isopropanol, another hour of incubation in fresh paraffin was performed before the embedment into paraffin blocks. Finally, the tissue was sectioned using a microtome. 5 µm sections were placed onto adhesion slides, dried overnight at 60°C and stored at 4°C until usage.

Immunofluorescence staining of FFPE cochleae

To remove remaining paraffin, the sections were rehydrated in xylene, 99 % isopropanol and a series of ethanol solutions of decreasing concentration (95, 80 and 70 %) for 15 minutes each. Antigen retrieval was achieved via incubation in citrate buffer at 95°C for 15 minutes. Following, the sections were incubated in blocking solution containing 5 % bovine serum albumin to block any unspecific binding sites. The primary antibody of interest was applied overnight at 4°C, followed by one hour of secondary antibody incubation at room temperature without light exposure. The

sections were mounted using a non-fluorescent glycergel mounting medium and stored at 4°C until imaging. All antibodies used as well as applied dilutions of such are displayed in *Materials/Antibodies*.

Electron microscopy of cochleae

For electron microscopy, cochleae were either dissected as previously described in *Dissection of cochleae* or perfusion-fixated before dissection. Perfusion-fixation was performed by Anna-Lena Forst. Animals were anesthetised by isoflurane administration and the abdominal aorta as well as vena cava were exposed. A catheter was inserted into the aorta while the vena cava was cut open to allow drainage of fixation solution. Animals were perfused with 50 mL of fixation solution at a perfusion rate of 1 mL per four seconds. After perfusion, cochleae were dissected as described previously. Dissected cochleae meant for electron microscopy were carefully fixed by applying glutaraldehyde solution through the round window after dissection, followed by three days of fixation in glutaraldehyde solution at 4°C. To prepare the bony tissue for sectioning, the cochleae were decalcified for 4 weeks in Osteosoft® solution with fresh solution added twice a week to maintain a high concentration of accessible EDTA. Cochleae were post-fixed in 1% OsO_4 solution and dehydrated through a series of graded alcohols and acetone. Tissue was embedded in resin and polymerised for 2 days at 60°C. Resin blocks were sectioned using an ultramicrotome Leica EM UC6. Thick sections (680 nm) were Richardson stained with Methylene Blue and used as overview images for subsequent morphological analysis. Blocks were thin-sectioned (50 nm) and placed on copper mesh grids. Dried grids were viewed with a transmission electron microscope Zeiss 902. A total of seven unperfused *Ehd1*$^{+/+}$ (four females, three males) aged 48 – 62 days and seven *Ehd1*$^{-/-}$ animals (three female, four male) aged 44 – 69 days was processed and analysed as described above. In addition, seven

Ehd1$^{-/-}$ and four *Ehd1*$^{+/+}$ animals (female) aged 150 – 151 days were processed and analysed. For better tissue preservation, three *Ehd1*$^{+/+}$(74 – 128 days old), three *Ehd1-/-* (74 – 130 days old) mice and one *Ehd1*^{R398W} mouse aged 233d were perfusion-fixated and visualised.

X-Gal staining of cochleae

For X-Gal staining, the dissected cochleae were fixed in 100 % acetone for 24 hours at 4°C with one change of solution after 12 hours. To remove any remaining acetone, the tissue was washed with X-Gal buffer for 5 minutes before incubation with X-Gal working solution for 24 hours at 37°C under constant motion of 500 rpm and protected from light. Cochleae were fixed with fixation solution for 24 hours and decalcified in Osteosoft® solution for four days. Post-fixation was achieved by incubation in postfixation solution for 6 hours. Sucrose was used as a cryoprotectant to prevent ice crystal formation within the tissue. As the post-fixation solution contains 17 % sucrose, the tissue was subsequently incubated in 50 mM HEPES buffer containing 30 % sucrose overnight at 4°C. Cochleae were embedded in TissueTek, which was introduced gradually by incubation in 50 % TissueTek dissolved in 30 % sucrose solution overnight before the final embedment. 5 µm sections were prepared using a cryostat. The slides were baked overnight at 60°C, washed with 1xPBS and mounted with glycergel mounting medium.

Transcriptomics of murine stria vascularis

To extract the stria vascularis from dissected cochleae, the drilled hole near the apex was used as a point of entry to carefully remove the bony structure from the coils. The stria vascularis was identified, gradually removed from the lateral wall, and immediately transferred to lysis buffer provided by Qiagen Rneasy®Micro. The lysate was

homogenised using QIAshredder columns and RNA was isolated and purified according to the Qiagen Rneasy®Micro kit instructions. RNA was eluted in 14 µL Rnase-free water and sent for analysis to the Kompetenzzentrum Fluoreszente Bioanalytik (KFB) of the University of Regensburg. Samples of 4 *Ehd1*$^{+/+}$ and 5 *Ehd1*$^{-/-}$ animals of mixed sex aged 55 to 58 days were prepared. Sample processing on an Affymetrix GeneChip® Clariom S mouse microarray as well as downstream analysis was carried out at the Genomics Core Facility KFB. Samples were analysed with the Applied Biosystems™ GeneChip™ Expression Console v1.4 software and probe sets with unadjusted p-values lower than 0.05 (Student's t-test) and a fold change above 2.0 fold were considered significantly regulated.

Proteomics of murine stria vascularis

To extract stria vascularis from dissected cochleae, the tissue was carefully removed as described in *Transcriptomics of murine stria vascularis*. The isolated striae were transferred to a PCR cup containing 8% SDS in ddH_2O and incubated at 95°C at 500 rpm for 5 minutes before storage at -80°C. Samples of 10 *Ehd1*$^{+/+}$ (4 females, 6 males) and 7 *Ehd1*$^{-/-}$ (4 females, 3 males) animals aged 57 to 62 days were sent for analysis to Prof. Dr. Markus Rinschen and Prof. Dr. Fatih Demir at Aarhus Institute of Advanced Studies of Aarhus University, Denmark. In addition, unrelated control animals of SV129 background were processed for comparison of EHD1 availability with *Ehd1*$^{+/+}$ and *Ehd1*$^{-/-}$ animals (8 females aged 56 – 76 days). Diluted samples were boiled, and protein concentrations were determined by BCA assay. Subsequently, cysteines were carbamidomethylated and proteins were purified with super-paramagnetic SP3 beads. Concentrations of cleaned peptides were determined by the NanoDrop A_{280} assay. Mass spectrometry runs were queried by Markus Rinschen's team on an UltiMate3000 nano-HPLC system/Exploris 480 mass spectrometer

including FAIMS pro interface (Thermo Fisher Scientific) using Spectronaut (version 18.6.231227.55695, Biognosys) utilizing data independent acquisition proteomics (directDIA+) against the mouse canonical reference proteome from UniProt (21,989 entries from 2022/09) with standard settings: Trypsin/P specificity with 2 missed cleavages and a 7-52 amino acid peptide length, acetylated protein N-termini and oxidized methionine as variable modifications, and fixed carbamidomethylation on cysteines. Identifications for PSM/peptide/protein groups were handled at a 0.01 false-discovery (FDR) rate. Due to significantly lower peptide and protein IDs (> 20% deviation from mean IDs), some mice samples were excluded from the database search and the subsequent analysis. Thus, samples of 6 *Ehd1*$^{+/+}$ (3 females, 3 males) and 6 *Ehd1*$^{-/-}$ (3 females, 3 males) animals aged 57 to 61 days were considered for data analysis.

β_2-microglobulin uptake in stria vascularis

Murine stria vascularis was extracted following protocols described in *Dissection of cochleae* and *Transcriptomics of murine stria vascularis* and immediately incubated in MEM medium containing 0.5 µM fluorescently-labelled β_2-microglobulin (b2m) for 30 minutes at 37°C. Tissue was washed for five minutes in ice-cold PBS solution before incubation in fixation solution containing 3% PFA for 10 minutes on ice. Striae were washed in ice-cold PBS solution for 5 minutes before being transferred to blocking solution for 10 minutes at room temperature. After another two rounds of washing in ice-cold PBS, the tissue was incubated in primary antibody (anti-Kcnq1) solution for 30 minutes at room temperature to later visualise marginal cells. After two rounds of washing in PBS solution on ice, the striae were added to secondary antibody solution for 30 minutes at room temperature. To wash off unbound secondary antibody, the samples were washed in PBS solution at room temperature twice before being

transferred to a microscope slide. There, remaining PBS solution was carefully removed with a 10 µL pipette and tissue was mounted with Dako mounting medium.

Whole mount of Organ of Corti

Cochleae were dissected as described in *Dissection of cochleae*. Fixation solution was applied through the round window. The carefully drilled hole near the apex provided thorough flushing of the coils. The tissue was incubated in ice-cold fixation solution for one hour before being transferred to a petri dish filled with PBS. With a stereomicroscope for better visualisation, the bony structures as well as the Reissner's membrane and stria vascularis were carefully removed. The bony modiulus and connected structures including the Organ of Corti were decalcified in PBS solution containing 140 mM EDTA at 4°C overnight. The cochleae were separated into their three coils using surgical scissors. Each coil was washed in PBS solution containing 0.1% Triton X-100 for 5 minutes before incubation in blocking solution for one hour. This step was followed by primary antibody incubation overnight at 4°C. After washing off any remaining primary antibody solution with 0.3% Triton X-100 in PBS, secondary antibody incubation was applied for 2 hours under light-free conditions. The coils were washed in 0.3% Triton X-100 as well as pure PBS solution before being transferred to a microscope slide and mounted.

Quantitative realtime PCR

Possible differences in mRNA expression in striae vascularis of *Ehd1*$^{+/+}$ and *Ehd1*$^{-/-}$ animals were examined via quantitative realtime polymerase chain-reaction (qPCR). Therefore, striae were dissected as described in *Dissection of cochleae* and *Transcriptomics of murine stria vascularis* and pooled per animal. Samples were lysed in RLT buffer by Qiagen containing β-mercaptoethanol to inactivate RNases, sonicated

for 5 minutes and homogenized using QIAshredder columns according to the manufacturer's guide. Total RNA was isolated and purified according to Quiagen RNeasy®Micro kit instructions and eluted in 14 µL RNase-free water. RNA concentration and quality was measured using a Nanodrop spectrophotometer with samples of low quality being excluded from further experiments. Therefore, the absorption of ultraviolet light at 260 nm provides information regarding the RNA concentration per sample as it constitutes the absorption peak for nucleic acids. As 280 nm defines the absorption peak of proteins, the ratio of wavelengths 260 nm to 280 nm reveals information about the purity of the RNA sample with a ratio of 2.0 being considered a pure, high-quality sample. As the polymerase activity is limited to double-stranded DNA templates, harvested RNA had to be reverse transcribed into complementary DNA (cDNA) first. Therefore, the following protocol was performed for each sample:

14 µL	purified RNA
1 µL	random primer

Following primer annealing, a master mix containing dNTPs and reverse transcriptase was added and processed, accordingly:

5 µL	M-MLV 5x reaction buffer	20°C, 10 minutes 50°C, 50 minutes 70°C, 15 minutes 4°C
1.25 µL	dNTPs	
1 µL	RNase inhibitor	
2.75 µL	H_2O (RNase-free)	
0.8 µL	M-MLV reverse transcriptase	

Each sample was processed without reverse transcriptase in parallel to detect possible contamination with genomic DNA and thus prevent incorrect evaluation of downstream qPCR measurements.

For qPCR experiments, Gapdh was used as reference gene as its expression levels across the two genotypes proved to be stable. A dilution series of all samples enabled the establishment of a standard curve. Therefore, an equal amount of all samples was pooled, and dilutions of this pooled sample were applied to each qPCR run (undiluted, 1:5, 1:25, 1:50 and 1:125). The log of each dilution was plotted against its C_t value to assess the efficiency per reaction. To ensure similar consistency of all probes during detection, a master mix of all ingredients was prepared before adding the template cDNA. Therefore, a SYBR Green I hot start reaction mix by Roche came to use according to the protocol below.

qPCR master mix:

Forward primer [10 µM]	0.5 µL
Reverse primer [10 µM]	0.5 µL
LightCycler® 480 SYBR Green I Master	5 µL
H_2O	3 µL
∑	9 µL

A volume of 9 µL of thoroughly mixed master mix was applied per well into a 96-well PCR plate. 1 µL of each template cDNA was added accordingly. The samples were processed by a LightCycler® 480 as follows. Customized annealing temperatures as well as the number of cycles are displayed in *Primers for qPCR*.

Activation of polymerase	95°C	10 min	
Denaturation	95°C	15s	n cycles
Annealing	x°C	20s	
Elongation	72°C	20s	
Melting curve analysis			
Denaturation	95°C	10s	
Renaturation	56°C	1min	

Statistics

For statistical analysis, GraphPad Prism came to use. Gaussian distribution of each set of data was examined and statistical analysis was carried out accordingly.

For analysis of f-ABR measurements, outliers were identified by calculating the interquartile range and defined as such for values 1.5 times lower than the first quartile or 1.5 times greater than the third quartile, accordingly. Mann-Whitney U tests were performed to calculate significant differences in hearing abilities between *Ehd1*$^{+/+}$ and *Ehd1*$^{-/-}$ as well as *Ehd1*$^{+/+}$ and *Ehd1*^{R398W} animals, respectively. P-values ≤ 0.05 were considered significant and indicated with an asterisk.

Fluorescence intensities of key player IF staining were normalised to the fluorescence intensities of nuclear staining per section and significant differences between *Ehd1*$^{+/+}$ and *Ehd1*$^{-/-}$ animals were investigated by applying Mann-Whitney U tests. Data are indicated as mean and SEM. P-values were Bonferroni corrected and values ≤ 0.01 were considered significant.

The mRNA expression of key players in *Ehd1*$^{-/-}$ samples was normalised to their expression in *Ehd1*$^{+/+}$ samples. Data were indicated as mean and SEM. Mann-Whitney-U tests were conducted to analyse significant differences between the two genotypes. Bonferroni corrected p-values ≤ 0.008 were considered significant.

To quantify morphological differences in the size of scala media, cell density within the spiral ganglion as well as the thickness of the stria vascularis, outliers were identified and eliminated by calculating the interquartile range and defined as such for values 1.5 times lower than the first quartile or 1.5 times greater than the third quartile, accordingly. Mann-Whitney-U tests were applied to identify significant differences

between the two genotypes for the morphological features mentioned above. Bonferroni-corrected p-values ≤ 0.0167 were considered significant.

Results

Localisation of EHD1 within the mouse inner ear

To determine the localisation of EHD1 within the mouse inner ear, immunofluorescence staining was performed using an antibody against EHD1 as well as an antibody against β-galactosidase on FFPE cochleae of *Ehd1*$^{-/-}$ and *Ehd1*$^{+/+}$ animals. In addition, β-galactosidase activity within the inner ear was detected via X-gal staining procedure.

Immunofluorescence staining of EHD1

In FFPE cochleae of *Ehd1*$^{+/+}$ mice, the stria vascularis, tectorial membrane, spiral ganglion and inner hair cells stained positive for EHD1 (**Figure 8**). To some extent, type II fibrocytes of the spiral ligament also showed positive staining for EHD1. However, tissue of *Ehd1*$^{-/-}$ animals also stained positive for EHD1 in named areas except stria vascularis and spiral ligament. It must be noted, that staining of the spiral ligament wasn't consistent in *Ehd1*$^{+/+}$ animals (**Figure 9**). This suggests that the stria vascularis is the only area of specific EHD1 staining within the cochlea. The positive staining seen in *Ehd1*$^{-/-}$ spiral ganglion, hair cells and tectorial membrane are most likely due to unspecific binding of the used antibody.

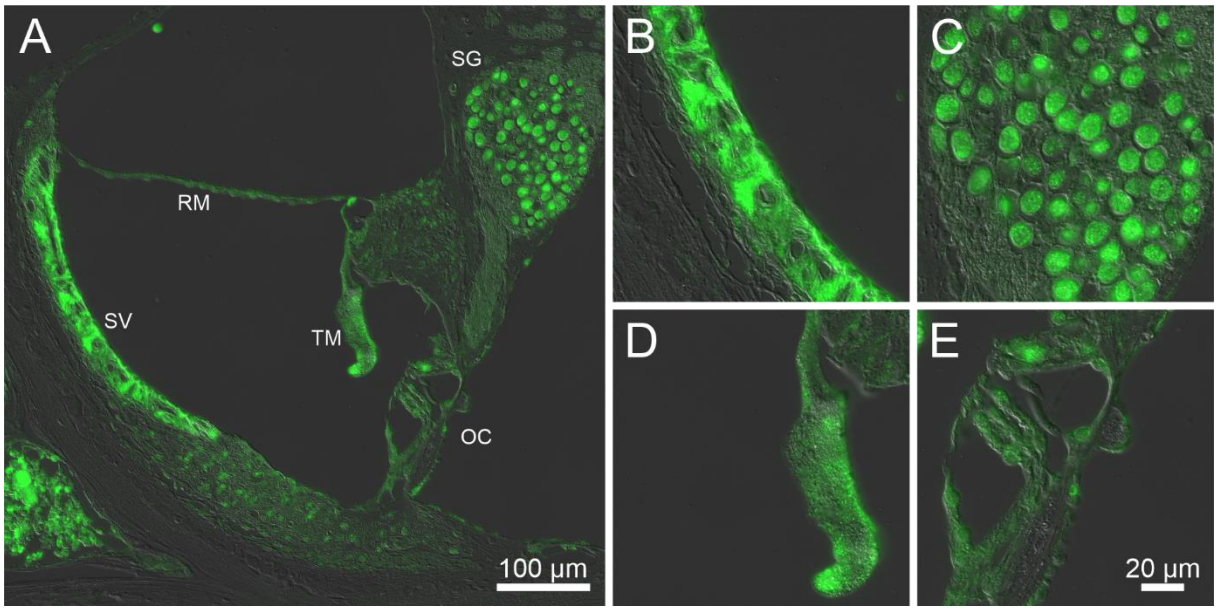

***Figure 8* IF detection of EHD1 in *Ehd1*$^{+/+}$ cochleae.** (A) overview image of a cochlear cross-section with positive staining for EHD1 depicted in green. (B) Close-up section of the stria vascularis. (C) Close-up section of the spiral ganglion. (D) Close-up section of the tectorial membrane. (E) Close-up section of the Organ of Corti with outer and inner hair cells. RM = Reissner's membrane, SV = stria vascularis, TM = tectorial membrane, OC = Organ of Corti, SG = spiral ganglion.

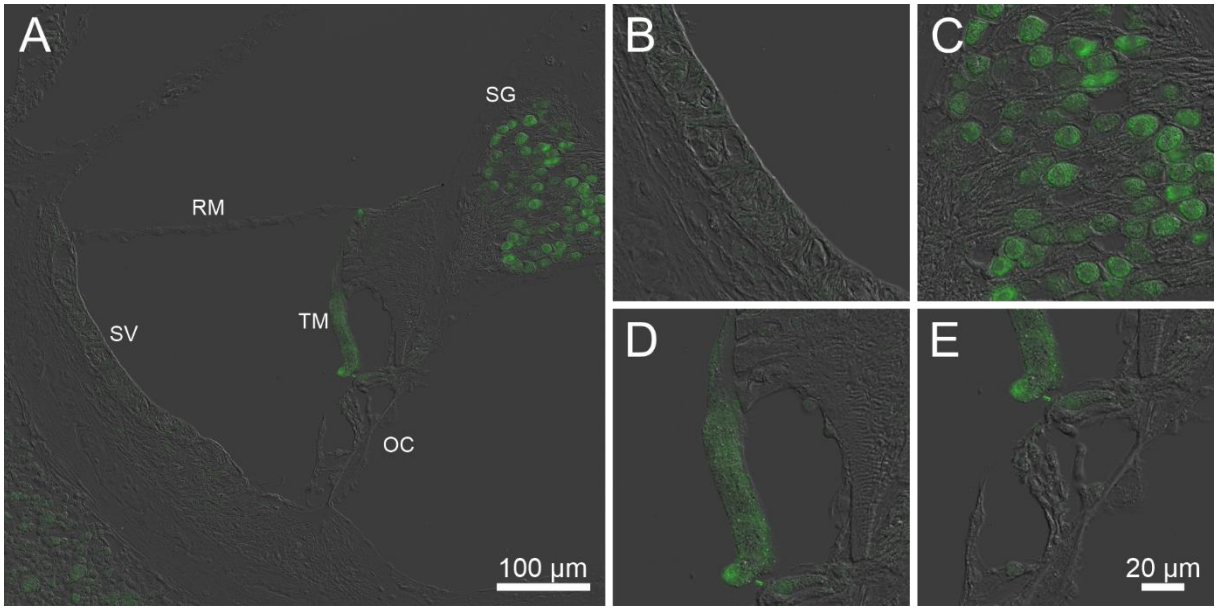

***Figure 9* IF detection of EHD1 in *Ehd1*$^{-/-}$ cochleae.** (A) overview image of a cochlear cross-section with positive staining for EHD1 depicted in green. (B) Close-up section of the stria vascularis. (C) Close-up section of the spiral ganglion. (D) Close-up section of the tectorial membrane. (E) Close-up section of the Organ of Corti with outer and inner hair cells. RM = Reissner's membrane, SV = stria vascularis, TM = tectorial membrane, OC = Organ of Corti, SG = spiral ganglion.

Immunofluorescence staining of β-galactosidase

To further evaluate the alleged unspecific staining of the EHD1 antibody observed in *Ehd1*$^{-/-}$ cochleae, an antibody binding to β-galactosidase came to use. The staining of this bacterial protein was possible due to its promoter lac Operon expressed within the *Ehd1*$^{-/-}$ mouse lineage. Immunofluorescence staining of *Ehd1*$^{-/-}$ cochleae revealed the detection of said protein within the stria vascularis (**Figure 10**). Moreover, the distinct staining of the strial area bordering the endolymphatic space suggests β-galactosidase expression in marginal cells of the stria vascularis.

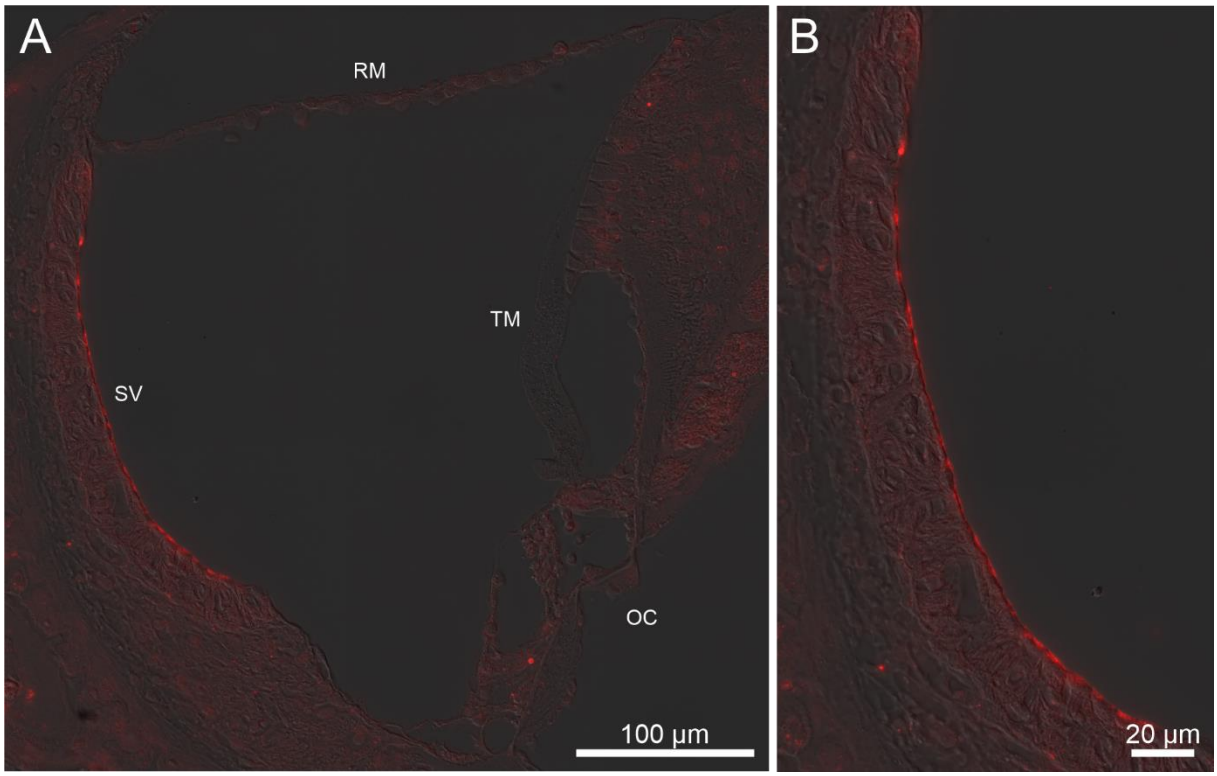

Figure 10 **IF detection of β-galactosidase in *Ehd1*$^{-/-}$ cochleae.** (A) Overview image of a cochlear cross-section with positive staining for β-galactosidase depicted in red. (B) Close-up of the stria vascularis with positive staining for β-galactosidase in the marginal cell layer. RM = Reissner's membrane, SV = stria vascularis, TM = tectorial membrane, OC = Organ of Corti.

X-gal staining

In addition to immunofluorescence staining of β-galactosidase, LacZ expression within the cochlea of *Ehd1*$^{-/-}$ animals was visualised by applying the X-gal staining technique. As the lacZ promoter is present in *Ehd1*$^{-/-}$ animals, applying X-gal as a substrate for β-galactosidase results in a characteristic blue precipitate on cells expressing its promoter. In *Ehd1*$^{-/-}$ cochleae, the marginal cell layer of the stria vascularis as well as the spiral ligament presented with said precipitate (**Figure 11**).

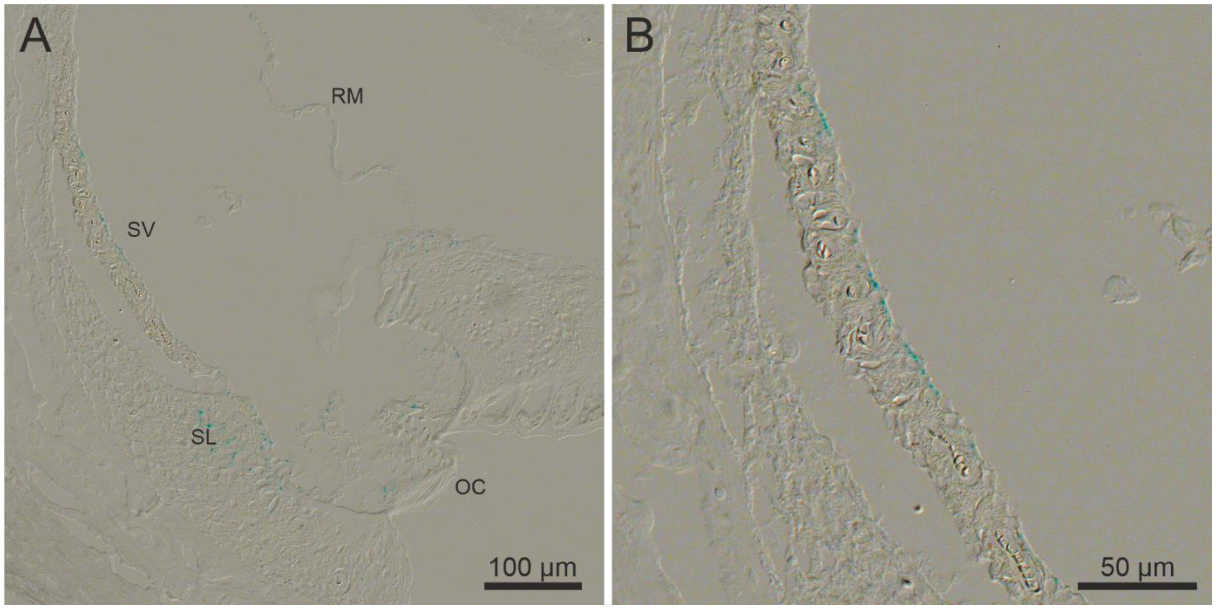

***Figure 11* Xgal staining of *Ehd1*$^{-/-}$ cochlea.** (A) Overview cross-section of *Ehd1*$^{-/-}$ cochlea with LacZ expression presenting as a blue stain most prominent in stria vascularis and spiral ligament. (B) Close-up of the stria vascularis showing distinct staining of marginal cells. RM = Reissner's membrane, SV = stria vascularis, OC = Organ of Corti, SL = spiral ligament.

f-ABR measurements

To assess the hearing capability of *Ehd1*$^{+/+}$, *Ehd1*$^{-/-}$ and *Ehd1*^{R398W} mice, f-ABR measurements were carried out. F-ABR measurements of *Ehd1*^{R398W} animals and their wildtype litter mates were done before this doctorate [98] and showed hearing loss at intermediate and high frequency ranges in animals carrying the mutation (**Figure 12**). Named animals were of a mixed BL6 and 129/SV background [98]. Sara Afonso also carried out measurements of *Ehd1*$^{-/-}$ animals of mixed genetic background and found a tendency of a higher threshold for the tested high frequency compared to *Ehd1*$^{+/+}$ animals but no differences at low and intermediate frequencies. [132] In addition, f-ABR measurements of *Ehd1*$^{-/-}$ animals and their wildtype litter mates of 129/SV background were carried out. Those measurements revealed significant hearing loss in the low and intermediate frequency ranges in *Ehd1*$^{-/-}$ animals compared to *Ehd1*$^{+/+}$ mice (**Figure 12**).

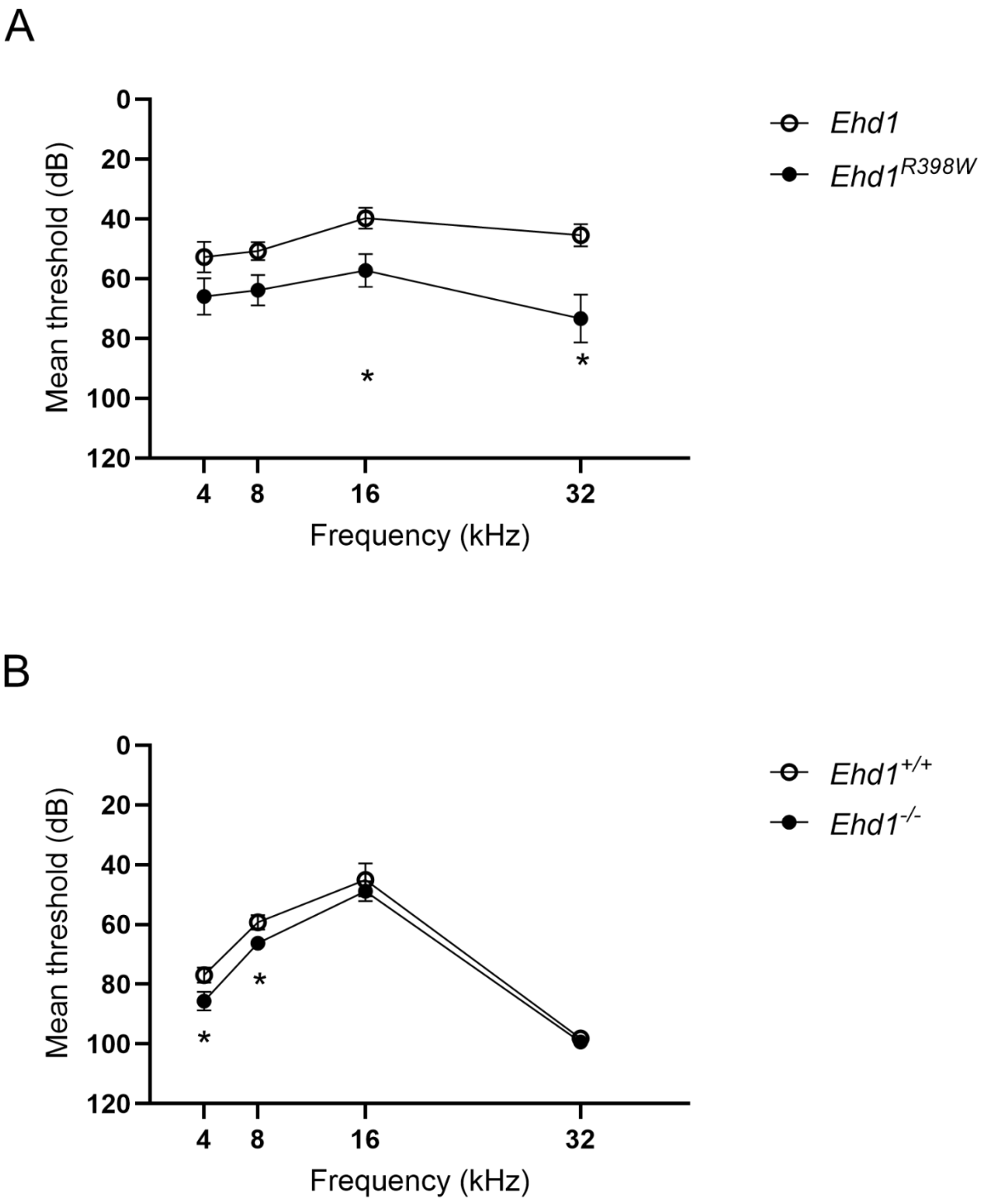

Figure 12 **Hearing impairment in *Ehd1*$^{-/-}$ and *Ehd1*^{R398W} animals.** (A) Auditory brainstem response measurements of *Ehd1*^{R398W} animals and their wildtype litter mates (*Ehd1*) showed hearing impairment in intermediate and high frequency ranges (mixed genetic background). (B) *Ehd1*$^{-/-}$ as well as *Ehd1*$^{+/+}$ animals (both of 129/SV background) showed hearing impairment throughout all frequencies tested compared to animals of mixed genetic background. *Ehd1*$^{-/-}$ animals presented with significantly worse hearing for low and moderate frequency ranges. * Indicates p≤0.05 between groups (Mann-Whitney-U test).

Influence of EHD1 knockout on key players of potassium cycling

As the stria vascularis is mainly responsible for the composition of the endolymph as well as of upholding the EP, possible alterations in the expression of key proteins responsible for K^+ cycling and generation of the EP needed to be investigated. Therefore, the expression of Na^+,K^+-ATPase, Kir4.1, Nkcc1, Barttin and Kcnq1 in *Ehd1*$^{+/+}$ and *Ehd1*$^{-/-}$ mice was measured to uncover a potential involvement of EHD1 in their subcellular distribution or expression levels.

Immunofluorescence staining of key players

Immunofluorescence staining of subunit 1 of Na^+K^+ATPase (Atp1a1), Nkcc1, Kir4.1, Barttin and Kcnq1 were performed. 5 *Ehd1*$^{+/+}$ and 7 *Ehd1*$^{-/-}$ animals used for these experiments were six to ten weeks old. No changes in staining patterns due to EHD1 knockout were detected for any of the proteins tested (**Figure 13**, **Figure 14**). Thus, the localisation of said key players within the stria vascularis remains unaffected by the presence or absence of EHD1: In addition, fluorescence intensities of the sections were quantified and normalised to the fluorescence intensity of nuclear staining, accordingly. No significant differences in fluorescence intensity of observed key players in *Ehd1*$^{-/-}$ and *Ehd1*$^{+/+}$ animals was found (**Figure 15**).

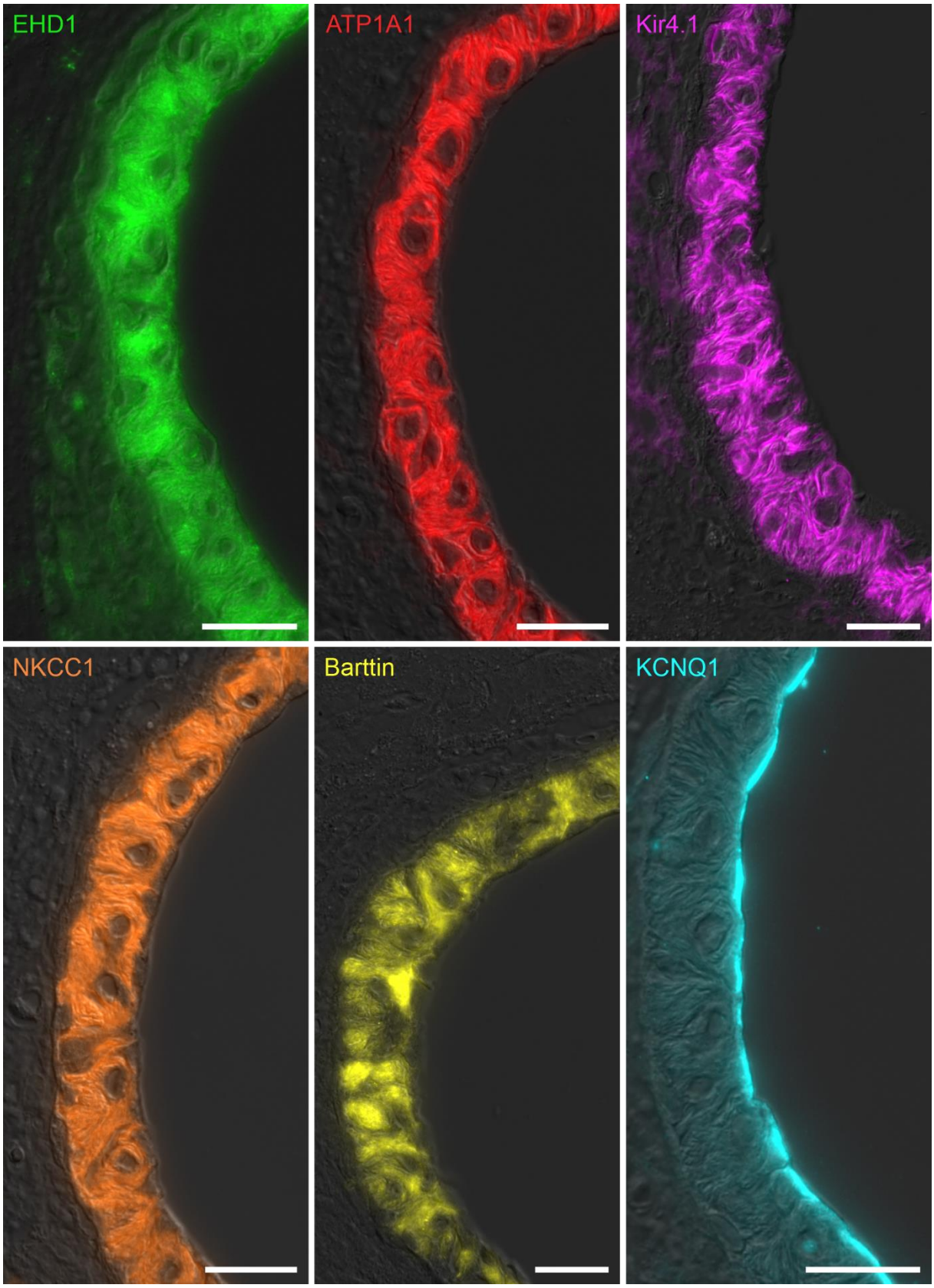

Figure 13 **IF staining of key players of K^+ cycling.in *Ehd1*$^{+/+}$ stria vascularis.** Localisation of subunit ATP1A1 of Na+K+ATPase (red), Kir4.1 (violet), NKCC1 (orange), Barttin (yellow) and KCNQ1 (turquoise) in stria vascularis compared to EHD1 expression (green) in *Ehd1*$^{+/+}$ mice. Scalebars 20 µm.

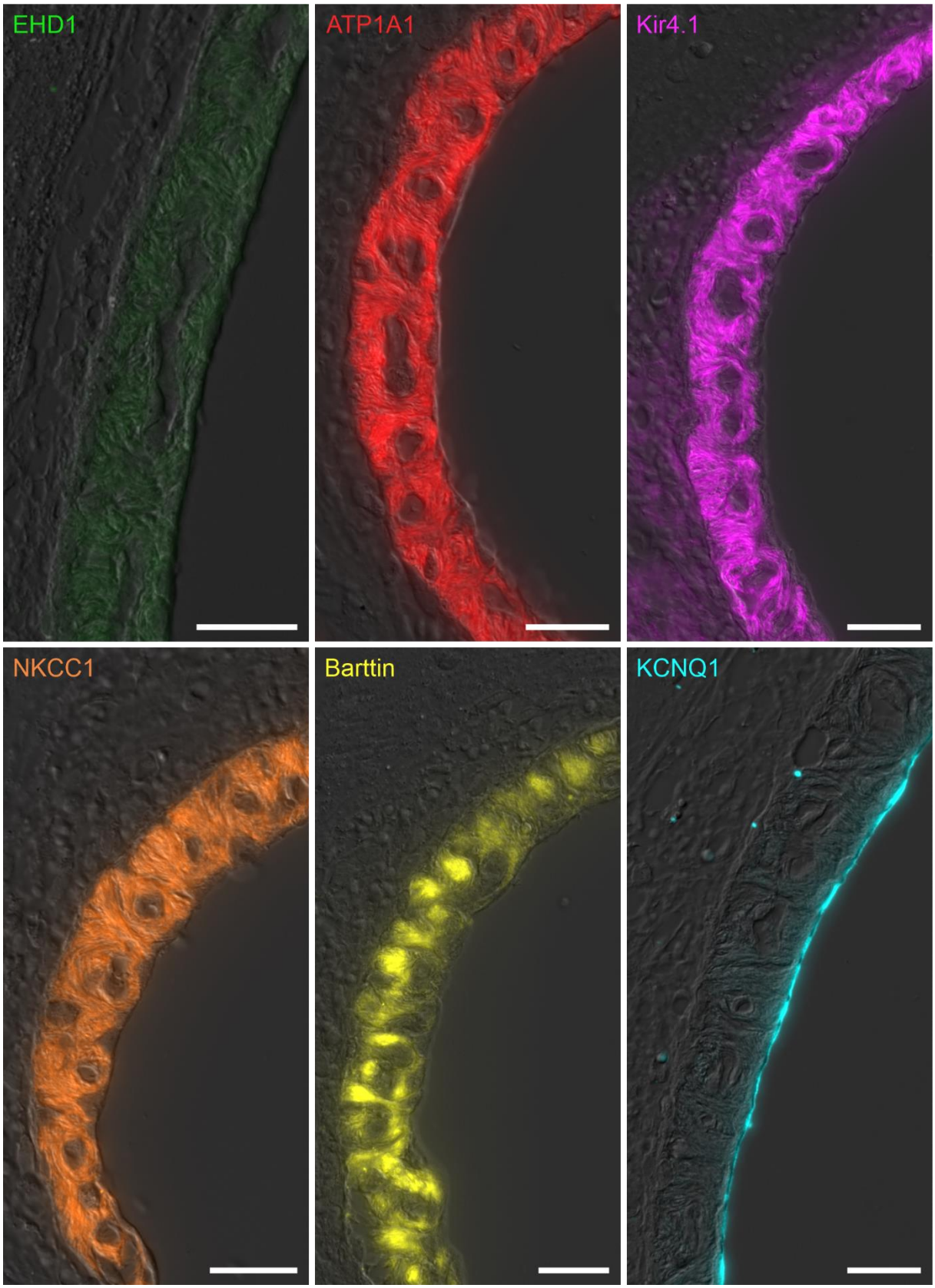

Figure 14 **IF staining of key players of K^+ cycling.in *Ehd1*$^{-/-}$ stria vascularis.** Localisation of subunit ATP1A1 of Na+K+ATPase (red), Kir4.1 (violet), NKCC1 (orange), Barttin (yellow) and KCNQ1 (turquoise) in stria vascularis compared to EHD1 expression (green) in *Ehd1*$^{-/-}$ mice. Scalebars 20 µm.

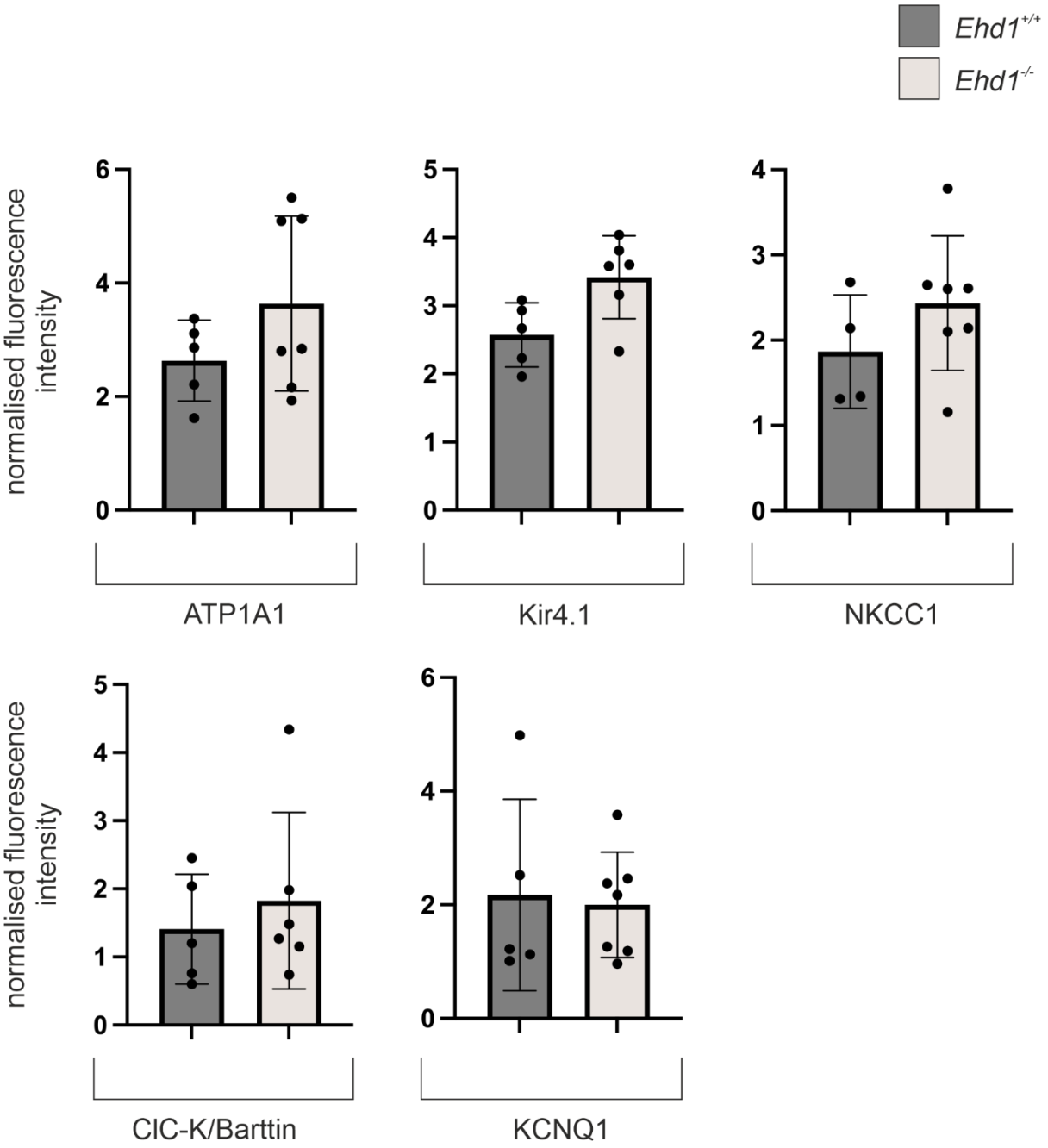

Figure 15 **Normalised fluorescence intensities of key player IF staining.** The fluorescence intensities of key player proteins of 5 *Ehd1*$^{+/+}$ and 7 *Ehd1*$^{-/-}$ animals normalised to fluorescence intensities of nuclear staining per section is shown. p-values ≤ 0.01 between groups were considered significant (Mann-Whitney-U test, Bonferroni corrected). Data are indicated as mean and SEM.

mRNA expression of key players

In addition to the immunofluorescence staining of key player proteins, their mRNA expression within the stria vascularis was measured via real-time PCR. *Ehd1*$^{+/+}$ and *Ehd1*$^{-/-}$ animals used for these experiments were three months and older. Primers were designed to detect genes of key players Na^+,K^+-ATPpase (*Atp1a1*), Kir4.1 (*Kcnj10*), NKCC1 (*Slc12a2*), Barttin (*Bsnd*), *Kcnq1* and *Ehd1*. No significant changes in mRNA expression of the genes tested could be found in *Ehd1*$^{-/-}$ animals compared to their wildtype litter mates (**Figure 16**). *Ehd1* gene expression was significantly lower but not fully diminished in *Ehd1*$^{-/-}$ striae due to the binding sites of the primers used.

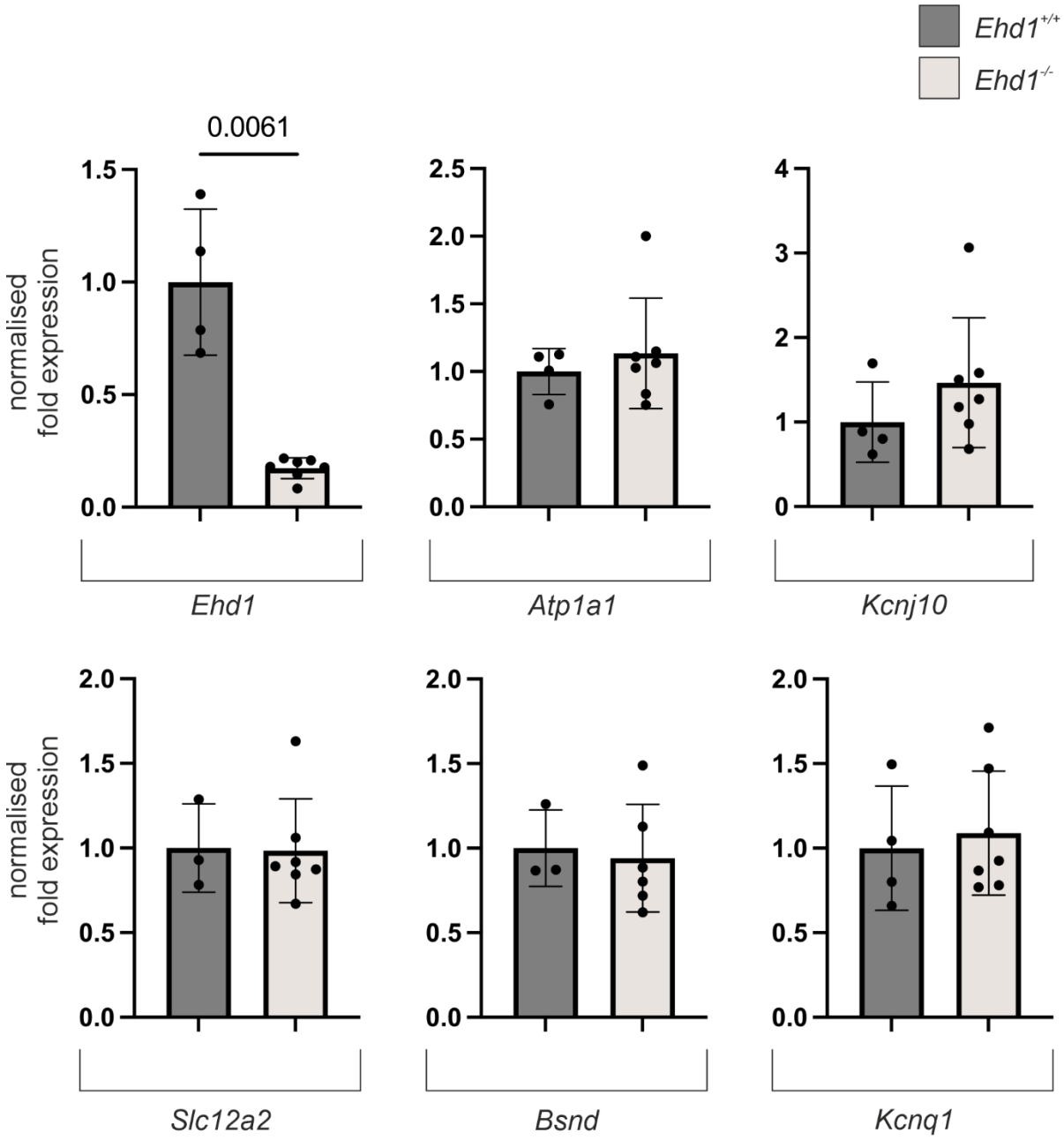

***Figure 16* mRNA expression of key player proteins within stria vascularis of *Ehd1*$^{+/+}$ and *Ehd1*$^{-/-}$ mice.** mRNA expression of EHD1 and key players in *Ehd1*$^{-/-}$ striae was normalised to their expression in stria vascularis of *Ehd1*$^{+/+}$ mice. n = 4 (EHD1$^{+/+}$) and n = 7 (EHD1$^{-/-}$). P-values ≤ 0.008 between groups are shown (Mann-Whitney-U test, Bonferroni corrected). Data are indicated as mean and SEM.

Morphological changes in mouse inner ear due to *Ehd1*$^{-/-}$

Various causes of sensorineural hearing loss have been shown to result in morphological changes within the inner ear such as the collapse of the Reissner's membrane, loss of hair cells and neuronal degeneration. [11, 40, 41, 64, 72, 135] In addition, characteristic morphological changes of the stria vascularis have been found and linked to deafness. [37, 64, 136, 137]. Therefore, possible morphological changes due to the absence of EHD1 have been investigated via imaging of Richardson staining sections as well as the analysis of transmission electron micrographs.

Morphology of overview images of murine cochleae

Possible morphological alterations in *Ehd1*$^{-/-}$ cochleae of eight-week-old mice were analysed using sections of Richardson staining of tissue destined for transmission electron microscopy. Besides visually analysing the sections for broad morphological changes such as hair cell degeneration, the widths of striae vascularis as well as the cell density and size of the endolymph-filled scalae media was measured. Therefore, middle turns of seven *Ehd1*$^{-/-}$ as well as six *Ehd1*$^{+/+}$ cochleae of mice aged six to ten weeks were analysed. To determine possible neuronal degeneration, the cell density within the spiral ganglion was assessed visually and by counting the number of neuronal cells present within a section of the cochlear middle turn. Visual analysis revealed a seemingly lower neuronal cell density in *Ehd1*$^{-/-}$ animals compared to their wildtype litter mates (**Figure 17**, **Figure 18**). Although quantitative analysis showed no significant changes in the number of neuronal cells due to the absence of EHD1, a trend towards lower cell counts in *Ehd1*$^{-/-}$ animals was detected (**Figure 19, B**). Depending on the underlying cause of SNHL, neuronal degeneration is often preceded by a considerate loss of hair cells. Although the Organ of Corti in both *Ehd1*$^{+/+}$ and *Ehd1*$^{-/-}$ animals seemed intact (**Figure 17**, **Figure 18**), a beginning degeneration of

hair cells cannot be detected by analysing overview cross-sections of cochleae. Thus, these data need to be considered with caution. As changes in endolymph composition can result in a change of volume and size of the scala media as well as a collapse of the Reissner's membrane, the area of the scala media of middle turns was analysed. The measurement revealed no significant changes in surface area (**Figure 19, A**) nor was a collapse of the Reissner's membrane found (**Figure 17**, **Figure 18**) due to the absence of EHD1. In addition, the average thickness of the stria vascularis was analysed by measuring the width of the stria vascularis in seven segments of each section. No significant changes in strial thickness could be found in *Ehd1*$^{-/-}$ animals compared to their wildtype litter mates (**Figure 19, C**).

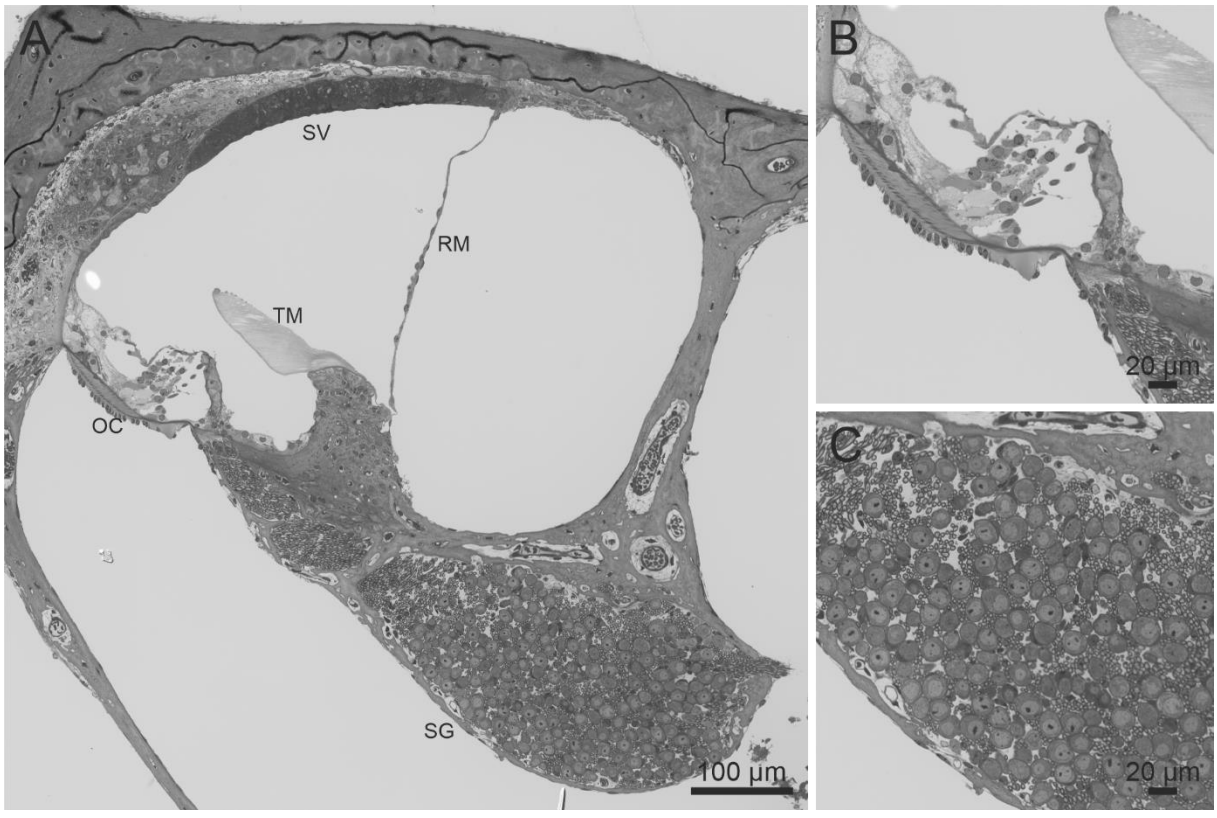

Figure 17 **Richardson staining of the cochlear middle turn of an *Ehd1*$^{+/+}$ mouse.** (A) Overview image of the cochlear middle turn with stria vascularis (SV), Organ of Corti (OC), Reissner's membrane (RM), tectorial membrane (TM) and spiral ganglion (SG). (B) Close-up section of the Organ of Corti with inner and outer hair cells. (C) Close-up section of the spiral ganglion.

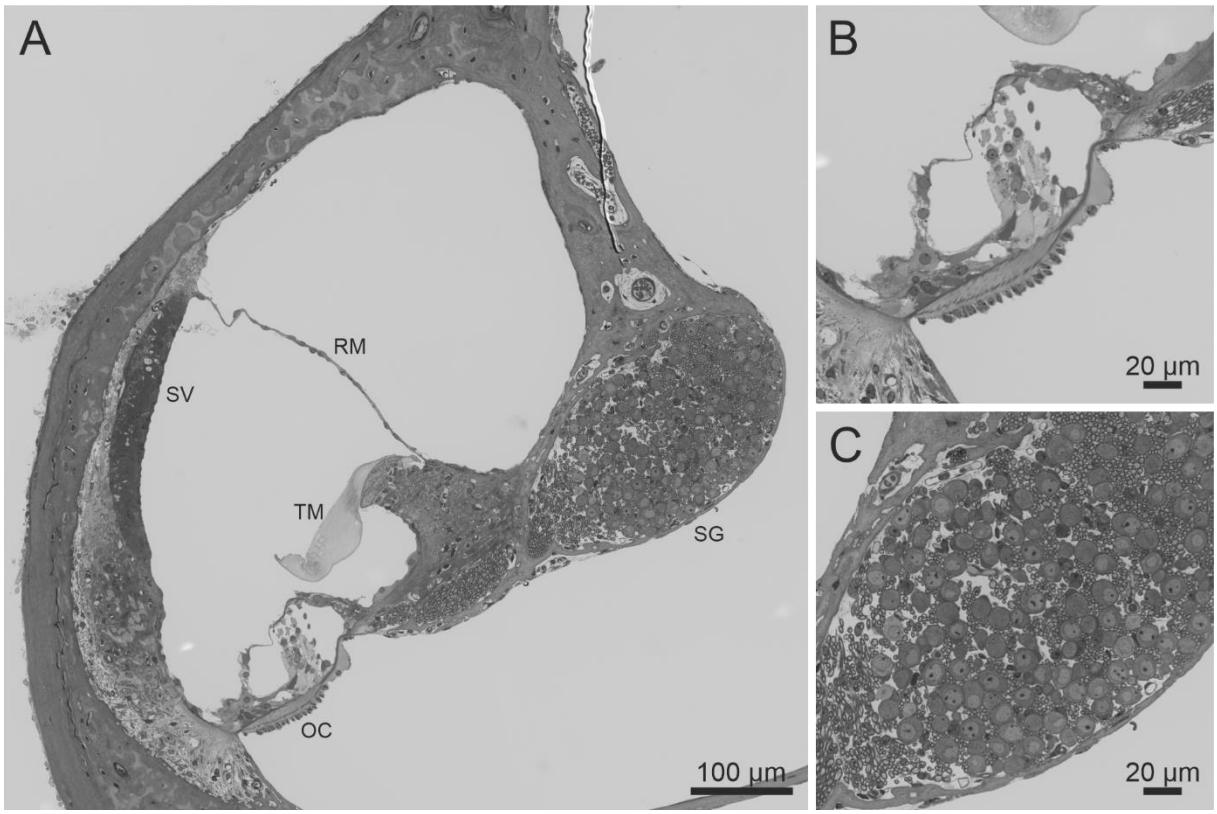

Figure 18 **Richardson staining of cochlear middle turn of an *Ehd1*$^{-/-}$ mouse**. (A) Overview image of the cochlear middle turn with stria vascularis (SV), Organ of Corti (OC), Reissner's membrane (RM), tectorial membrane (TM) and spiral ganglion (SG). (B) Close-up section of the Organ of Corti with inner and outer hair cells. (C) Close-up section of the spiral ganglion.

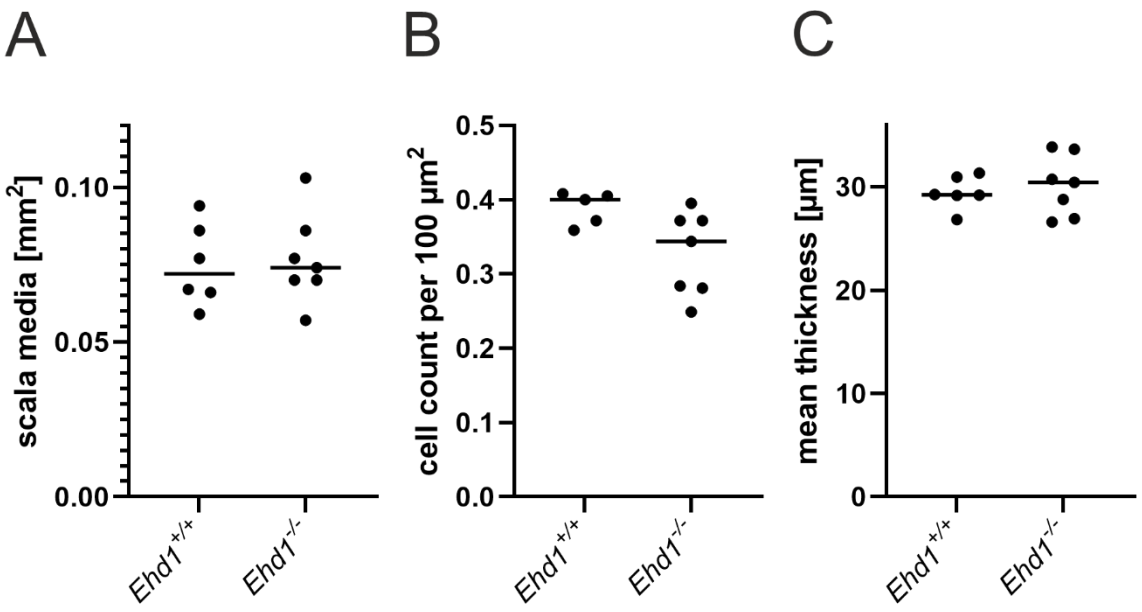

Figure 19 **Quantitative analysis of the morphology of *Ehd1*$^{+/+}$ and *Ehd1*$^{-/-}$ cochleae.** (A) Size of the scala media in mm^2. (B) Cell density of the spiral ganglion in cells per 100 µm^2. (C) Thickness of the stria vascularis in µm. n = 6 (*Ehd1*$^{+/+}$) and 7 (Ehd1$^{-/-}$). P-values ≤ 0.0167 between groups were considered significant (Mann-Whitney-U test, Bonferroni corrected). Mean values are indicated.

Transmission electron microscopy of the stria vascularis

To gain insight into possible morphological changes within the stria vascularis due to the absence of EHD1, transmission electron microscopic imaging of a total of 17 *Ehd1*$^{-/-}$ and 15 *Ehd1*$^{+/+}$ was performed. In addition, cochleae of one *Ehd1*^{R398W} animal were analysed to reveal possible similarities or differences between striae containing the mutated protein and those with or without wildtype EHD1. The morphological differences between the genotypes were distinguishable for most animals but nonetheless some animals presented with rather indistinct differences. Taken together, the main differences presented as follows. In stria vascularis of wildtype animals, the delicate membranes forming the interdigitations between marginal and intermediate cells as well as the mitochondrial cristae could be clearly identified (**Figure 20**). Both *Ehd1*$^{-/-}$ and *Ehd1*^{R398W} striae presented with diminished mitochondrial cristae as well as a deterioration of the characteristic intercellular spaces (**Figure 21**, **Figure 22**). In addition, *Ehd1*$^{-/-}$ striae presented with a noticeably higher proportion of diminished mitochondrial cristae as well as myelinated bodies.

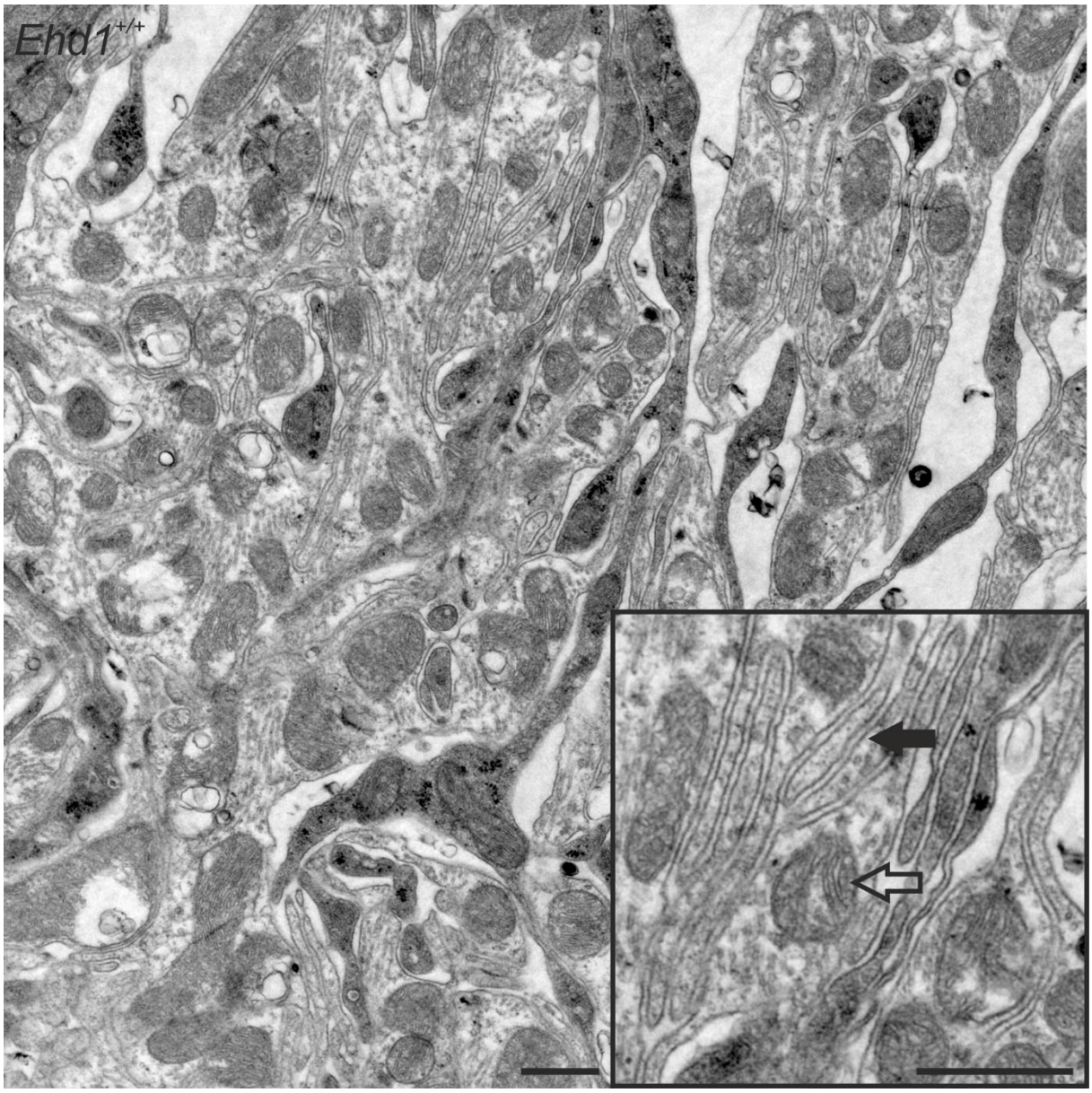

Figure 20 **Transmission electron micrograph of Ehd1$^{+/+}$ stria vascularis.** Characteristic interdigitations (filled arrow) between marginal and intermediate cells and mitochondrial cristae (open arrow) can be seen in striae of wildtype animals.

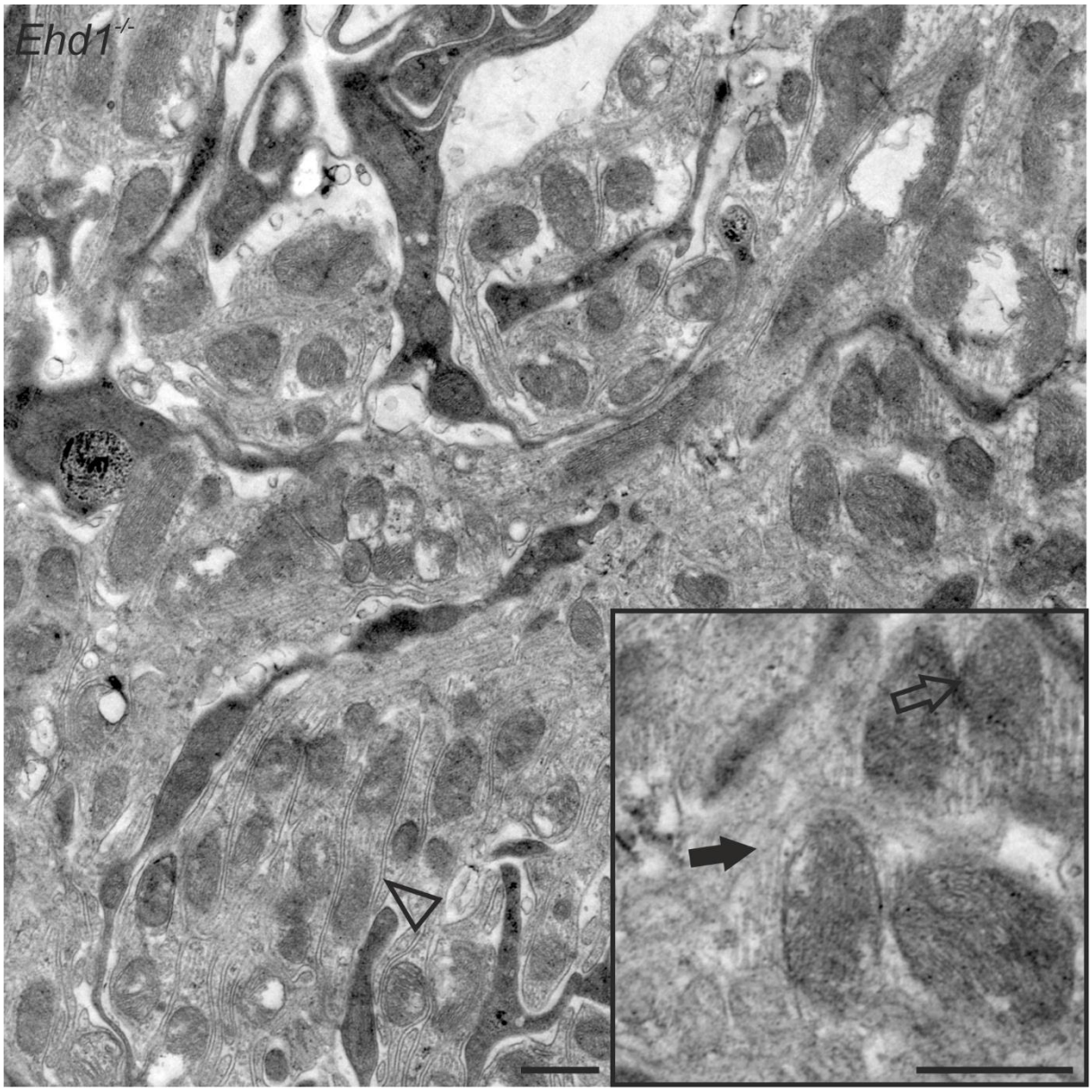

Figure 21 **Morphological consequences in stria vascularis of *Ehd1*$^{-/-}$ mice.** Absent or diminished mitochondrial cristae (open arrow) as well as a deterioration of interdigitations between marginal and intermediate cells (filled arrow) define striae vascularis of *Ehd1*$^{-/-}$ animals. Scarce areas of normal morphology (open arrowhead) guarantee focused images were generated. Scalebars 500 nm.

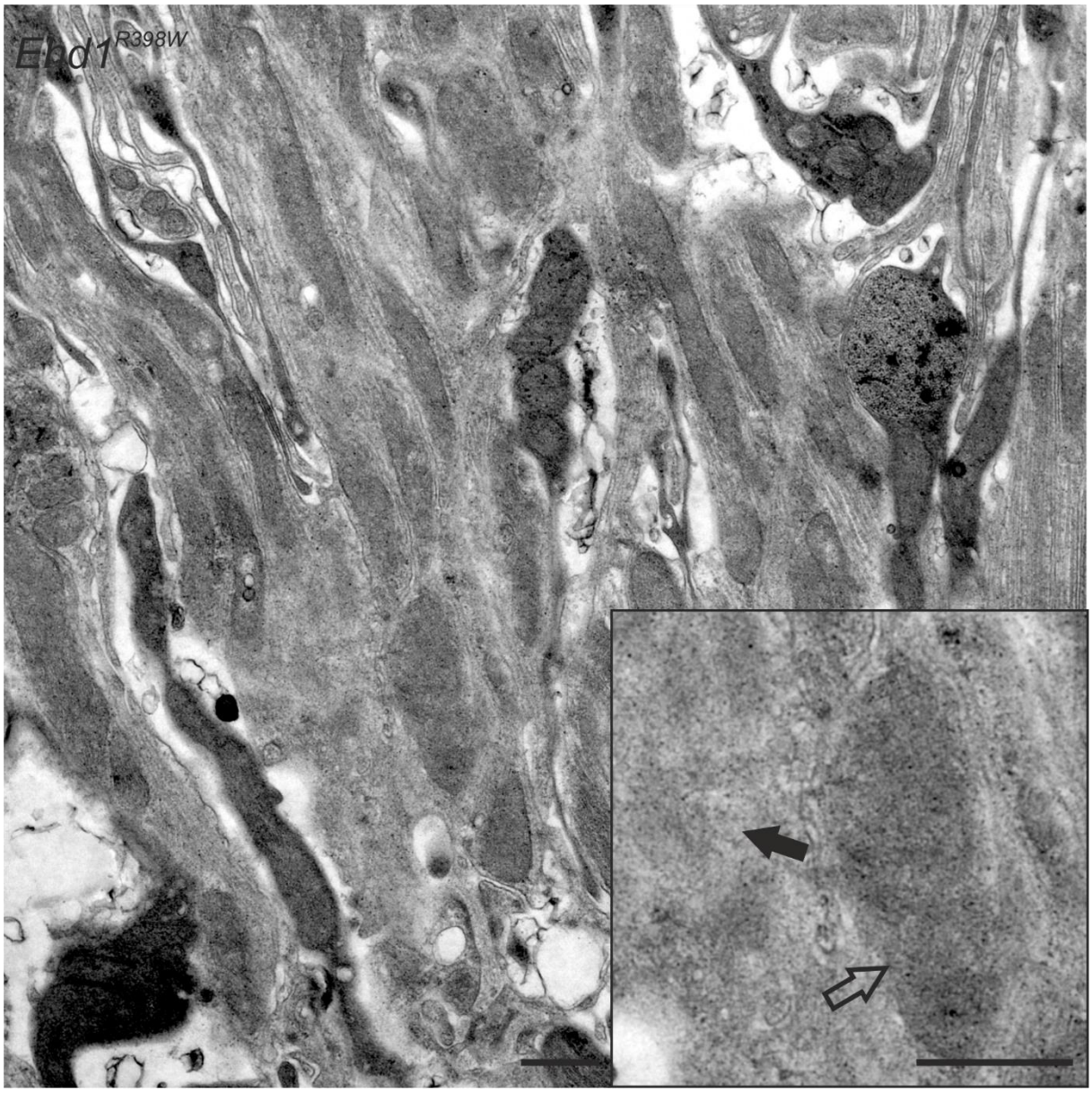

Figure 22 **Morphological consequences in stria vascularis of *Ehd1*^{R398W} mice.** Absent or diminished mitochondrial cristae (open arrow) as well as a deterioration of interdigitations between marginal and intermediate cells (filled arrow) define striae vascularis of *Ehd1*^{R398W} animals. Scalebars 500 nm.

Transcriptomics of stria vascularis

To identify pathways influenced by the loss of EHD1 within the strial unit, transcriptome analysis of stria vascularis of *Ehd1*$^{-/-}$ and their wildtype litter mates was carried out via GeneChip™ microarray assay. The significant downregulation of *Ehd1* in *Ehd1*$^{-/-}$ compared to *Ehd1*$^{+/+}$ striae confirmed the genotypes of animals used for the experiment. (**Table 2**) As exon 2 of *Ehd1* is missing in *Ehd1*$^{-/-}$ mice, low detection of other fragments of *Ehd1* mRNA was to be expected in those animals. Due to the functions and biological pathways allocated to EHD1 and the SNHL of patients as well as *Ehd1*$^{-/-}$ and *Ehd1*^{R398W} mice, the dataset was examined regarding significant differences in the expression of genes involved in said pathways. Thus, genes encoding for proteins involved in endocytic recycling as well as known binding partners and cargo of EHD1 were analysed. In addition, key player proteins of strial K^+ cycling as well as SNHL genes were examined regarding their significant representation within the dataset. No genes identified to cause SNHL were significantly regulated in *Ehd1*$^{-/-}$ striae compared to their wildtype litter mates. Similarly, no matches were found for genes encoding for key players in K^+ cycling, endocytosis and genes related to EHD1. Instead, 29 genes with no known link to any of the pathways named above have been identified to be significantly regulated within the strial unit. Predominantly, they're related to immune response and inflammatory pathways (**Table 2**).

Table 2

Significantly regulated genes in Ehd1$^{-/-}$ stria vascularis

Gene description	Gene symbol	Log2 fold change	P-value
Phosphatidylserine decarboxylase, pseudogene 3	*Pisd-ps3*	-13,32	2,44743E-08
Interferon regulatory factor 7	*Irf7*	-6,26	0,023570393
Interferon-induced protein 44	*Ifi44*	-5,62	0,000433716
Bone marrow stromal cell antigen 2	*Bst2*	-4,50	0,0034961
Tripartite motif-containing 30A	*Trim30a*	-4,41	0,001039188
Gene description	Gene symbol	Log2 fold change	P-value
Predicted gene 12185	*Gm12185*	-3,98	0,00784196
Interferon, alpha-inducible protein 27 like 2A	*Ifi27l2a*	-3,42	0,003879627
2-5 oligoadenylate synthetase 1G	*Oas1g*	-3,15	0,000633658
T cell specific GTPase 2	*Tgtp2*	-3,12	0,046429293
2-5 oligoadenylate synthetase 1A	*Oas1a*	-2,99	0,008899595
PHD finger protein 11D	*Phf11d*	-2,74	0,022193
Galectin 3 binding protein	*Lgals3bp*	-2,73	0,027920193
Proteasome subunit, β type 8	*Psmb8*	-2,71	0,002132779
EH-domain containing 1	*Ehd1*	2,50	4,7765E-05
ISG15 ubiquitin-like modifier	*Isg15*	-2,46	0,029611232
Receptor transporter protein 4	*Rtp4*	-2,43	0,004907031
Leucine-rich repeats and guanylate kinase domain containing	*Lrguk*	2,30	0,013538235
interferon regulatory factor 9	*Irf9*	-2,22	0,012233039
Chemokine ligand 13	*Cxcl13*	-2,19	0,023109796
Guanylate binding protein 4	*Gbp4*	-2,19	0,007789443
Tumor-associated calcium signal transducer 2	*Tacstd2*	2,16	0,042868863
ubiquitin specific peptidase 18	*Usp18*	-2,15	0,028312176
2-5 oligoadenylate synthetase-like 2	*Oasl2*	-2,11	0,004491729
Interferon induced with helicase C domain 1	*Ifih1*	-2,11	0,002382763
Secretoglobin family 2A member 2-like	*LOC102639117*	-2,06	0,008933328
Poly (ADP-ribose) polymerase family member 12	*Parp12*	-2,02	0,001003373
myosin light chain 1	*Myl1*	2,02	0,029980428
Guanylate-binding protein 10	*Gbp10*	-2,01	0,025537797
DEXH-box helicase 58	*Dhx58*	-2,00	0,035472748
Hermansky-Pudlak syndrome 4 homolog	*Hps4*	2,00	0,009191014

Significantly regulated genes in Ehd1$^{+/+}$ striae compared to Ehd1$^{-/-}$ animals. Fold changes and unadjusted p-values of Ehd1$^{+/+}$ versus Ehd1$^{-/-}$ are shown.

Proteomics of stria vascularis

To gain insight into pathways and identify single proteins affected by the absence of EHD1 within the strial unit, striae vascularis of *Ehd1*$^{-/-}$ mice, their wildtype litter mates, and unrelated SV129 control animals (Charles River) were subjected to proteome analysis. The absence of intact EHD1 protein in tissue of *Ehd1*$^{-/-}$ animals was confirmed by position mapping of peptides allocated to EHD1. There, peptides within exon 2 of the protein could not be detected in *Ehd1*$^{-/-}$ striae, whereas their availability in corresponding *Ehd1*$^{+/+}$ and control tissue was verified (**Figure 23**).

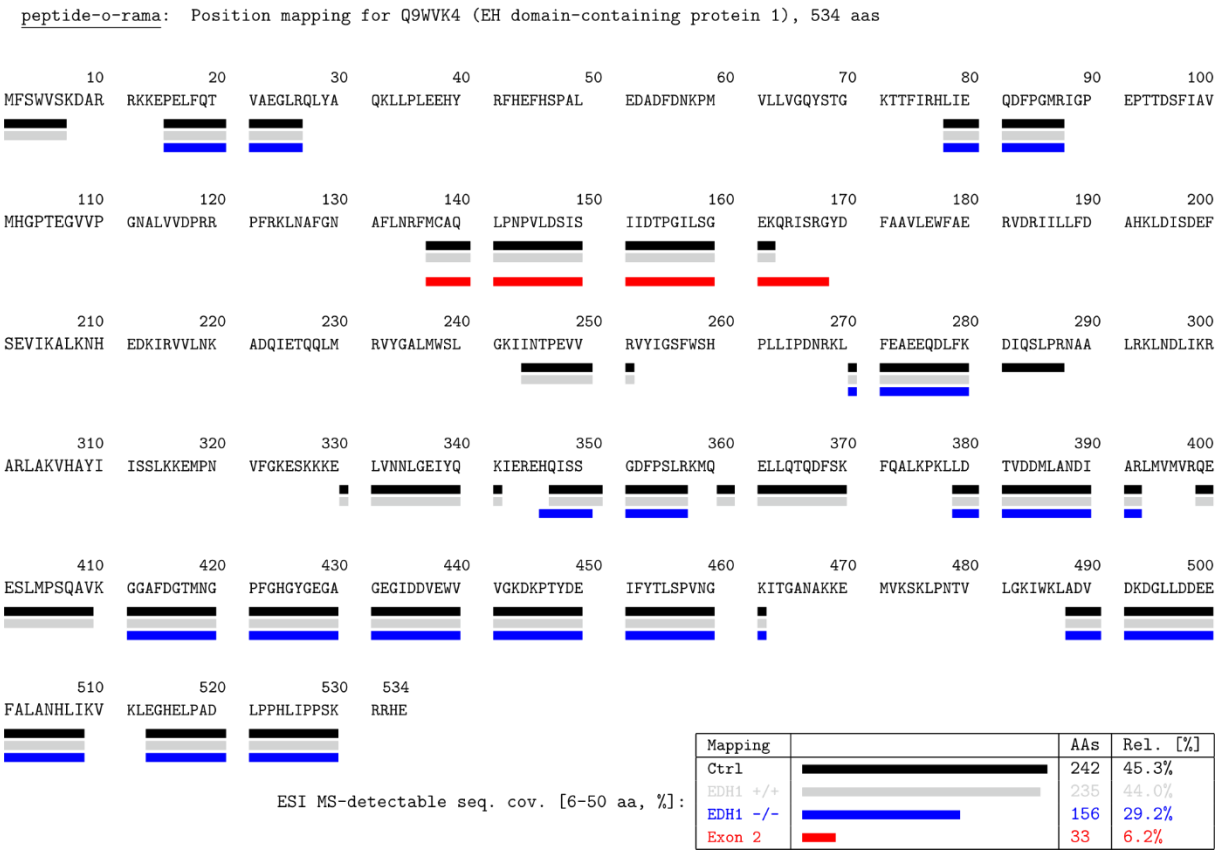

***Figure 23* Position mapping for peptides of EHD1.** Shown are peptides of EHD1 found in *Ehd1*$^{+/+}$ (grey), *Ehd1*$^{-/-}$ (blue) and unrelated control animals of SV129 background (Charles River) (black). Peptides of exon 2 of the protein are highlighted in red.

Similar to the approach described in *Transcriptomics of stria vascularis*, proteins involved in SNHL, strial K^+ cycling, endocytosis and proteins interacting with EHD1 have been analysed regarding a possible up- or downregulation due to the loss of EHD1. None of the key players in strial K^+ cycling identified so far were significantly affected by the loss of EHD1 (**Figure 24**). Three proteins with known SNHL gene mutations were found to be significantly altered in *Ehd1*$^{-/-}$ striae compared to *Ehd1*$^{+/+}$ tissue. (**Table 3**)

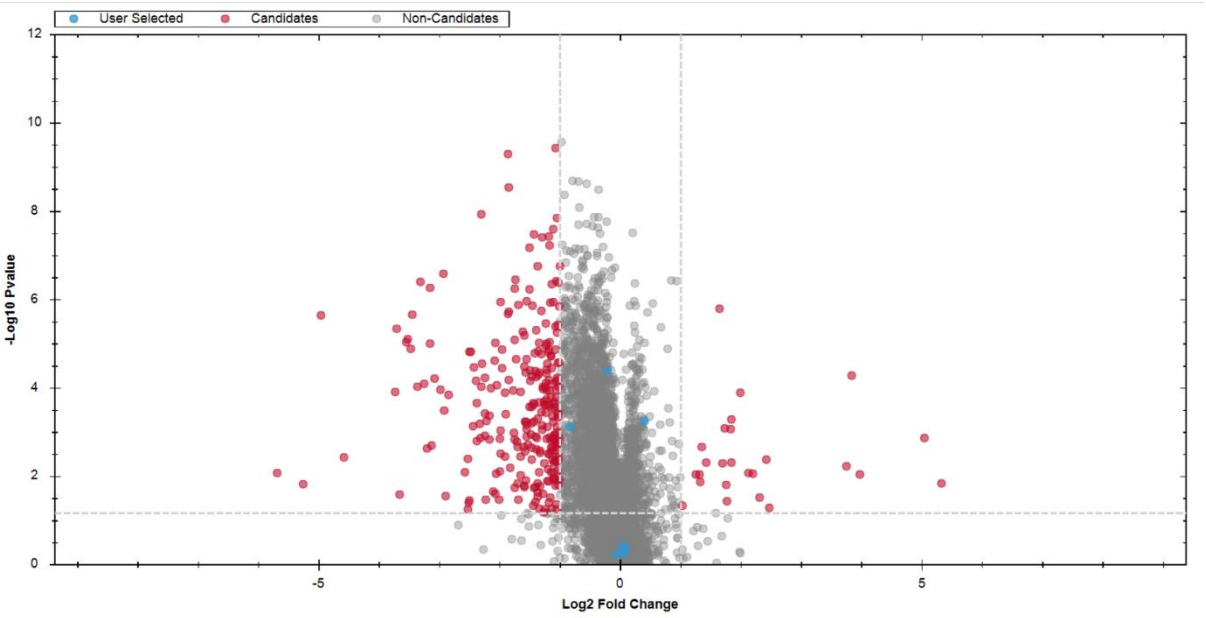

Figure 24 **Volcano plot of *Ehd1*$^{+/+}$ versus *Ehd1*$^{-/-}$ samples.** Significant (red) and non-significant (grey) proteins are shown. Marked in blue are key player proteins ATP1A1, Kir4.1, KCNQ1, NKCC1 and Barttin subunits BSND, CLCKA and CLCKB.

Table 3

Significantly altered SNHL-related proteins

Protein name	Gene symbol	Log2 fold change	P-value
Collagen alpha-1(XI) chain	*Col11a1*	-1,43	0,0006
Gap junction alpha-1 protein	*Gja1*	-1,38	0,0014
Collagen alpha-1(II) chain	*Col2a1*	-1,06	0,0018

SNHL genes with significant differences in protein expression in Ehd1$^{+/+}$ *striae compared to Ehd1*$^{-/-}$ *animals. Average Log2 ratios and adjusted p-values of Ehd1*$^{+/+}$ *versus Ehd1*$^{-/-}$ *are shown.*

While no binding partners of EHD1 were influenced within the stria vascularis due to the loss of EHD1, a significant increase in glucose transporter type 4 (GLUT4) expression in *Ehd1*$^{-/-}$ striae was detected. (**Table 4**)

Table 4
Significantly altered EHD1-related proteins

Protein name	Gene symbol	Log2 fold change	P-value
Glucose transporter type 4	*Slc2a4*	-1,05	0,0022
Gap junction alpha-1 protein	*Gja1*	-1,38	0,0014

Known cargo proteins of EHD1 with significant differences in protein expression in Ehd1$^{+/+}$ *striae compared to Ehd1*$^{-/-}$ *animals. Average Log2 ratios and adjusted p-values of Ehd1*$^{+/+}$ *versus Ehd1*$^{-/-}$ *are shown*.

Data was analysed regarding endocytic recycling, including components of the retromer complex and proteins involved in membrane fusion as well as proteins involved in endocytic pathways in general. No significant changes could be found due to the loss of EHD1 except for one protein previously linked to the trans-Golgi network (**Table 5**). [138]

Table 5
Significantly altered endocytic proteins

Protein name	Gene symbol	Log2 fold change	P-value
RAB6-interacting golgin	*Gorab*	-1,02	0,0036

Proteins involved in endocytosis with significant differences in protein expression in Ehd1$^{+/+}$ *striae compared to Ehd1*$^{-/-}$ *animals. Average Log2 ratios and adjusted p-values of Ehd1*$^{+/+}$ *versus Ehd1*$^{-/-}$ *are shown.*

In addition to the analysis targeting SNHL, strial key players and EHD1-related proteins and pathways, the thirty most up- or down-regulated proteins due to the loss of EHD1 are listed in **Table 6**. There, expression of proteins involved in cell contractility, as well as inflammatory processes, autophagy, mitochondrial metabolism, protein synthesis and trafficking pathways were altered. (**Table 6**)

Table 6

Top 30 of proteins with highest overall log2 fold changes

Protein name	Gene symbol	Log2 fold change	P-value
Keratin, type II cytoskeletal 2 oral	*Krt76*	5,05	0,0014
Myosin-4	*Myh4*	-4,97	2,2946E-06
Lys-63-specific deubiquitinase BRCC36	*Brcc3*	-4,58	0,0038
Keratin, type I cuticular Ha3-I	*Krt33a*	3,84	5,3486E-05
L-aminoadipate-semialdehyde dehydrogenase-phosphopantetheinyl transferase	*Aasdhppt*	3,75	0,0060
Coiled-coil-helix-coiled-coil-helix domain-containing protein 7	*Chchd7*	-3,72	0,0001
Myosin regulatory light chain 2, skeletal muscle isoform	*Mylpf*	-3,70	4,6246E-06
Myomesin 2	*Myom2*	-3,54	9,126E-06
Myosin light chain 1/3, skeletal muscle isoform	*Myl1*	-3,52	8,0059E-06
Myosin-1	*Myh1*	-3,47	1,3105E-05
Tropomyosin β chain	*Tpm2*	-3,44	2,1533E-06
Myozenin-1	*Myoz1*	-3,37	9,5292E-05
Myosin light chain 3	*Myl3*	-3,31	4,0321E-07
Alpha-actinin-3	*Actn3*	-3,24	7,9316E-05
Myosin regulatory light chain 2, ventricular/cardiac muscle isoform	*Myl2*	-3,21	0,0024
Myomesin-1	*Myom1*	-3,15	9,8291E-06
CtBP-interacting BTB zinc finger protein	*Zbtb38*	-3,15	5,5071E-07
Keratin, type I cytoskeletal 15	*Krt15*	-3,13	0,0020
SH3 domain-containing protein	*Neb*	-3,08	6,2595E-05
Reticulon-2	*Rtn2*	-2,98	0,0001
40S ribosomal protein S5	*Rps5*	-2,93	2,5626E-07
Dynactin subunit 6	*Dctn6*	-2,92	0,0003
Troponin C, skeletal muscle	*Tnnc2*	-2,84	0,0001
Glial fibrillary acidic protein	*Gfap*	-2,52	0,0040
Kelch-like protein 41	*Klhl41*	-2,50	1,5239E-05
Calsequestrin-1	*Casq1*	-2,48	1,5069E-05
LIM domain-binding protein 3	*Ldb3*	-2,44	0,0007
EH domain-containing protein 1	*Ehd1*	2,43	0,0042
Troponin I, fast skeletal muscle	*Tnni2*	-2,42	3,4088E-05
Myosin-binding protein C, fast-type	*Mybpc2*	-2,39	7,0242E-05

Top 30 proteins with highest log2 fold change in $Ehd1^{+/+}$ striae compared to $Ehd1^{-/-}$ animals. Average Log2 ratios and adjusted p-values of $Ehd1^{+/+}$ versus $Ehd1^{-/-}$ are shown.

In addition to EHD1, two other proteins presented with significantly altered expressions while also showing significantly altered gene expression in transcriptome analysis (**Table 7**).

Table 7

Significantly altered genes in both proteome and transcriptome analysis

	transcriptomics		proteomics	
Gene symbol	Log2 fold change	P-value	Log2 fold change	P-value
Ehd1	2,50	4,7765E-05	2,43	0,004247699
Ifi44	-5,62	0,000433716	-1,44	0,000221773
Myl1	2,02	0,029980428	-3,52	8,00586E-06

Significantly regulated genes and proteins in Ehd1$^{+/+}$ compared to Ehd1$^{-/-}$ stria vascularis. Log2 fold changes and p-values of gene regulation as well as log2 fold changes and adjusted p-values of protein expression in Ehd1$^{+/+}$ versus Ehd1$^{-/-}$ are shown

A full list of proteins significantly altered due to the absence of EHD1 can be found in Supplements (**Table 8**).

Protein uptake in stria vascularis

Due to the well-known role of EHD1 in endocytosis [99], a method to determine possible EHD1-dependent protein uptake by strial marginal cells was established. Whole-mounted striae of *Ehd1*$^{+/+}$ animals were used to demonstrate the uptake of fluorescently labelled β_2-microglobulin. Immunofluorescent staining of Kcnq1 enabled the visualisation of marginal cells and showed a co-localisation of absorbed β_2-microglobulin with said cell population, accumulating in distinct vesicle-like structures (**Figure 25**).

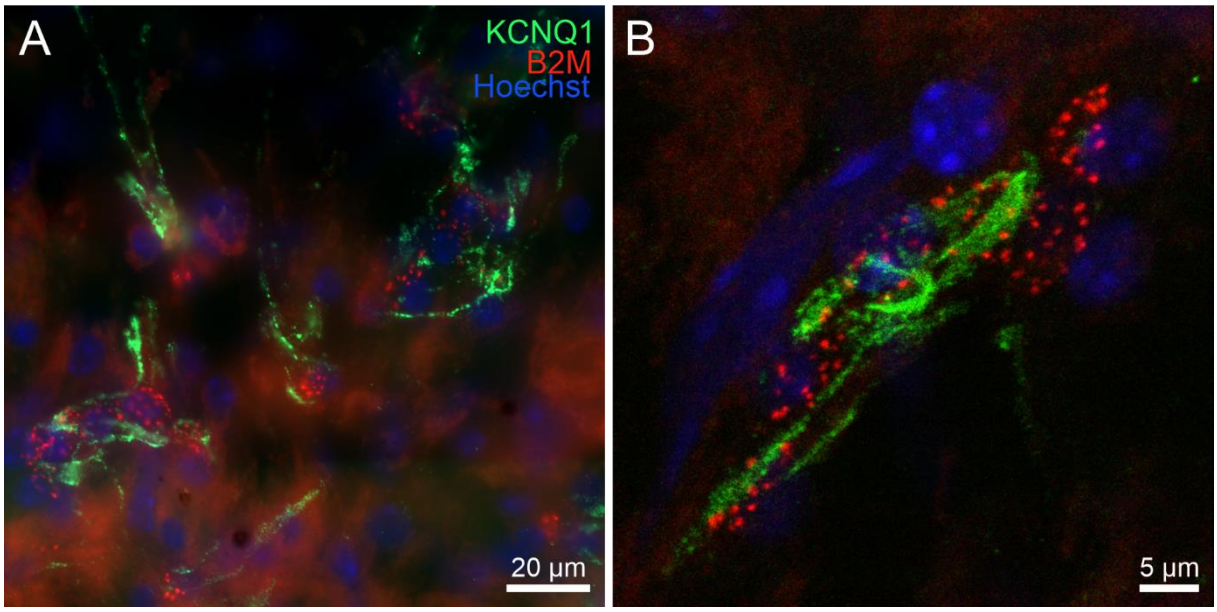

Figure 25 **Protein uptake in *Ehd1*$^{+/+}$ stria vascularis.** (A) Shown is the absorption of fluorescently labelled β_2-microglobulin (B2M; red) in whole-mounted stria vascularis. B2M co-localises with KCNQ1 positive marginal cells (green). Nuclear staining (blue). (B) A close-up of the same tissue reveals B2M staining of distinct vesicle-like structures. Nuclear staining is depicted in blue.

Whole mount cochleae

For analysis of possible hair cell damage due to the knockout of *Ehd1*, the preparation of whole cochleae and subsequent mounting of whole cochlear turns was established. The dissection of whole cochleae without damaging the delicate hair cells, the separation of each turn as well as the staining process and mounting of the turns was developed successfully. (**Figure 26)**. Hair cell damage can be visualised by immunofluorescent staining of phalloidin, a protein present in stereocilia of hair cells. Both *Ehd1*$^{+/+}$ and *Ehd1*$^{-/-}$ cochleae were stained successfully. (**Figure 26**, **D, E**) However, the number of experiments run was insufficient to assess possible differences between the two genotypes.

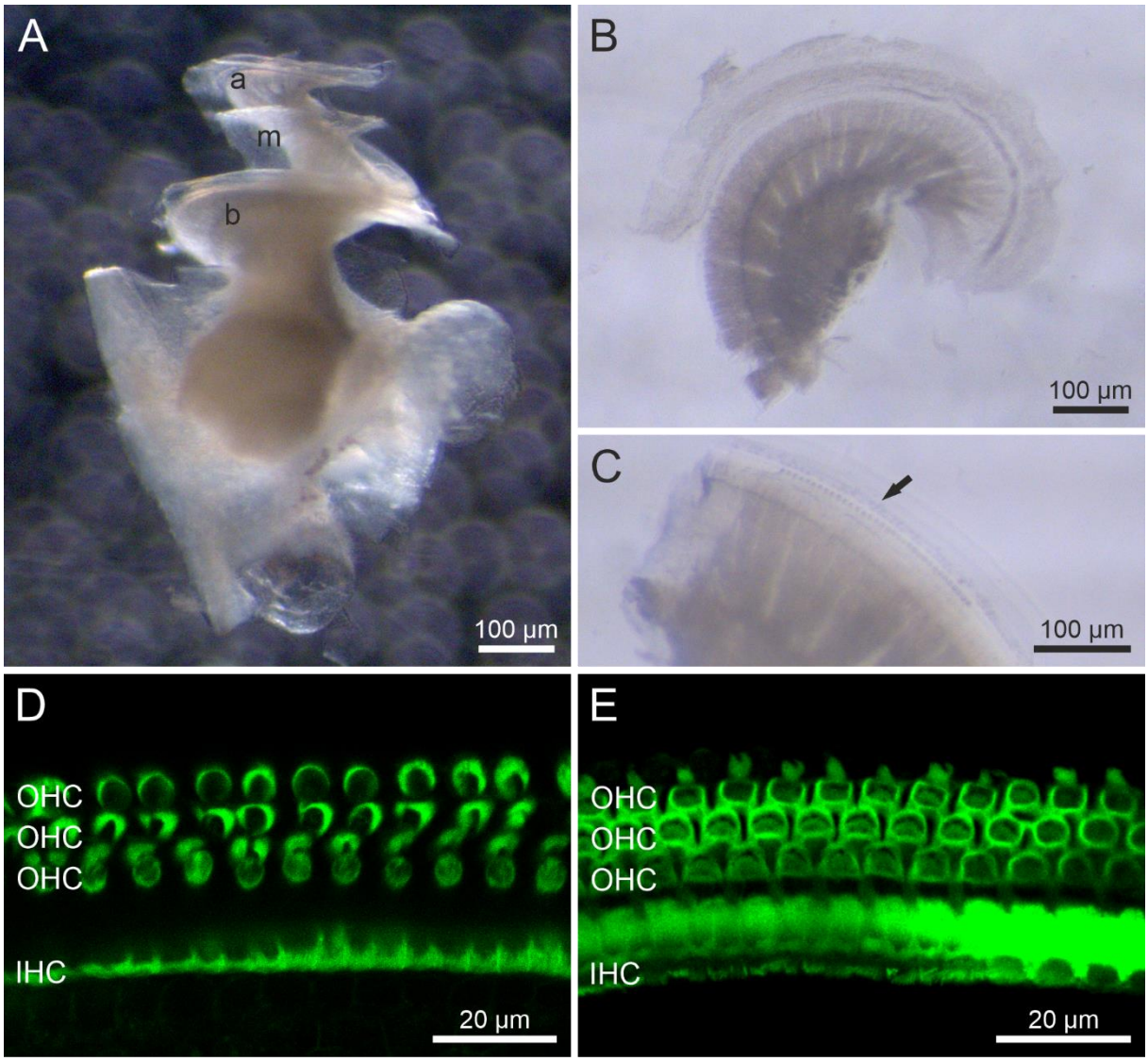

***Figure 26* Establishment of whole mounted cochlear turns.** (A) Dissected murine cochlea with the apical (a), middle (m), and basal (b) cochlear turns typically seen in mice. (B) Separated middle turn of murine cochlea. (C) Separated middle turn with three rows of outer and one row of inner hair cells (arrow). (D) Phalloidin staining (green) of *Ehd1*$^{+/+}$ Organ of Corti with outer hair cells (OHC) and inner hair cells (IHC). (E) Phalloidin staining (green) of *Ehd1*$^{-/-}$ Organ of Corti with OHC and IHC.

Discussion

This doctorate aimed to investigate the pathophysiology of hearing impairment related to EHD1 – a protein known to be involved in endocytic recycling. Therefore, the localisation of EHD1 within the murine inner ear had to be uncovered and effects on cochlear functioning due to the loss of EHD1 were examined.

Localisation of EHD1 in the murine cochlea

The localisation of EHD1 in the murine cochlea was investigated via anti-EHD1, anti-β-galactosidase IF staining as well as X-Gal staining.

IF staining against EHD1 and β-galactosidase as well as X-Gal staining of *Ehd1*$^{+/+}$ and *Ehd1*$^{-/-}$ mice indicated the presence of EHD1 mainly within the stria vascularis. In addition, type II fibrocytes of the spiral ligament seemed to express EHD1 to some extent. As the spiral ganglion neurons, tectorial membrane and IHC of *Ehd1*$^{-/-}$ animals also stained positive for EHD1, these results are most likely caused by unspecific staining of the anti-EHD1 antibody. This might – at least to some extent – be due to the structural similarity of the EHD proteins [139-141], causing the anti-EHD1 antibody to bind to other EHDs present within the cochlea in addition to its main target. RNAseq data obtained from the gEAR database [102] (Supplements **Figure 27** and **Figure 28**) suggested the presence of EHD3 within the spiral ganglion cells as well as IHCs of adult mice. [142, 143] In addition, single cell RNAseq data suggested EHD3 and EHD4 expression within the stria vascularis of adult mice. [102, 103] *Ehd1* mRNA was found throughout different cell populations of stria vascularis and the spiral ligament, which is consistent with staining results. These results suggest the unspecific binding of anti-EHD1 antibody to EHD3 and possibly also EHD4 in IHC and the spiral ganglion. IF staining of β-galactosidase and X-gal staining of *Ehd1*$^{-/-}$ cochleae confirmed, however,

the presence of EHD1 within the stria vascularis and its absence in IHCs, tectorial membrane and the spiral ganglion. Interestingly, type II fibrocytes of the spiral ligament stained positive via X-gal staining but remained unstained in IF staining of β-galactosidase.

Taken together, EHD1 seems to be localised mainly in the stria vascularis of the murine cochlea, subsequently leading to a thorough investigation of this tissue and its functional properties.

Assessment of effects on hearing capability due to loss of EHD1

To assess the functionality of EHD1 within the inner ear, its impact on hearing capability in mice was examined via f-ABR measurements.

As mentioned in the introductory section *EHD1 mutation R398W*, patients presenting with SNHL due to the *EHD1*^{R398W} mutation show hearing loss in the high frequency range. Therefore, f-ABR measurements of mice also carrying the mutation were conducted before this doctorate and showed hearing impairment in *Ehd1*^{R398W} animals compared to their wildtype litter mates in the moderate and high frequency range. [98] Most importantly, those mice were of a mixed BL6 and 129/SV background. *Ehd1*$^{-/-}$ mice were also examined regarding their hearing capability as they were used for this doctorate to investigate the role of EHD1 within the inner ear. It was crucial, therefore, to know whether those animals also showed hearing impairment due to the absence of EHD1. Before this doctorate, f-ABR measurements of *Ehd1*$^{-/-}$ animals of mixed genetic background showed a tendency of hearing loss in the high frequency range. Since then, mice had been backcrossed to a 129/SV background. Those animals presented with significant hearing impairment in the low and intermediate frequency range compared to their wildtype litter mates. Surprisingly, even the wildtype mice

showed severe hearing loss in the high frequency range alongside their *Ehd1*$^{-/-}$ litter mates when looking at data obtained by [144]. In this study, Zheng et al. assessed the hearing of 80 mice strains, including four 129-related strains. While young *Ehd1*$^{+/+}$ animals showed complete loss of hearing at 32 kHz, SV129 sub-strains observed by [144] presented with slightly elevated ABR thresholds at a young age which progressed to intermediate or severe hearing loss over time. The severe hearing loss found in young *Ehd1*$^{+/+}$ animals used for this thesis confirms the concerns about using SV129 sub-strains to study hearing impairment (**Figure 12**). It must be kept in mind that due to the mouse strain itself, any results can be confounded in their effect size and thus, must be interpreted most carefully. To avoid a presbycusis-related confounding of results, a different mouse lineage should be used for further investigations. For example, CBA/CaJ mice are often used in hearing research, as they show a consistently good hearing ability throughout different ages. [144]

Overall, the model used in this study isn't ideal for studying the influence of EHD1 on the process of hearing and results obtained should be reviewed using an appropriate mouse strain. Nevertheless, *Ehd1*$^{-/-}$ mice presented with a significantly elevated threshold in low and moderate frequency ranges compared to their wildtype litter mates, confirming EHD1's impact on their capability to hear.

Morphological changes due to the absence of EHD1

Due to its localisation within the stria vascularis and the hearing loss occurring due to its absence, EHD1 might contribute to the generation of the EP and / or the composition of the endolymph. Thus, the absence of EHD1 would eventually cause hair cell damage and neuronal degeneration, leading to hearing loss as seen in patients and mice. Therefore, the morphology of the cochlear duct needed to be investigated more closely. In some cases, changes in endolymph composition and EP have been

reported to cause certain morphological changes such as a collapse of the Reissner's membrane [64, 145] or a change in the thickness of the stria vascularis [146]. In addition, progressive hearing loss due to changes in EP or endolymph ultimately leads to the degeneration of hair cells, and the spiral ganglion neurons. Hypothesising that the absence of EHD1 does, indeed, lead to changes in endolymph composition and / or the EP, morphological changes of the scales mentioned above could be present and were, therefore, evaluated. Therefore, Richardson staining sections were analysed. Given the localisation of EHD1 within the stria vascularis, this tissue was also studied by electron microscopy.

Richardson staining sections of cochleae destined for electron microscopy revealed no major changes in strial thickness or a collapse of the Reissner's membrane due to fluid pressure within the scala vestibuli (**Figure 17**, **Figure 18**). In addition, no changes within the spiral ganglion or the Organ of Corti were found in *Ehd1*$^{-/-}$ animals. Electron micrographs revealed a disturbed morphology of the strial unit in mice lacking EHD1. There, interdigitations between marginal and intermediate cells were diminished and mitochondrial cristae presented blurred or absent. Most wildtype mice presented with clearly defined interdigitations, and a normal morphology of mitochondria was observed. Some wildtype animals, however, also showed signs of degeneration as seen in *Ehd1*$^{-/-}$ animals.

The disturbed morphology of *Ehd1*$^{-/-}$ striae observed via transmission electron microscopy indicates functional disruption of the strial unit and, thus, changes in EP and / or endolymph composition are likely. Even though no degeneration of the spiral ganglion could be quantified in 8-week-old animals, this doesn't rule out neuronal degeneration in general. Depending on the cause of hearing loss, hair cell damage can precede neuronal degeneration. Thus, possible neuronal damage might not be as

pronounced yet as to be quantifiable. This assumption inevitably needs to be verified by quantification of hair cell damage. As demonstrated above, the method of whole mount IF staining of cochlear hair cells via Phalloidin has been established and can be used to further investigate hair cell damage due to the absence of EHD1 (**Figure 26**). In addition, the ion composition of the endolymph as well as measurements of the EP should be obtained. However, special expertise and equipment are required for this and access to those proved to be difficult. The – in hindsight - rather unfortunately chosen mouse strain used for this study could also explain why no difference in neuronal cell count was found. As seen in f-ABR measurements and described by Zheng et al.[144] SV129 mouse lineages tend to present with presbycusis at an early age. Therefore, wildtype animals might show similar neuronal degeneration as EHD1$^{-/-}$ mice. In addition, the heterogeneity observed in strial morphology is probably also a result of the confounding effects of the sub-strain of mice used for this study. Indeed, age-related degeneration of the stria vascularis has been observed besides a decrease in hair cell survival and elevated ABR thresholds. [23, 147, 148] The early-onset presbycusis in wildtype animals can therefore explain the beginning degeneration of the stria vascularis seen in some wildtype animals, making it difficult to assess the characteristics of the *Ehd1*$^{-/-}$ phenotype. However, most *Ehd1*$^{-/-}$ striae observed via electron microscopy were clearly distinguishable from their wildtype litter mates as the degeneration observed was much more progressed in those animals. Thus, the morphological findings described above do not diminish the likelihood of changes in EP and / or the endolymph itself. In fact, the localisation of EHD1 along with the degeneration witnessed in electron micrographs of the stria vascularis rather substantiate the likelihood of downstream damage to hair cells and spiral ganglion neurons. The observed phenotype of stria vascularis in the absence of EHD1 strongly hints towards functional disruption of the strial unit. Disrupted mitochondria of the

marginal cells along with signs of cell death of intermediate cells indicate the involvement of the stria vascularis as a whole, rather than just one cell type (**Figure 20**, **Figure 21**, **Figure 22**). The mitochondrial phenotype especially demonstrates the severity of functional limitations arising from the absence of EHD1. Thus, it is highly unlikely that the stria vascularis can still operate to the extent of upholding the EP and fulfilling the task of undisrupted K+ cycling and EP generation. A definitive proof of altered endolymph composition and EP, however, can only be rendered by measuring the EP and ion composition within the endolymph. The quantification of hair cell damage via whole-mounted cochleae is more approachable and might substantiate the matter, even though it doesn't provide with definitive evidence for endolymph alterations.

Functional properties of EHD1-related hearing loss

To further investigate the functional properties of EHD1-related hearing loss, proteome, and transcriptome analyses as well as IF staining of key player proteins of the stria vascularis were conducted and interpreted in conjunction with the findings described above.

Disruption of the endocytic machinery of marginal cells

When hypothesising about the pathophysiology of *Ehd1*$^{-/-}$ within the stria vascularis, EHD1s known role in endocytic recycling comes to mind. Thus, the loss of EHD1 might lead to a disruption of the endocytic machinery within the stria vascularis which might lead to the observed phenotype in human and mouse. Xgal staining as well as anti-beta galactosidase IF staining suggested EHD1 to be localised mainly in marginal cells of the stria vascularis (**Figure 10**, **Figure 11**). As these epithelial cells border the cochlear duct containing the endolymph, their apical membrane bordering the endolymph is of interest, especially. Studies have shown that marginal cells of the stria

vascularis can take up proteins from the endolymph. [149-153] In addition, endocytosis is thought to contribute to the uptake of Na^+ from the endolymph via the recycling of epithelial Na^+-selective channels, suggesting a role of the endocytic machinery of marginal cells in taking up ions to uphold their low concentration within the endolymph and therefore contributing to the endolymph composition. [154] In addition, the absorption of waste material, designated for removal via the many capillaries within the stria vascularis is a possibility as the stria vascularis is the only vascularised place within the cochlea. Indeed, the established method of β_2-microglobulin uptake into the stria vascularis complements the results obtained from Kakigi et al (**Figure 25**). [149-153] Marginal cells can take up β_2-microglobulin from the endolymphatic space and the established method needs to be used to test for possible differences in the ability to take up protein in *Ehd1*$^{-/-}$ and *Ehd1*$^{+/+}$ striae. Information regarding the quantity and speed to take up β_2-microglobulin might help to assess the functionality of the endocytic machinery of marginal cells in the absence of EHD1. However, no changes in the endocytic machinery within the marginal cells were observed via transmission electron microscopy. Proteome analysis did, indeed, detect proteins whose expression is unknown of within the stria vascularis according to the gEAR database. This might indicate that those proteins weren't synthesised within the stria vascularis but taken up from the endolymph. [41, 44] For example, Keratins type I (*Krt15*, *Krt33a*) and type II (*Krt76*) but also muscle related proteins Myosin-4 (*Myh4*), Myosin-1 (*Myh1*) and Myomesin-1 (*Myom1*) were among those proteins with virtually absent gene expression in the lateral wall (**Table 6**). However, the alleged lack of expression in the lateral wall might also be due to the limitations of RNAseq of this tissue and ultimately doesn't prove those proteins to be foreign to the strial unit.

Disturbed key player functioning

In addition to the uptake of material from the endolymph, the involvement of the endocytic machinery in the recycling of one or more key player proteins might also provide an explanation for the observed phenotype in *Ehd1*$^{-/-}$ animals. As the stria vascularis is responsible for maintaining the unique endolymph composition and upholding the EP, a disruption of this process due to the absence of EHD1 seems likely. EHD1 is known to be involved in the recycling of a variety of receptors, [108-112] and thus might also contribute to the availability of ion channels responsible for K^+ cycling within the stria vascularis. However, IF staining of known key players Kir4.1, Nkcc1, Na^+,K^+-ATPase, Barttin and Kcnq1 revealed no changes in distribution of said proteins within the stria vascularis (**Figure 13**, **Figure 14**). In addition, mRNA expression of genes encoding for those ion channels remained unchanged in *Ehd1*$^{-/-}$ animals (**Figure 16**). Transcriptome and proteome analysis confirmed these findings as none of the genes or proteins showed significant changes in their mRNA or protein expression, respectively (**Table 2**, **Figure 24**). Nonetheless, a contribution of EHD1 to the expression and or functioning of proteins involved in K^+ cycling cannot be ruled out in general. For one, not all key players are identified yet. Therefore, the possibility of regulation of an unknown ion channel via EHD1-dependent endocytic recycling remains. In fact, proteomics data of stria vascularis revealed chloride intracellular channel protein 6 (*Clic6*) to be downregulated in *Ehd1*$^{-/-}$ striae (Supplements **Table 8**). However, no link of this chloride channel to K^+ cycling within the stria vascularis or hearing impairment in general is known of. In addition, Na^+,K^+-ATPase subunit alpha 4 (*Atp1a4*) was significantly upregulated in *Ehd1*$^{-/-}$ striae (Supplements **Table 8**). Curiously, *Atp1a4* couldn't be detected within the stria vascularis in previous studies and thus, has not been linked to K^+ cycling so far. [155] In addition, the possibility

remains that proper functioning of one or more ion channels involved in K^+ cycling is affected by the absence of EHD1, for example due to changes in pH within the cells. This, however, cannot be examined morphologically, nor can it be quantified by any methods used for this thesis. A different approach would be needed to investigate the matter further, for example via life cell imaging to gain insight into the electrophysiological properties of the cells or measure the pH. Furthermore, K^+ cycling and the upholding of the EP not only depends on ion channels but also on protein complexes such as gap and tight junctions. For example, one of the most common causes of NSHL involves gap junctional protein Cx26 (*Gjb2*) and $Cx26^{-/-}$ mice have been shown to present with a loss of EP. [72] Interestingly, proteome analysis revealed the upregulation of connexin 43 in *Ehd1*$^{-/-}$ striae. Besides Glut4 (*Slc2a4*), connexin 43 (*Gja1*) is the only proteome candidate with which EHD1 is known to interact (**Table 4**). [108, 113] Unlike Glut4, however, connexin 43 is also known to contribute to SNHL. [156-158]

Disruption of pericyte function

Quite in contrast to the hypotheses discussed above, findings concerning connexin 43 in addition to other data obtained from proteomics and transcriptomics suggest an explanation for the hearing loss observed in *Ehd1*$^{-/-}$ mice involving pericytes of the stria vascularis. Pericytes are known to be contractile and feature protein expression patterns commonly seen in muscle cells and which are linked to muscle contraction. [159] Interestingly, proteome analysis of *Ehd1*$^{-/-}$ striae revealed significantly elevated levels of a variety of proteins involved in muscle contractility, such as Myosin-4 (*Myh4*), Myomesin 2 (*Myom2*), Myosin-1 (*Myh1*) and Myozenin-1 (*Myoz1*). In fact, the majority of the top 30 protein candidates (**Table 6**) are muscle-related proteins. As pericytes are the only contractile strial cell type featuring muscle-cell specific proteins within the

stria vascularis, these data suggest that pericytes are greatly influenced by the absence of EHD1. Interestingly, interactions between endothelial cells, pericytes and macrophages have been shown to regulate the permeability of the intrastrial fluid-blood barrier. [22] In addition, endothelial cells and pericytes are known to be connected via gap junctions consisting of connexins 30 and 43. [159-161] As mentioned above, proteome analysis identified connexin 43 (*Gja1*) to be one of the protein candidates significantly upregulated in *Ehd1*$^{-/-}$ striae (**Table 3**, **Table 4**). Mutations in *GJA1* have been shown to be linked to non-syndromic hearing loss. [156, 158, 162, 163] Even though its contribution to hearing loss is inconclusive due to the low number of variants reported so far [158], it is nonetheless an interesting candidate for this study. For one, it is considered to play a key role in hearing. [156-158] While it is crucial for blood-brain barrier maintenance [164, 165], connexin 43 is the most abundant connexin in the cardiovascular system. Martins-Marques et al demonstrated the involvement of EHD1 in the internalisation of connexin 43 in the heart, therefore contributing to the intercellular coupling of cardiomyocytes. [113] What's more, [166] found connexin 43 to be expressed in endothelial cells as well as PVMs within the stria vascularis.[166] Their work also suggests macrophages and endothelial cells to share some, but not all, of the connexin-43 positive sites. However, throughout the endothelial cells, many more connexin-43 positive sites were visible, suggesting the gap junction protein to serve as a point of connection between endothelial cells and another cell type. Considering the findings of [166], pericytes presumably share connexin 43 containing gap junctions with endothelial cells of the stria vascularis. This suggestion is complemented by gEAR data, which shows *Gja1* expression present in an unknown cell type. While Hoa et al were able to distinguish between a variety of cell types including macrophages, pericytes are not listed and might contribute to the unknown cell type described in the gEAR data base. [102, 103] Meanwhile, connexin 43-

containing gap junctions have been shown to play an important role in the functioning of intercellular tight junctions of endothelial cells in vitro and hearing loss and a drop in EP in mice with suppressed connexin 43 expression was observed. These data suggest a role of connexin 43 in blood-strial barrier permeability and demonstrate the integrity of this barrier to be vital for upholding the EP. [166] It is therefore worthwhile to consider connexin 43 as one of the top candidates of the proteins physiologically interacting with EHD1 within the stria vascularis and therefore being affected by the absence of EHD1 in *Ehd1*$^{-/-}$ mice, contributing to their hearing loss. One may even consider a disrupted gap junction remodelling within the stria vascularis to be causative to the cochlear phenotype of the *Ehd1*$^{-/-}$ mice. Considering the coupling of endothelial cells to pericytes via connexin 43, this finding further underlines a possible role of disrupted pericyte function in EHD1-related hearing loss. Interestingly, pericytes also feature functions of immune regulation. They have been shown to be capable of phagocytosis, pinocytosis, and endocytosis in the brain [159, 167] and are involved in inflammatory responses due to their ability to secrete pro-inflammatory molecules such as cytokines, and chemokines. [168-170] Interestingly, transcriptome analysis pointed towards an ongoing immune response in *Ehd1*$^{-/-}$ striae as many genes involved in interferon-signalling are significantly altered (**Table 2**). For example, *Irf7* (Interferon regulatory factor 7), *Irf9* (Interferon regulatory factor 9), *Gbp4* (Guanylate Binding Protein 4) and *Ifih1* (Interferon induced with helicase C domain 1) were among the genes upregulated in *Ehd1*$^{-/-}$ striae. In addition, *Ifi44* (Interferon induced protein 44) was downregulated in *Ehd1*$^{-/-}$ striae in both proteome and transcriptome analysis (**Table 7**). Proteome analysis also revealed the significant upregulation of Lys-63-specific deubiquitinase BRCC36 (*Brcc3*) (**Table 6**), a protein known to regulate the inflammasome. [171, 172] To further investigate this theory, IF staining of connexin 43 could shed some light on a possibly altered distribution of the protein due to the

absence of EHD1. Unfortunately, no specific strial pericyte marker is known yet. Therefore, a direct approach via IF staining of the distribution of pericytes throughout the stria vascularis remains difficult. However, electron micrographs can, in a next step, be analysed regarding pericyte morphology as well as gap junctional coupling between endothelial cells and pericytes. In addition, the investigation of possible macrophage invasion of stria vascularis could further substantiate the suspicion of inflammation within the tissue due to the absence of EHD1.

Taken together, this dissertation reveals EHD1 to be localised in the stria vascularis of the inner ear, where it plays an important role in the process of hearing. These findings contribute to inner ear research in general alongside findings of Kleta et al. [98], as it further substantiates EHD1s role in hearing in human and mouse and its consideration as a new SNHL candidate. Further research is needed to unravel EHD1s functional properties within the stria vascularis as well as the pathophysiology underlying the cochlear phenotype seen in patients carrying the mutation R398W. In mice lacking EHD1, a thorough investigation of hair cell damage and endolymph composition is needed to further elucidate EHD1's impact on cochlear functioning. Interactions between EHD1 and connexin 43 within the stria vascularis are of particular interest and might be beneficial in uncovering the pathophysiology of the phenotype seen in patients and thus, providing with potential new targets and treatments of SNHL.

Conclusions

This research aimed to identify the localisation of EHD1 within the inner ear and its role in the process of hearing. Based on the histological examination of murine cochleae it can be concluded that EHD1 is mainly expressed within the stria vascularis of the inner ear. F-ABR measurements of *Ehd1*$^{-/-}$ animals and their wildtype litter mates further revealed hearing impairment in mice lacking EHD1. In addition, the SV129 sub-strain used for this study showed early-onset presbycusis which confirms previous findings of [144] regarding the problematic use of SV129 mouse lineages for hearing studies. The pathohistological observations indicated ongoing degeneration of the strial cell layers due to the absence of EHD1 and thus, a high probability of disrupted EP generation and / or endolymph composition. In addition, proteome and transcriptome analyses pointed towards an association of pericyte function with the phenotype seen in human and mouse and a possible interaction between EHD1 and connexin 43 within the stria vascularis. This study clearly illustrates an important role for EHD1 in the process of hearing and its consideration as a novel SNHL gene. Further research is needed to unravel the exact role of EHD1 within the stria vascularis and its contribution to the EP and endolymph composition. Therefore, the use of a different mouse lineage without early-onset presbycusis is recommended to better distinguish the morphological and functional features caused by the absence of EHD1 from presbycusis-induced changes. Future research of possible interactions between EHD1 and connexin 43 is advisable to uncover the pathophysiological properties of the disruption of the stria vascularis seen in mice. In addition, the endolymph composition as well as possible hair cell damage needs to be studied to further substantiate Ehd1's role in the process of hearing and its contribution to strial functions. Taken together, this doctorate contributes to the effort of inner ear research to unravel novel players in

SNHL and helps to pave the way to the discovery of new targets and treatments of hearing loss.

References

1. Organization, W.H. *Deafness and hearing loss*. 2015 March 2015; Available from: https://web.archive.org/web/20150516054114/http:/www.who.int/mediacentre/factsheets/fs300/en/.
2. Nin, F., et al., *The unique electrical properties in an extracellular fluid of the mammalian cochlea; their functional roles, homeostatic processes, and pathological significance.* Pflugers Arch, 2016. **468**(10): p. 1637-49.
3. Fettiplace, R. and C.M. Hackney, *The sensory and motor roles of auditory hair cells.* Nat Rev Neurosci, 2006. **7**(1): p. 19-29.
4. Tanna RJ, L.J., De Jesus O, *Sensorineural Hearing Loss*. Updated 2023 Aug 23, StatPearls [Internet]: StatPearls Publishing, Treasure Island (FL).
5. Bosher, S.K. and R.L. Warren, *Very low calcium content of cochlear endolymph, an extracellular fluid.* Nature, 1978. **273**(5661): p. 377-8.
6. Wangemann, P., *Supporting sensory transduction: cochlear fluid homeostasis and the endocochlear potential.* J Physiol, 2006. **576**(Pt 1): p. 11-21.
7. Recanzone, G.H., *Perception of auditory signals.* Ann N Y Acad Sci, 2011. **1224**: p. 96-108.
8. Oghalai, J.S., *The cochlear amplifier: augmentation of the traveling wave within the inner ear.* Curr Opin Otolaryngol Head Neck Surg, 2004. **12**(5): p. 431-8.
9. Zdebik, A.A., P. Wangemann, and T.J. Jentsch, *Potassium ion movement in the inner ear: insights from genetic disease and mouse models.* Physiology (Bethesda), 2009. **24**: p. 307-16.
10. Marcus, D.C., et al., *KCNJ10 (Kir4.1) potassium channel knockout abolishes endocochlear potential.* Am J Physiol Cell Physiol, 2002. **282**(2): p. C403-7.
11. Rickheit, G., et al., *Endocochlear potential depends on Cl- channels: mechanism underlying deafness in Bartter syndrome IV.* EMBO J, 2008. **27**(21): p. 2907-17.
12. Dallos, P., *The active cochlea.* J Neurosci, 1992. **12**(12): p. 4575-85.
13. Richard, E.M., T. Maurice, and B. Delprat, *Calcium signaling and genetic rare diseases: An auditory perspective.* Cell Calcium, 2023. **110**: p. 102702.
14. Liu, S., et al., *Mechanisms in cochlear hair cell mechano-electrical transduction for acquisition of sound frequency and intensity.* Cell Mol Life Sci, 2021. **78**(12): p. 5083-5094.
15. Corey, D.P. and A.J. Hudspeth, *Ionic basis of the receptor potential in a vertebrate hair cell.* Nature, 1979. **281**(5733): p. 675-677.
16. Ottersen, O.P., et al., *Molecular organization of a type of peripheral glutamate synapse: the afferent synapses of hair cells in the inner ear.* Prog Neurobiol, 1998. **54**(2): p. 127-48.
17. Uetsuka, S., et al., *Molecular architecture of the stria vascularis membrane transport system, which is essential for physiological functions of the mammalian cochlea.* Eur J Neurosci, 2015. **42**(3): p. 1984-2002.
18. Hibino, H., et al., *How is the highly positive endocochlear potential formed? The specific architecture of the stria vascularis and the roles of the ion-transport apparatus.* Pflugers Arch, 2010. **459**(4): p. 521-33.
19. Shi, X., *Pathophysiology of the cochlear intrastrial fluid-blood barrier (review).* Hear Res, 2016. **338**: p. 52-63.
20. Zhang, W., et al., *Perivascular-resident macrophage-like melanocytes in the inner ear are essential for the integrity of the intrastrial fluid-blood barrier.* Proc Natl Acad Sci U S A, 2012. **109**(26): p. 10388-93.

21. Ito, T., N. Kurata, and Y. Fukunaga, *Tissue-Resident Macrophages in the Stria Vascularis.* Front Neurol, 2022. **13**: p. 818395.
22. Neng, L., et al., *Endothelial cell, pericyte, and perivascular resident macrophage-type melanocyte interactions regulate cochlear intrastrial fluid-blood barrier permeability.* J Assoc Res Otolaryngol, 2013. **14**(2): p. 175-85.
23. Thulasiram, M.R., J.M. Ogier, and A. Dabdoub, *Hearing Function, Degeneration, and Disease: Spotlight on the Stria Vascularis.* Front Cell Dev Biol, 2022. **10**: p. 841708.
24. Juhn, S.K. and L.P. Rybak, *Labyrinthine barriers and cochlear homeostasis.* Acta Otolaryngol, 1981. **91**(5-6): p. 529-34.
25. Pfenniger, A., A. Wohlwend, and B.R. Kwak, *Mutations in connexin genes and disease.* Eur J Clin Invest, 2011. **41**(1): p. 103-16.
26. Srinivas, M., V.K. Verselis, and T.W. White, *Human diseases associated with connexin mutations.* Biochim Biophys Acta Biomembr, 2018. **1860**(1): p. 192-201.
27. Del Castillo, F.J. and I. Del Castillo, *Genetics of isolated auditory neuropathies.* Front Biosci (Landmark Ed), 2012. **17**(4): p. 1251-65.
28. Mikstiene, V., et al., *The high frequency of GJB2 gene mutation c.313_326del14 suggests its possible origin in ancestors of Lithuanian population.* BMC Genet, 2016. **17**: p. 45.
29. Li, H., et al., *SNPscan as a high-performance screening tool for mutation hotspots of hearing loss-associated genes.* Genomics, 2015. **106**(2): p. 83-7.
30. Xu, J. and B.J. Nicholson, *The role of connexins in ear and skin physiology - functional insights from disease-associated mutations.* Biochim Biophys Acta, 2013. **1828**(1): p. 167-78.
31. Zhao, H.B., et al., *Gap junctions and cochlear homeostasis.* J Membr Biol, 2006. **209**(2-3): p. 177-86.
32. Locher, H., et al., *Development of the stria vascularis and potassium regulation in the human fetal cochlea: Insights into hereditary sensorineural hearing loss.* Dev Neurobiol, 2015. **75**(11): p. 1219-40.
33. Faridi, R., et al., *Mutational and phenotypic spectra of KCNE1 deficiency in Jervell and Lange-Nielsen Syndrome and Romano-Ward Syndrome.* Hum Mutat, 2019. **40**(2): p. 162-176.
34. Békésy, G.v., *DC Potentials and Energy Balance of the Cochlear Partition.* Journal of the Acoustical Society of America, 1951. **23**: p. 576-582.
35. Gagov, H., M. Chichova, and M. Mladenov, *Endolymph composition: paradigm or inevitability?* Physiol Res, 2018. **67**(2): p. 175-179.
36. Scheibe, F., H. Haupt, and H. Ising, *Total magnesium concentrations of perilymph, cerebrospinal fluid and blood in guinea pigs fed different magnesium-containing diets.* Eur Arch Otorhinolaryngol, 1999. **256**(5): p. 215-9.
37. Cohen-Salmon, M., et al., *Connexin30 deficiency causes instrastrial fluid-blood barrier disruption within the cochlear stria vascularis.* Proc Natl Acad Sci U S A, 2007. **104**(15): p. 6229-34.
38. Takeuchi, S. and M. Ando, *Dye-coupling of melanocytes with endothelial cells and pericytes in the cochlea of gerbils.* Cell Tissue Res, 1998. **293**(2): p. 271-5.
39. Salt, A.N., I. Melichar, and R. Thalmann, *Mechanisms of endocochlear potential generation by stria vascularis.* Laryngoscope, 1987. **97**(8 Pt 1): p. 984-91.
40. Boettger, T., et al., *Deafness and renal tubular acidosis in mice lacking the K-Cl co-transporter Kcc4.* Nature, 2002. **416**(6883): p. 874-8.
41. Boettger, T., et al., *Loss of K-Cl co-transporter KCC3 causes deafness, neurodegeneration and reduced seizure threshold.* EMBO J, 2003. **22**(20): p. 5422-34.
42. Hama, K. and K. Saito, *Gap junctions between the supporting cells in some acoustico-vestibular receptors.* J Neurocytol, 1977. **6**(1): p. 1-12.

43. Mammano, F., et al., *Ca2+ signaling in the inner ear.* Physiology (Bethesda), 2007. **22**: p. 131-44.
44. Schulte, B.A. and J.C. Adams, *Distribution of immunoreactive Na+,K+-ATPase in gerbil cochlea.* J Histochem Cytochem, 1989. **37**(2): p. 127-34.
45. Schulte, B.A. and K.P. Steel, *Expression of alpha and beta subunit isoforms of Na,K-ATPase in the mouse inner ear and changes with mutations at the Wv or Sld loci.* Hear Res, 1994. **78**(1): p. 65-76.
46. Crouch, J.J., et al., *Immunohistochemical localization of the Na-K-Cl co-transporter (NKCC1) in the gerbil inner ear.* J Histochem Cytochem, 1997. **45**(6): p. 773-8.
47. Sakaguchi, N., et al., *Na-K-Cl cotransporter expression in the developing and senescent gerbil cochlea.* Hear Res, 1998. **118**(1-2): p. 114-22.
48. Konishi, T. and M. Mendelsohn, *Effect of ouabain on cochlear potentials and endolymph composition in guinea pigs.* Acta Otolaryngol, 1970. **69**(3): p. 192-9.
49. Kuijpers, W. and S.L. Bonting, *The cochlear potentials. I. The effect of ouabain on the cochlear potentials of the guinea pig.* Pflugers Arch, 1970. **320**(4): p. 348-58.
50. Marcus, D.C., N.Y. Marcus, and R. Thalmann, *Changes in cation contents of stria vascularis with ouabain and potassium-free perfusion.* Hear Res, 1981. **4**(2): p. 149-60.
51. Hibino, H., et al., *Expression of an inwardly rectifying K+ channel, Kir5.1, in specific types of fibrocytes in the cochlear lateral wall suggests its functional importance in the establishment of endocochlear potential.* Eur J Neurosci, 2004. **19**(1): p. 76-84.
52. Hibino, H., et al., *An ATP-dependent inwardly rectifying potassium channel, KAB-2 (Kir4. 1), in cochlear stria vascularis of inner ear: its specific subcellular localization and correlation with the formation of endocochlear potential.* J Neurosci, 1997. **17**(12): p. 4711-21.
53. Takeuchi, S. and M. Ando, *Inwardly rectifying K+ currents in intermediate cells in the cochlea of gerbils: a possible contribution to the endocochlear potential.* Neurosci Lett, 1998. **247**(2-3): p. 175-8.
54. Takeuchi, S., M. Ando, and A. Kakigi, *Mechanism generating endocochlear potential: role played by intermediate cells in stria vascularis.* Biophys J, 2000. **79**(5): p. 2572-82.
55. Ando, M. and S. Takeuchi, *mRNA encoding 'ClC-K1, a kidney Cl(-)- channel' is expressed in marginal cells of the stria vascularis of rat cochlea: its possible contribution to Cl(-) currents.* Neurosci Lett, 2000. **284**(3): p. 171-4.
56. Estevez, R., et al., *Barttin is a Cl- channel beta-subunit crucial for renal Cl- reabsorption and inner ear K+ secretion.* Nature, 2001. **414**(6863): p. 558-61.
57. Sage, C.L. and D.C. Marcus, *Immunolocalization of ClC-K chloride channel in strial marginal cells and vestibular dark cells.* Hear Res, 2001. **160**(1-2): p. 1-9.
58. Takeuchi, S., et al., *Ion channels in basolateral membrane of marginal cells dissociated from gerbil stria vascularis.* Hear Res, 1995. **83**(1-2): p. 89-100.
59. Birkenhager, R., et al., *Mutation of BSND causes Bartter syndrome with sensorineural deafness and kidney failure.* Nat Genet, 2001. **29**(3): p. 310-4.
60. Schlingmann, K.P., et al., *Salt wasting and deafness resulting from mutations in two chloride channels.* N Engl J Med, 2004. **350**(13): p. 1314-9.
61. Casimiro, M.C., et al., *Targeted disruption of the Kcnq1 gene produces a mouse model of Jervell and Lange-Nielsen Syndrome.* Proc Natl Acad Sci U S A, 2001. **98**(5): p. 2526-31.
62. Nicolas, M., et al., *KCNQ1/KCNE1 potassium channels in mammalian vestibular dark cells.* Hear Res, 2001. **153**(1-2): p. 132-45.
63. Sakagami, M., et al., *Cellular localization of rat Isk protein in the stria vascularis by immunohistochemical observation.* Hear Res, 1991. **56**(1-2): p. 168-72.

64. Vetter, D.E., et al., *Inner ear defects induced by null mutation of the isk gene.* Neuron, 1996. **17**(6): p. 1251-64.
65. Wangemann, P., et al., *Loss of KCNJ10 protein expression abolishes endocochlear potential and causes deafness in Pendred syndrome mouse model.* BMC Med, 2004. **2**: p. 30.
66. Scholl, U.I., et al., *Seizures, sensorineural deafness, ataxia, mental retardation, and electrolyte imbalance (SeSAME syndrome) caused by mutations in KCNJ10.* Proc Natl Acad Sci U S A, 2009. **106**(14): p. 5842-7.
67. Bockenhauer, D., et al., *Epilepsy, ataxia, sensorineural deafness, tubulopathy, and KCNJ10 mutations.* N Engl J Med, 2009. **360**(19): p. 1960-70.
68. Kitajiri, S., et al., *Compartmentalization established by claudin-11-based tight junctions in stria vascularis is required for hearing through generation of endocochlear potential.* J Cell Sci, 2004. **117**(Pt 21): p. 5087-96.
69. Kitajiri, S.I., et al., *Expression patterns of claudins, tight junction adhesion molecules, in the inner ear.* Hear Res, 2004. **187**(1-2): p. 25-34.
70. Gow, A., et al., *Deafness in Claudin 11-null mice reveals the critical contribution of basal cell tight junctions to stria vascularis function.* J Neurosci, 2004. **24**(32): p. 7051-62.
71. Boulay, A.C., et al., *Hearing is normal without connexin30.* J Neurosci, 2013. **33**(2): p. 430-4.
72. Cohen-Salmon, M., et al., *Targeted ablation of connexin26 in the inner ear epithelial gap junction network causes hearing impairment and cell death.* Curr Biol, 2002. **12**(13): p. 1106-11.
73. Shearer AE, H.M., Schaefer AM, et al., *Genetic Hearing Loss Overview*. 1999 Feb 14 [Updated 2023 Sep 28] ed. GeneReviews®, ed. F.J. Adam MP, Mirzaa GM, et al.,. 1993-2024, Seattle (WA): University of Washington, Seattle.
74. Walls, W.D., H. Azaiez, and R.J.H. Smith. *Hereditary Hearing Loss Homepage*. Available from: https://hereditaryhearingloss.org.
75. Priestley, L., D. Kumar, and B. Sykes, *Amplification of the COL2A1 3' variable region used for segregation analysis in a family with the Stickler syndrome.* Hum Genet, 1990. **85**(5): p. 525-6.
76. Francomano, C.A., et al., *The Stickler syndrome: evidence for close linkage to the structural gene for type II collagen.* Genomics, 1987. **1**(4): p. 293-6.
77. Brunner, H.G., et al., *A Stickler syndrome gene is linked to chromosome 6 near the COL11A2 gene.* Hum Mol Genet, 1994. **3**(9): p. 1561-4.
78. Tassabehji, M., V.E. Newton, and A.P. Read, *Waardenburg syndrome type 2 caused by mutations in the human microphthalmia (MITF) gene.* Nat Genet, 1994. **8**(3): p. 251-5.
79. Tassabehji, M., et al., *Waardenburg's syndrome patients have mutations in the human homologue of the Pax-3 paired box gene.* Nature, 1992. **355**(6361): p. 635-6.
80. Zlotogora, J., et al., *Homozygosity for Waardenburg syndrome.* Am J Hum Genet, 1995. **56**(5): p. 1173-8.
81. Pingault, V., et al., *SOX10 mutations in patients with Waardenburg-Hirschsprung disease.* Nat Genet, 1998. **18**(2): p. 171-3.
82. Everett, L.A., et al., *Pendred syndrome is caused by mutations in a putative sulphate transporter gene (PDS).* Nat Genet, 1997. **17**(4): p. 411-22.
83. Mishra, S., et al., *Connexin 26 (GJB2) Mutations Associated with Non-Syndromic Hearing Loss (NSHL).* Indian J Pediatr, 2018. **85**(12): p. 1061-1066.
84. Kelsell, D.P., et al., *Connexin 26 mutations in hereditary non-syndromic sensorineural deafness.* Nature, 1997. **387**(6628): p. 80-3.
85. Mutai, H., et al., *Variants encoding a restricted carboxy-terminal domain of SLC12A2 cause hereditary hearing loss in humans.* PLoS Genet, 2020. **16**(4): p. e1008643.

86. Riazuddin, S., et al., *Molecular basis of DFNB73: mutations of BSND can cause nonsyndromic deafness or Bartter syndrome.* Am J Hum Genet, 2009. **85**(2): p. 273-80.
87. Walsh, T., et al., *From flies' eyes to our ears: mutations in a human class III myosin cause progressive nonsyndromic hearing loss DFNB30.* Proc Natl Acad Sci U S A, 2002. **99**(11): p. 7518-23.
88. Wang, A., et al., *Association of unconventional myosin MYO15 mutations with human nonsyndromic deafness DFNB3.* Science, 1998. **280**(5368): p. 1447-51.
89. Greenberg, D., N.D. Rosenblum, and M. Tonelli, *The multifaceted links between hearing loss and chronic kidney disease.* Nat Rev Nephrol, 2024.
90. Phelan, P.J. and M.N. Rheault, *Hearing loss and renal syndromes.* Pediatr Nephrol, 2018. **33**(10): p. 1671-1683.
91. Hudson, B.G., et al., *Alport's syndrome, Goodpasture's syndrome, and type IV collagen.* N Engl J Med, 2003. **348**(25): p. 2543-56.
92. Jefferson, J.A., et al., *Autosomal dominant Alport syndrome linked to the type IV collage alpha 3 and alpha 4 genes (COL4A3 and COL4A4).* Nephrol Dial Transplant, 1997. **12**(8): p. 1595-9.
93. Mochizuki, T., et al., *Identification of mutations in the alpha 3(IV) and alpha 4(IV) collagen genes in autosomal recessive Alport syndrome.* Nat Genet, 1994. **8**(1): p. 77-81.
94. Barker, D.F., et al., *Identification of mutations in the COL4A5 collagen gene in Alport syndrome.* Science, 1990. **248**(4960): p. 1224-7.
95. Seri, M., et al., *MYH9-related disease: May-Hegglin anomaly, Sebastian syndrome, Fechtner syndrome, and Epstein syndrome are not distinct entities but represent a variable expression of a single illness.* Medicine (Baltimore), 2003. **82**(3): p. 203-15.
96. Janssen, A.G., et al., *Disease-causing dysfunctions of barttin in Bartter syndrome type IV.* J Am Soc Nephrol, 2009. **20**(1): p. 145-53.
97. Janer, A., et al., *RMND1 deficiency associated with neonatal lactic acidosis, infantile onset renal failure, deafness, and multiorgan involvement.* Eur J Hum Genet, 2015. **23**(10): p. 1301-7.
98. Issler, N., et al., *A Founder Mutation in EHD1 Presents with Tubular Proteinuria and Deafness.* J Am Soc Nephrol, 2022. **33**(4): p. 732-745.
99. Bhattacharyya, S. and T.J. Pucadyil, *Cellular functions and intrinsic attributes of the ATP-binding Eps15 homology domain-containing proteins.* Protein Sci, 2020. **29**(6): p. 1321-1330.
100. Naslavsky, N. and S. Caplan, *EHD proteins: key conductors of endocytic transport.* Trends Cell Biol, 2011. **21**(2): p. 122-31.
101. Fagerberg, L., et al., *Analysis of the human tissue-specific expression by genome-wide integration of transcriptomics and antibody-based proteomics.* Mol Cell Proteomics, 2014. **13**(2): p. 397-406.
102. Orvis, J., et al., *gEAR: Gene Expression Analysis Resource portal for community-driven, multi-omic data exploration.* Nat Methods, 2021. **18**(8): p. 843-844.
103. Korrapati, S., et al., *Single Cell and Single Nucleus RNA-Seq Reveal Cellular Heterogeneity and Homeostatic Regulatory Networks in Adult Mouse Stria Vascularis.* Front Mol Neurosci, 2019. **12**: p. 316.
104. O'Sullivan, M.J. and A.J. Lindsay, *The Endosomal Recycling Pathway-At the Crossroads of the Cell.* Int J Mol Sci, 2020. **21**(17).
105. Sharma, M., et al., *MICAL-L1: An unusual Rab effector that links EHD1 to tubular recycling endosomes.* Commun Integr Biol, 2010. **3**(2): p. 181-3.
106. Sharma, M., et al., *MICAL-L1 links EHD1 to tubular recycling endosomes and regulates receptor recycling.* Mol Biol Cell, 2009. **20**(24): p. 5181-94.

107. Naslavsky, N., et al., *Interactions between EHD proteins and Rab11-FIP2: a role for EHD3 in early endosomal transport.* Mol Biol Cell, 2006. **17**(1): p. 163-77.
108. Guilherme, A., et al., *Role of EHD1 and EHBP1 in perinuclear sorting and insulin-regulated GLUT4 recycling in 3T3-L1 adipocytes.* J Biol Chem, 2004. **279**(38): p. 40062-75.
109. Lin, S.X., et al., *Rme-1 regulates the distribution and function of the endocytic recycling compartment in mammalian cells.* Nat Cell Biol, 2001. **3**(6): p. 567-72.
110. Walseng, E., O. Bakke, and P.A. Roche, *Major histocompatibility complex class II-peptide complexes internalize using a clathrin- and dynamin-independent endocytosis pathway.* J Biol Chem, 2008. **283**(21): p. 14717-27.
111. Jovic, M., et al., *EHD1 regulates beta1 integrin endosomal transport: effects on focal adhesions, cell spreading and migration.* J Cell Sci, 2007. **120**(Pt 5): p. 802-14.
112. Rotem-Yehudar, R., E. Galperin, and M. Horowitz, *Association of insulin-like growth factor 1 receptor with EHD1 and SNAP29.* J Biol Chem, 2001. **276**(35): p. 33054-60.
113. Martins-Marques, T., et al., *EHD1 Modulates Cx43 Gap Junction Remodeling Associated With Cardiac Diseases.* Circ Res, 2020. **126**(10): p. e97-e113.
114. Seaman, M.N., *The retromer complex - endosomal protein recycling and beyond.* J Cell Sci, 2012. **125**(Pt 20): p. 4693-702.
115. Gokool, S., D. Tattersall, and M.N.J. Seaman, *EHD1 Interacts with Retromer to Stabilize SNX1 Tubules and Facilitate Endosome-to-Golgi Retrieval.* Traffic, 2007. **8**(12): p. 1873-1886.
116. Zhang, J., et al., *Rabankyrin-5 interacts with EHD1 and Vps26 to regulate endocytic trafficking and retromer function.* Traffic, 2012. **13**(5): p. 745-57.
117. Dhawan, K., N. Naslavsky, and S. Caplan, *Sorting nexin 17 (SNX17) links endosomal sorting to Eps15 homology domain protein 1 (EHD1)-mediated fission machinery.* J Biol Chem, 2020. **295**(12): p. 3837-3850.
118. Cullen, P.J. and F. Steinberg, *To degrade or not to degrade: mechanisms and significance of endocytic recycling.* Nat Rev Mol Cell Biol, 2018. **19**(11): p. 679-696.
119. Doherty, K.R., et al., *The endocytic recycling protein EHD2 interacts with myoferlin to regulate myoblast fusion.* J Biol Chem, 2008. **283**(29): p. 20252-60.
120. Posey, A.D., Jr., et al., *Endocytic recycling proteins EHD1 and EHD2 interact with fer-1-like-5 (Fer1L5) and mediate myoblast fusion.* J Biol Chem, 2011. **286**(9): p. 7379-88.
121. Posey, A.D., Jr., et al., *EHD1 mediates vesicle trafficking required for normal muscle growth and transverse tubule development.* Dev Biol, 2014. **387**(2): p. 179-90.
122. Demonbreun, A.R., et al., *Eps 15 Homology Domain (EHD)-1 Remodels Transverse Tubules in Skeletal Muscle.* PLoS One, 2015. **10**(9): p. e0136679.
123. Demonbreun, A.R., et al., *An actin-dependent annexin complex mediates plasma membrane repair in muscle.* J Cell Biol, 2016. **213**(6): p. 705-18.
124. Breslow, D.K. and A.J. Holland, *Mechanism and Regulation of Centriole and Cilium Biogenesis.* Annu Rev Biochem, 2019. **88**: p. 691-724.
125. Bhattacharyya, S., et al., *Endocytic recycling protein EHD1 regulates primary cilia morphogenesis and SHH signaling during neural tube development.* Sci Rep, 2016. **6**: p. 20727.
126. Meindl, K., et al., *A missense mutation in Ehd1 associated with defective spermatogenesis and male infertility.* Front Cell Dev Biol, 2023. **11**: p. 1240558.
127. Lu, Q., et al., *Early steps in primary cilium assembly require EHD1/EHD3-dependent ciliary vesicle formation.* Nat Cell Biol, 2015. **17**(4): p. 531.
128. Xie, S., et al., *Vesicular trafficking plays a role in centriole disengagement and duplication.* Mol Biol Cell, 2018. **29**(22): p. 2622-2631.
129. Stoeber, M., et al., *Oligomers of the ATPase EHD2 confine caveolae to the plasma membrane through association with actin.* EMBO J, 2012. **31**(10): p. 2350-64.

130. Hansen, C.G., G. Howard, and B.J. Nichols, *Pacsin 2 is recruited to caveolae and functions in caveolar biogenesis.* J Cell Sci, 2011. **124**(Pt 16): p. 2777-85.
131. Yeow, I., et al., *EHD Proteins Cooperate to Generate Caveolar Clusters and to Maintain Caveolae during Repeated Mechanical Stress.* Curr Biol, 2017. **27**(19): p. 2951-2962 e5.
132. Afonso, S., *Role of EHD1 in Renal Proximal Tubular Endocytosis and Recycling*. 2017, University of Regensburg: Regensburg.
133. Skarnes, W.C., et al., *A conditional knockout resource for the genome-wide study of mouse gene function.* Nature, 2011. **474**(7351): p. 337-42.
134. Tziridis, K., et al., *Deficit in acoustic signal-in-noise detection in glycine receptor alpha3 subunit knockout mice.* Eur J Neurosci, 2017. **45**(4): p. 581-586.
135. Chu, H., et al., *Localization of NKCC1 in the cochlea and morphology of the cochlea in NKCC1-knockout mice.* J Huazhong Univ Sci Technolog Med Sci, 2006. **26**(3): p. 374-7.
136. Meyer zum Gottesberge, A.M., et al., *Inner ear defects and hearing loss in mice lacking the collagen receptor DDR1*. Lab Invest, 2008. **88**(1): p. 27-37.
137. Trowe, M.O., et al., *Impaired stria vascularis integrity upon loss of E-cadherin in basal cells.* Dev Biol, 2011. **359**(1): p. 95-107.
138. Witkos, T.M., et al., *GORAB scaffolds COPI at the trans-Golgi for efficient enzyme recycling and correct protein glycosylation.* Nat Commun, 2019. **10**(1): p. 127.
139. Pohl, U., et al., *EHD2, EHD3, and EHD4 encode novel members of a highly conserved family of EH domain-containing proteins.* Genomics, 2000. **63**(2): p. 255-62.
140. Naslavsky, N. and S. Caplan, *C-terminal EH-domain-containing proteins: consensus for a role in endocytic trafficking, EH?* J Cell Sci, 2005. **118**(Pt 18): p. 4093-101.
141. George, M., et al., *Shared as well as distinct roles of EHD proteins revealed by biochemical and functional comparisons in mammalian cells and C. elegans.* BMC Cell Biol, 2007. **8**: p. 3.
142. Liu, H., et al., *Cell-Specific Transcriptome Analysis Shows That Adult Pillar and Deiters' Cells Express Genes Encoding Machinery for Specializations of Cochlear Hair Cells.* Front Mol Neurosci, 2018. **11**: p. 356.
143. Li, C., et al., *Comprehensive transcriptome analysis of cochlear spiral ganglion neurons at multiple ages.* Elife, 2020. **9**.
144. Zheng, Q.Y., K.R. Johnson, and L.C. Erway, *Assessment of hearing in 80 inbred strains of mice by ABR threshold analyses.* Hear Res, 1999. **130**(1-2): p. 94-107.
145. Belal, A., Jr. and J. Ylikoski, *Pathologic significance of Meniere's symptom complex. A histopathologic and electron microscopic study.* Am J Otolaryngol, 1980. **1**(4): p. 275-84.
146. Kurata, N., et al., *Histopathologic Evaluation of Vascular Findings in the Cochlea in Patients With Presbycusis.* JAMA Otolaryngol Head Neck Surg, 2016. **142**(2): p. 173-8.
147. Carraro, M. and R.V. Harrison, *Degeneration of stria vascularis in age-related hearing loss; a corrosion cast study in a mouse model.* Acta Otolaryngol, 2016. **136**(4): p. 385-90.
148. Gratton, M.A., R.A. Schmiedt, and B.A. Schulte, *Age-related decreases in endocochlear potential are associated with vascular abnormalities in the stria vascularis.* Hear Res, 1996. **102**(1-2): p. 181-90.
149. Kakigi, A., et al., *Endocytosis of microperoxidase in the marginal cells of stria vascularis.* Auris Nasus Larynx, 2007. **34**(1): p. 39-43.
150. Kakigi, A., et al., *Actin filaments and microtubules regulate endocytosis in marginal cells of the stria vascularis.* Acta Otolaryngol, 2008. **128**(8): p. 856-60.

151. Kakigi, A., et al., *Endocytosis of cationized ferritin in marginal cells of the stria vascularis is regulated by protein kinase, protein phosphatase, and MEK/ERK and PI3-K signaling pathways.* Otol Neurotol, 2011. **32**(5): p. 856-62.
152. Kakigi, A., et al., *Endocytosis of MPO in marginal cells is regulated by PKC, protein phosphatase, ERK and PI3-K signaling cascades, but not by PKA and MEK signaling cascades.* ORL J Otorhinolaryngol Relat Spec, 2010. **72**(4): p. 188-95.
153. Kakigi, A., et al., *Endocytosis of CF in marginal cells of stria vascularis regulated by ROCK and MLCK signaling cascade, but not G-proteins.* Auris Nasus Larynx, 2019. **46**(5): p. 790-796.
154. Kakigi, A., et al., *Presence and regulation of epithelial sodium channels in the marginal cells of stria vascularis.* Acta Otolaryngol, 2008. **128**(3): p. 233-8.
155. Ding, B., et al., *Age-related changes in Na, K-ATPase expression, subunit isoform selection and assembly in the stria vascularis lateral wall of mouse cochlea.* Hear Res, 2018. **367**: p. 59-73.
156. Liu, X.Z., et al., *Mutations in GJA1 (connexin 43) are associated with non-syndromic autosomal recessive deafness.* Hum Mol Genet, 2001. **10**(25): p. 2945-51.
157. Bult, C.J., et al., *Mouse Genome Database (MGD) 2019.* Nucleic Acids Res, 2019. **47**(D1): p. D801-D806.
158. Adadey, S.M., et al., *Connexin Genes Variants Associated with Non-Syndromic Hearing Impairment: A Systematic Review of the Global Burden.* Life (Basel), 2020. **10**(11).
159. Zhang, Z.S., et al., *Research advances in pericyte function and their roles in diseases.* Chin J Traumatol, 2020. **23**(2): p. 89-95.
160. Hirschi, K.K., et al., *Gap junction communication mediates transforming growth factor-beta activation and endothelial-induced mural cell differentiation.* Circ Res, 2003. **93**(5): p. 429-37.
161. Armulik, A., G. Genove, and C. Betsholtz, *Pericytes: developmental, physiological, and pathological perspectives, problems, and promises.* Dev Cell, 2011. **21**(2): p. 193-215.
162. Yang, J.J., et al., *Identification of mutations in members of the connexin gene family as a cause of nonsyndromic deafness in Taiwan.* Audiol Neurootol, 2007. **12**(3): p. 198-208.
163. Yang, J.J., et al., *Prospective variants screening of connexin genes in children with hearing impairment: genotype/phenotype correlation.* Hum Genet, 2010. **128**(3): p. 303-13.
164. Nagy, J.I. and J.E. Rash, *Connexins and gap junctions of astrocytes and oligodendrocytes in the CNS.* Brain Res Brain Res Rev, 2000. **32**(1): p. 29-44.
165. Boulay, A.C., S. Cisternino, and M. Cohen-Salmon, *Immunoregulation at the gliovascular unit in the healthy brain: A focus on Connexin 43.* Brain Behav Immun, 2016. **56**: p. 1-9.
166. Zhang, J., et al., *Suppression of Connexin 43 Leads to Strial Vascular Hyper-Permeability, Decrease in Endocochlear Potential, and Mild Hearing Loss.* Front Physiol, 2020. **11**: p. 974.
167. Thomas, W.E., *Brain macrophages: on the role of pericytes and perivascular cells.* Brain Res Brain Res Rev, 1999. **31**(1): p. 42-57.
168. Smyth, L.C.D., et al., *Unique and shared inflammatory profiles of human brain endothelia and pericytes.* J Neuroinflammation, 2018. **15**(1): p. 138.
169. Kovac, A., M.A. Erickson, and W.A. Banks, *Brain microvascular pericytes are immunoactive in culture: cytokine, chemokine, nitric oxide, and LRP-1 expression in response to lipopolysaccharide.* J Neuroinflammation, 2011. **8**: p. 139.
170. Jansson, D., et al., *A role for human brain pericytes in neuroinflammation.* J Neuroinflammation, 2014. **11**: p. 104.

171. Py, B.F., et al., *Deubiquitination of NLRP3 by BRCC3 critically regulates inflammasome activity.* Mol Cell, 2013. **49**(2): p. 331-8.
172. Song, N., et al., *NLRP3 Phosphorylation Is an Essential Priming Event for Inflammasome Activation.* Mol Cell, 2017. **68**(1): p. 185-197 e6.

Supplements

Proteome candidates

Table 8

List of all significantly altered proteome candidates

Protein name	Gene symbol	Log2 fold change	P-value
GTP-+B4:B223binding nuclear protein Ran	1700009N14Rik	-1,55	0,000667007
L-aminoadipate-semialdehyde dehydrogenase-phosphopantetheinyl transferase	Aasdhppt	3,75	0,005975757
ABI gene family, member 3 (NESH)-binding protein	Abi3bp	-1,15	1,16E-06
Aggrecan core protein	Acan	-1,55	1,07E-06
1-aminocyclopropane-1-carboxylate synthase-like protein 1	Accs	-1,14	0,008024512
Acid phosphatase type 7	Acp7	1,84	0,004864578
Actin, alpha skeletal muscle	Acta1	-2,24	0,000381892
B-actin-like protein 2	Actbl2	-1,03	9,57E-05
Alpha-actinin-2	Actn2	-1,66	0,000122931
Alpha-actinin-3	Actn3	-3,24	7,93E-05
Manganese-dependent ADP-ribose/CDP-alcohol diphosphatase	Adprm	1,65	1,62E-06
Aldo-keto reductase family 1 member C13	Akr1c13	-1,46	0,004249761
Putative bifunctional UDP-N-acetylglucosamine transferase and deubiquitinase ALG13	Alg13	-1,03	0,00040081
Polyunsaturated fatty acid (12S)/(13S)-lipoxygenase, epidermal-type	Alox12e	-1,13	0,002768068
Protein angel homolog 2	Angel2	-1,03	0,007382703
AP-1 complex subunit sigma-3	Ap1s3	-1,23	0,000365049
Apolipoprotein C-III	Apoc3	-1,55	0,001245344
ADP-ribosylation factor 5	Arf5	-2,37	0,000218364
ADP-ribosylation factor-like protein 2-binding protein	Arl2bp	-2,38	0,001591443
Sodium/potassium-transporting ATPase subunit alpha-4	Atp1a4	-1,33	0,002950023
Sarcoplasmic/endoplasmic reticulum calcium ATPase 1	Atp2a1	-1,91	0,000127461
Phospholipid-transporting ATPase IC	Atp8b1	-1,57	4,45E-05
Cholinesterase	Bche	-1,39	5,63E-05

Protein name	Gene symbol	Log2 fold change	P-value
BolA-like protein 2	Bola2	-1,06	3,78E-07
BPI fold-containing family A member 1	Bpifa1	-1,12	0,002253965
BPI fold-containing family B member 1	Bpifb1	1,84	0,00086546
Lys-63-specific deubiquitinase BRCC36	Brcc3	-4,58	0,003775942
B-TFIID TATA-box-binding protein-associated factor 1	Btaf1	-1,23	3,48E-06
BTB/POZ domain-containing protein 9	Btbd9	1,43	0,004909001
Voltage-dependent L-type calcium channel subunit β-1	Cacnb1	-1,47	0,000268223
Calcium/calmodulin-dependent protein kinase type II subunit alpha	Camk2a	-1,57	0,00057193
Calsequestrin-1	Casq1	-2,48	1,51E-05
Calsequestrin-2	Casq2	-1,37	1,76E-07
Caveolae-associated protein 4	Cavin4	-1,53	0,001954881
ADP-ribosyl cyclase/cyclic ADP-ribose hydrolase 1	Cd38	-1,21	0,000767612
Pre-mRNA-processing factor 17	Cdc40	-1,00	2,64E-05
Chondroadherin	Chad	-1,59	3,28E-05
Coiled-coil-helix-coiled-coil-helix domain-containing protein 7	Chchd7	-3,72	0,000122845
Chloride intracellular channel protein 6	Clic6	1,70	0,005005733
CKLF-like MARVEL transmembrane domain-containing protein 5	Cmtm5	-1,42	1,67E-05
Calponin-1	Cnn1	-1,06	0,004186713
Collagen alpha-1(XI) chain	Col11a1	-1,43	0,00057778
Collagen alpha-1(II) chain	Col2a1	-1,06	0,001774585
Collagen alpha-1(IV) chain	Col4a1	-1,21	4,69E-05
Procollagen galactosyltransferase 2	Colgalt2	-1,36	5,14E-05
Cytochrome c oxidase assembly protein COX16 homolog, mitochondrial	Cox16	-1,09	0,001631354
Inactive carboxypeptidase-like protein X2	Cpxm2	-1,99	1,13E-06
CREB3 regulatory factor	Crebrf	-1,31	1,68E-05
Protein CREG1	Creg1	-1,43	0,000236843
Casein kinase II subunit β	Csnk2b	-1,09	0,000278132
Collagen triple helix repeat-containing protein 1	Cthrc1	-1,28	9,52E-05
CBP80/20-dependent translation initiation factor	Ctif	-1,11	0,001397954

Protein name	Gene symbol	Log2 fold change	P-value
Cytochrome P450 2A5	Cyp2a5	1,99	0,000129299
Decorin	Dcn	-1,26	0,000237343
Dynactin subunit 6	Dctn6	-2,92	0,000330826
Discoidin domain-containing receptor 2	Ddr2	-1,84	6,59E-05
Derlin-2	Derl2	-1,15	1,90E-05
Desmin	Des	-1,22	0,000184061
Deoxyguanosine kinase, mitochondrial	Dguok	-1,09	0,001170627
Dimethylglycine dehydrogenase, mitochondrial	Dmgdh	-1,23	1,11E-05
Dentin matrix acidic phosphoprotein 1	Dmp1	-1,90	0,003660855
Deoxyribonuclease-1-like 1	Dnase1l1	-1,30	0,000356515
Dedicator of cytokinesis protein 8	Dock8	-1,40	0,001249543
Probable C-mannosyltransferase DPY19L1	Dpy19l1	-1,11	0,000590934
Probable E3 ubiquitin-protein ligase DTX3	Dtx3	-1,23	7,80E-05
EH domain-containing protein 1	Ehd1	2,43	0,004247699
Probable RNA-binding protein EIF1AD	Eif1ad	-1,06	0,000109226
Protein eva-1 homolog A	Eva1a	-1,75	8,14E-06
Ecotropic viral integration site 5 protein	Evi5	-1,45	1,38E-06
Fibrillin-1	Fbn1	-1,02	0,00036431
Peptidyl-prolyl cis-trans isomerase FKBP10	Fkbp10	-1,82	0,006524264
Filamin-C	Flnc	-1,46	5,40E-05
Follistatin	Fst	-1,26	0,000205496
Growth arrest and DNA damage-inducible proteins-interacting protein 1	Gadd45gip1	-1,50	6,78E-08
Guanidinoacetate N-methyltransferase	Gamt	-1,11	2,57E-08
Glial fibrillary acidic protein	Gfap	-2,52	0,004048821
Glutathione hydrolase 7	Ggt7	-1,17	0,003179859
Gap junction alpha-1 protein	Gja1	-1,38	0,001388621
Glycolipid transfer protein	Gltp	-1,04	6,59E-05
RAB6-interacting golgin	Gorab	-1,02	0,003561893
Glycosylphosphatidylinositol anchor attachment 1 protein	Gpaa1	-1,03	4,07E-07
Histone H2AX	H2ax	-1,78	0,000116219
H-2 class I histocompatibility antigen, L-D alpha chain	H2-L	-1,61	5,28E-06
Heat shock protein β-6	Hspb6	-1,18	0,000246464
Heat shock protein β-7	Hspb7	-2,14	0,00010159

Protein name	Gene symbol	Log2 fold change	P-value
Bone sialoprotein 2	Ibsp	-2,21	0,000560136
Interferon-induced protein 44	Ifi44	-1,44	0,000221773
Integrin-linked kinase-associated serine/threonine phosphatase 2C	Ilkap	-1,18	6,58E-05
Inosine-5'-monophosphate dehydrogenase 1	Impdh1	-1,55	2,21E-05
Alpha-internexin	Ina	-1,74	0,001453449
Integrator complex subunit 1	Ints1	-1,01	1,45E-06
Integrator complex subunit 5	Ints5	-1,20	0,007032947
Importin-8	Ipo8	-1,05	1,42E-08
IST1 homolog	Ist1	-1,47	0,002220698
Inter-alpha-trypsin inhibitor heavy chain H3	Itih3	-1,20	1,52E-05
Junctophilin-1	Jph1	-1,39	0,002433209
Junctophilin-2	Jph2	-1,50	0,000272372
Junctional sarcoplasmic reticulum protein 1	Jsrp1	-1,95	3,62E-05
Inward rectifier potassium channel 2	Kcnj2	-1,21	3,84E-05
Keratocan	Kera	-2,00	0,007719529
Kelch-like protein 40	Klhl40	-1,12	0,000439507
Kelch-like protein 41	Klhl41	-2,50	1,52E-05
Keratin, type I cytoskeletal 15	Krt15	-3,13	0,001997203
Keratin, type I cuticular Ha3-I	Krt33a	3,84	5,35E-05
Keratin, type II cytoskeletal 2 oral	Krt76	5,05	0,001384749
Keratin, type II cytoskeletal 79	Krt79	-1,17	0,000115199
LIM domain-binding protein 3	Ldb3	-2,44	0,000726366
Galectin-8	Lgals8	-1,34	0,000213257
Acyl-CoA:lysophosphatidylglycerol acyltransferase 1	Lpgat1	-1,06	0,004641867
Protein LSM12 homolog	Lsm12	-1,28	0,000107741
Putative RNA-binding protein Luc7-like 1	Luc7l	-1,03	6,75E-05
Meiosis regulator and mRNA stability factor 1	Marf1	-1,01	0,001356609
Cartilage matrix protein	Matn1	-1,55	0,000869297
Multiple coagulation factor deficiency protein 2 homolog	Mcfd2	-1,13	0,002298645
MTOR-associated protein MEAK7	Meak7	-1,25	9,96E-05
Matrix extracellular phosphoglycoprotein	Mepe	-1,29	0,000900582
Uncharacterized protein CXorf38 homolog	MGI:1916405	-1,86	5,06E-10
Methylated-DNA--protein-cysteine methyltransferase	Mgmt	-1,15	0,000158871
Collagenase 3	Mmp13	-1,14	0,001506328

Protein name	Gene symbol	Log2 fold change	P-value
Mannose-P-dolichol utilization defect 1 protein	Mpdu1	-1,15	0,002221552
39S ribosomal protein L22, mitochondrial	Mrpl22	-1,03	0,001786259
39S ribosomal protein L35, mitochondrial	Mrpl35	-1,22	0,000112911
39S ribosomal protein L53, mitochondrial	Mrpl53	-1,10	0,005127569
ATP synthase subunit a	Mtatp6	-1,04	0,000765137
Murinoglobulin-2	Mug2	-1,22	9,77E-06
Myosin-binding protein C, slow-type	Mybpc1	-1,29	0,000697502
Myosin-binding protein C, fast-type	Mybpc2	-2,39	7,02E-05
Myosin-1	Myh1	-3,47	1,31E-05
Myosin, heavy polypeptide 2, skeletal muscle, adult	Myh2	-1,98	0,003113833
Myosin-4	Myh4	-4,97	2,29E-06
Myosin light chain 1/3, skeletal muscle isoform	Myl1	-3,52	8,01E-06
Myosin regulatory light chain 2, ventricular/cardiac muscle isoform	Myl2	-3,21	0,002364146
Myosin light chain 3	Myl3	-3,31	4,03E-07
Myosin regulatory light chain 2, skeletal muscle isoform	Mylpf	-3,70	4,62E-06
Myomesin-1	Myom1	-3,15	9,83E-06
Myomesin 2	Myom2	-3,54	9,13E-06
Myotilin	Myot	-1,35	1,49E-05
Myozenin-1	Myoz1	-3,37	9,53E-05
Myozenin-3	Myoz3	-2,33	0,000644803
Neutrophil cytosol factor 2	Ncf2	-1,05	5,87E-05
SH3 domain-containing protein	Neb	-3,08	6,26E-05
Neurofilament heavy polypeptide	Nefh	-1,89	0,00040195
Neurofilament light polypeptide	Nefl	-1,47	0,000639473
Neurofilament medium polypeptide	Nefm	-1,60	0,002214337
60S ribosomal export protein NMD3	Nmd3	-1,57	0,000585575
Nuclear speckle splicing regulatory protein 1	Nsrp1	-1,84	1,91E-06
Netrin-1	Ntn1	-1,75	5,60E-07
Protein numb homolog	Numb	-1,00	1,77E-07
Odorant-binding protein 2a	Obp2a	1,35	0,002176499
Obscurin	Obscn	-2,04	8,59E-05
Mimecan	Ogn	-1,15	1,87E-05
PDZ and LIM domain protein 3	Pdlim3	-1,31	1,79E-06

Protein name	Gene symbol	Log2 fold change	P-value
PPM-type phosphatase domain-containing protein	Pdp2	-2,07	9,50E-06
PEX5-related protein	Pex5l	-1,96	1,37E-05
Phosphorylase b kinase gamma catalytic chain, skeletal muscle/heart isoform	Phkg1	-1,49	4,07E-05
Phospholipid phosphatase 1	Plpp1	-1,23	0,000241304
Pancreatic triacylglycerol lipase	Pnlip	-1,02	0,004305802
Nuclear envelope pore membrane protein POM 121	Pom121	-1,03	0,000456253
Protein kinase C epsilon type	Prkce	-1,13	8,06E-05
Serine/threonine-protein kinase D1	Prkd1	-2,31	0,00135362
Serine/threonine-protein kinase D3	Prkd3	-2,08	2,44E-05
Prolactin	Prl	-1,33	0,002688558
Pre-mRNA-splicing factor 38B	Prpf38b	-1,10	0,000208943
Peripherin	Prph	-1,06	0,001042235
Proline-rich protein 33	Prr33	-2,17	0,001452051
Proteasome subunit β type-7	Psmb7	-1,06	7,12E-05
Phosphatidylserine synthase 2	Ptdss2	-1,04	5,62E-06
Retinol-binding protein 4	Rbp4	-1,74	3,48E-07
Receptor expression-enhancing protein 5	Reep5	-2,30	1,17E-08
E3 ubiquitin-protein ligase RNF169	Rnf169	1,74	0,000840121
E3 ubiquitin-protein ligase RNF181	Rnf181	-1,18	3,71E-08
40S ribosomal protein S5	Rps5	-2,93	2,56E-07
Reticulon-2	Rtn2	-2,98	0,000108869
Ryanodine receptor 1	Ryr1	-2,24	5,81E-05
Protein S100-A16	S100a16	-1,09	0,000241901
Protein S100-A4	S100a4	-1,13	4,54E-07
Protein S100-A6	S100a6	-1,25	0,005082362
SR-related and CTD-associated factor 8	Scaf8	-1,17	0,001307985
Secretogranin-3	Scg3	-1,30	3,96E-08
Protein transport protein Sec61 subunit β	Sec61b	-1,68	1,35E-06
Serine incorporator 3	Serinc3	-1,85	2,92E-09
Serine protease inhibitor A3N	Serpina3n	-1,07	4,09E-06
SH3 domain-binding glutamic acid-rich protein	Sh3bgr	-1,07	1,34E-05
Paired amphipathic helix protein Sin3b	Sin3b	-1,65	0,003608724
Monocarboxylate transporter 4	Slc16a3	-1,72	2,29E-05

Protein name	Gene symbol	Log2 fold change	P-value
Solute carrier family 2, facilitated glucose transporter member 4	Slc2a4	-1,05	0,002180486
Zinc transporter 7	Slc30a7	-1,08	0,004574617
Vesicular inhibitory amino acid transporter	Slc32a1	-1,36	0,000495172
Zinc transporter ZIP6	Slc39a6	-1,39	4,92E-06
Solute carrier organic anion transporter family member 1A5	Slco1a5	-1,14	0,000292437
Histone-lysine N-methyltransferase Smyd1	Smyd1	-1,86	2,07E-06
Spermatogenesis-associated serine-rich protein 2	Spats2	-1,48	0,001108652
Striated muscle-specific serine/threonine-protein kinase	Speg	-1,21	2,85E-05
Testican-2	Spock2	-1,18	6,06E-08
Sarcalumenin	Srl	-2,29	2,87E-05
SH3 and cysteine-rich domain-containing protein 3	Stac3	-1,06	0,000163336
Transcription elongation factor SPT4-A;Transcription elongation factor SPT4-B	Supt4h1a;Supt4h1b	-1,51	5,95E-07
Tyrosine-protein kinase SYK	Syk	-1,05	0,002644363
Synaptophysin-like protein 2	Sypl2	-1,57	0,002708888
Transgelin-3	Tagln3	-2,24	0,001192874
TBC1 domain family member 23	Tbc1d23	-1,76	0,001034633
Protein-glutamine gamma-glutamyltransferase E	Tgm3	1,85	0,00052267
Thrombospondin-4	Thbs4	-1,03	2,73E-05
Transmembrane emp24 domain-containing protein 3	Tmed3	-2,17	0,000430933
Protein TMED8	Tmed8	-1,34	4,51E-05
Trimeric intracellular cation channel type A	Tmem38a	-1,98	0,000936935
Transmembrane protein 53	Tmem53	-1,13	3,64E-05
Troponin C, skeletal muscle	Tnnc2	-2,84	0,000142366
Troponin I, fast skeletal muscle	Tnni2	-2,42	3,41E-05
Troponin T, fast skeletal muscle	Tnnt3	-2,31	9,37E-05
Tropomyosin alpha-1 chain	Tpm1	-1,71	0,001642412
Tropomyosin β chain	Tpm2	-3,44	2,15E-06
Transformer-2 protein homolog alpha	Tra2a	-1,17	9,10E-06
Trafficking protein particle complex subunit 3	Trappc3	-1,49	6,94E-05
Tripartite motif-containing protein 72	Trim72	-1,20	0,003072148
Transient receptor potential cation channel subfamily V member 2	Trpv2	-1,40	4,16E-05

Protein name	Gene symbol	Log2 fold change	P-value
Tetraspanin-9	Tspan9	-1,10	1,11E-06
Translocator protein	Tspo	-1,43	3,35E-08
Titin	Ttn	-1,70	0,002157318
Transthyretin	Ttr	-1,03	3,71E-06
RING finger protein unkempt homolog	Unk	-1,99	0,00140608
U3 small nucleolar RNA-associated protein 4 homolog	Utp4	-1,19	1,37E-05
Synaptic vesicle membrane protein VAT-1 homolog-like	Vat1l	-1,34	9,66E-06
V-set and immunoglobulin domain-containing protein 10	Vsig10	-1,21	0,001423959
Methylosome protein 50	Wdr77	-1,07	3,80E-10
CtBP-interacting BTB zinc finger protein	Zbtb38	-3,15	5,51E-07
Zinc finger MYM-type protein 3	Zmym3	-1,06	0,001050188
Zinc finger MYM-type protein 4	Zmym4	-1,07	0,00122026
Zinc finger protein 652	Znf652	-1,12	0,004209978
E3 ubiquitin-protein ligase ZNRF2	Znrf2	-1,58	6,40E-06

Average Log2 ratios and adjusted p-values of EHD1$^{+/+}$ versus EHD1$^{-/-}$ striae are shown for all proteins with significantly altered expression due to the loss of Ehd1.

gEAR data

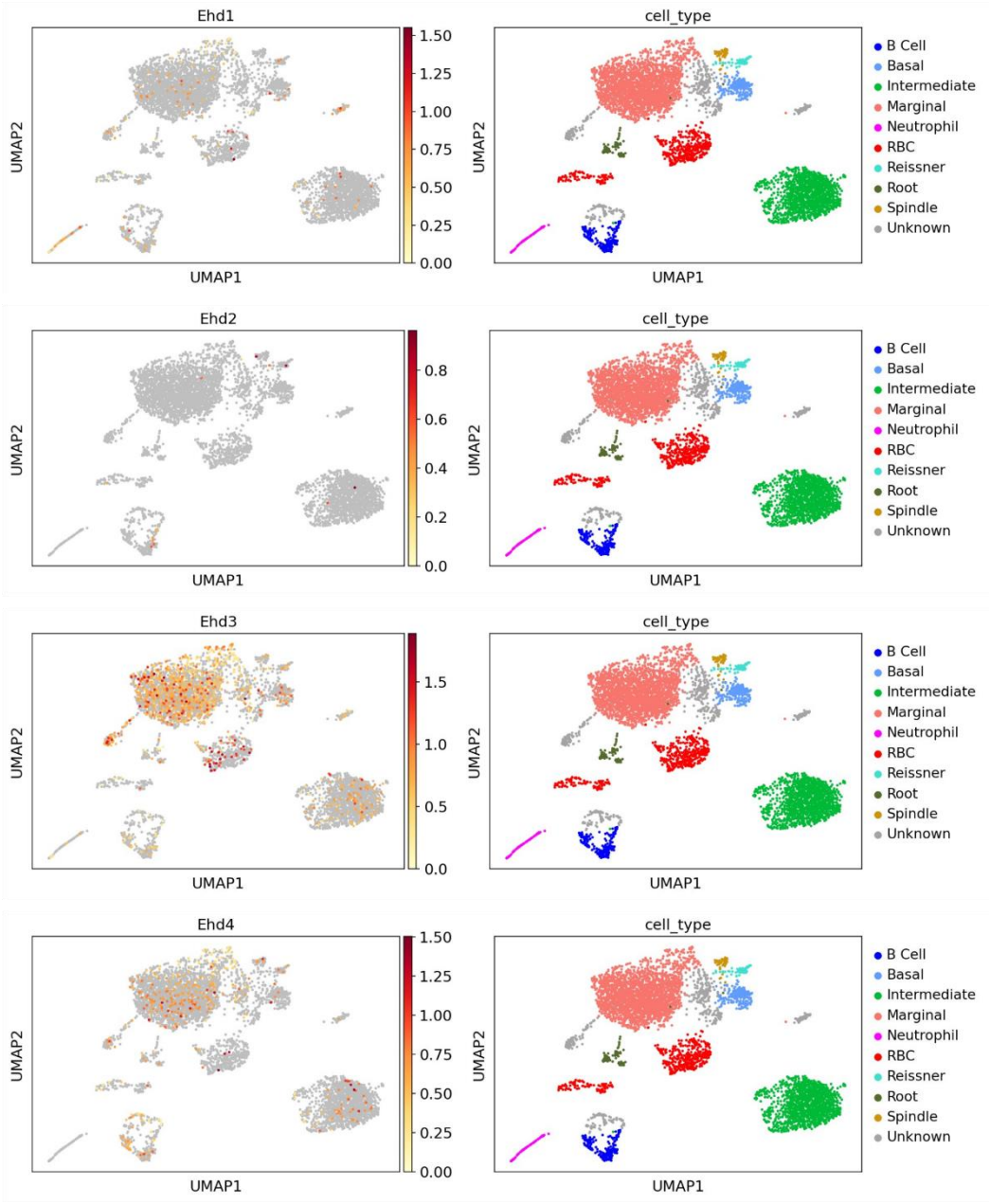

***Figure 27* RNA expression of *Ehd1 – 4* in cells of the murine lateral wall.** Adult mouse snRNA-seq data obtained from [102, 103].

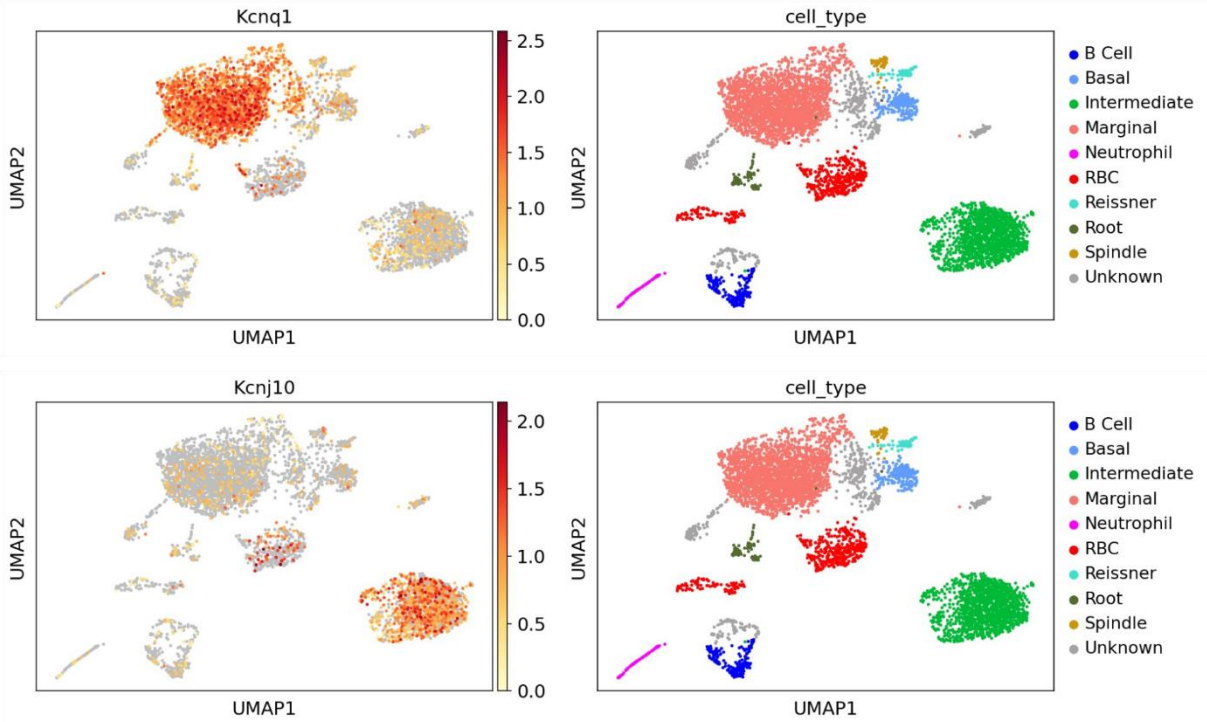

Figure 28 **RNA expression of *Kcnq1* and *Kcnj10* in cells of the murine lateral wall.** Reference of high expression in marginal (*Kcnq1*) and intermediate cells (*Kcnj10*). Adult mouse snRNA-seq data obtained from [102, 103].

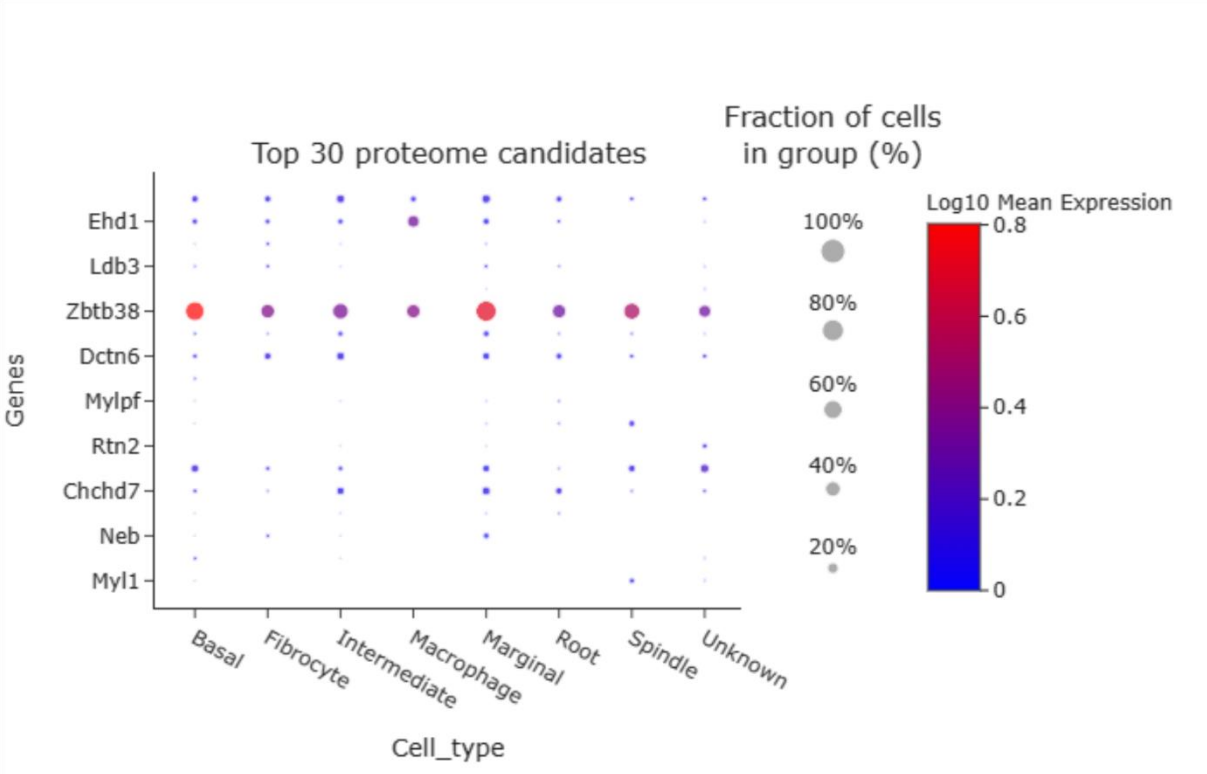

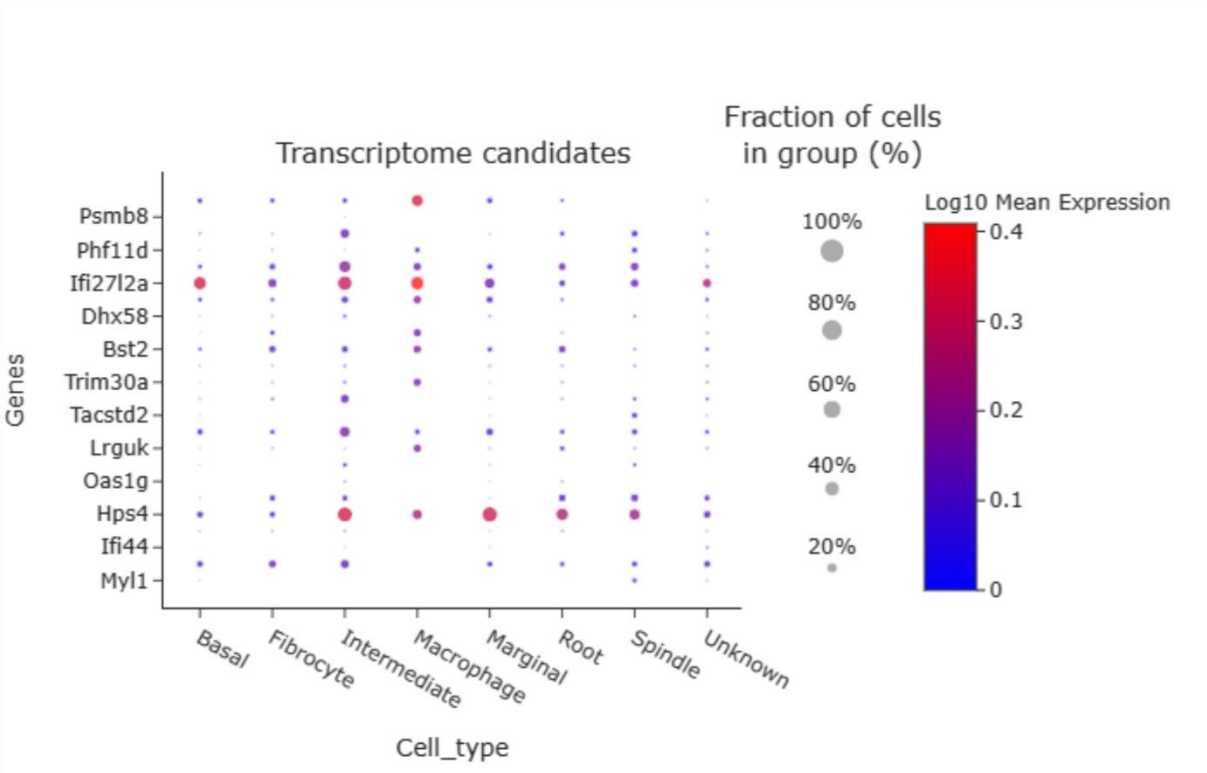

Figure 29 **Distribution of significantly altered proteins and genes in *Ehd1*$^{-/-}$ stria vascularis.** High proportion of proteome candidates are expressed in marginal, intermediate, and basal cells while many transcriptome candidates are present in intermediate cells and macrophages. Data obtained from [102, 103].

Hereditary hearing loss homepage data

Table 9

Genes listed on the hereditary hearing loss homepage

Locus (OMIM)	Gene (OMIM)	Key Gene References (PubMed)
ATS1	COL4A5	Barker et al., 1990
ATS2	COL4A4	Mochizuki et al., 1994
ATS3A	COL4A3	Jefferson et al., 1997
ATS3B	COL4A3	Mochizuki et al., 1994
AUNX1	AIFM1	Zong et al., 2015
BOR1, BOS1	EYA1	Abdelhak et al., 1997; Vincent et al., 1997
BOS3	SIX1	Ruf et al., 2004
DFNA1	DIAPH1	Lynch et al., 1997
DFNA10	EYA4	Wayne et al., 2001
DFNA11	MYO7A	Liu et al., 1997
DFNA15	POU4F3	Vahava et al., 1998
DFNA17	MYH9	Lalwani et al., 2000
DFNA20/26	ACTG1	Zhu et al., 2003
DFNA22	MYO6	Melchionda et al., 2001
DFNA2A	KCNQ4	Kubisch et al., 1999
DFNA36	TMC1	Kurima et al., 2002
DFNA5	GSDME/DFNA5	Van Laer et al., 1998
DFNA6/14/38	WFS1	Bespalova et al., 2001; Young et al., 2001
DFNA8/12	TECTA	Verhoeven et al., 1998
DFNA9	COCH	Robertson et al., 1998
DFNB12	CDH23	Bork et al., 2001
DFNB15/72/95	GIPC3	Charizopoulou et al., 2011; Rehman et al., 2011
DFNB16	STRC	Verpy et al., 2001
DFNB18B	OTOG	Schraders et al., 2012
DFNB1A	GJB2	Kelsell et al., 1997
DFNB21	TECTA	Mustapha et al., 1999
DFNB22	OTOA	Zwaenepoel et al., 2002
DFNB24	RDX	Khan et al., 2007
DFNB25	GRXCR1	Schraders et al., 2010
DFNB28	TRIOBP	Shahin et al., 2006; Riazuddin et al., 2006
DFNB29	CLDN14	Wilcox et al., 2001
DFNB3	MYO15A	Wang et al., 1998
DFNB35	ESRRB	Collin et al., 2008
DFNB36	ESPN	Naz et al., 2004
DFNB4	SLC26A4	Everett et al., 1997
DFNB42	ILDR1	Borck et al., 2011

Locus (OMIM)	Gene (OMIM)	Key Gene References (PubMed)
DFNB48	CIB2	Riazuddin et al., 2012
DFNB49	MARVELD2	Riazuddin et al., 2006
DFNB57	PDZD7	Booth et al., 2015
DFNB59	PJVK	Delmaghani et al., 2006
DFNB6	TMIE	Naz et al., 2002
DFNB63	LRTOMT/COMT2	Du et al., 2008
DFNB67	LHFPL5	Shabbir et al., 2006; Kalay et al., 2006
DFNB7/11	TMC1	Kurima et al., 2002
DFNB73	BSND	Riazuddin et al., 2009
DFNB74	MSRB3	Ahmed et al., 2011
DFNB77	LOXHD1	Grillet et al., 2009
DFNB79	TPRN	Rehman et al., 2010; Li et al., 2010
DFNB8/10	TMPRSS3	Scott et al., 2001
DFNB84A	PTPRQ	Schraders et al., 2010
DFNB84B	OTOGL	Yariz et al., 2012
DFNB86	TBC1D24	Rehman et al., 2014
DFNB9	OTOF	Yasunaga et al., 1999
DFNB93	CABP2	Schrauwen et al., 2012
DFNX1	PRPS1	Liu et al., 2010
DFNX2	POU3F4	de Kok et al., 1995
DFNX4	SMPX	Huebner et al., 2011; Schraders et al., 2011
DFNX5	AIFM1	Zong et al., 2015
JLNS1	KNCQ1	Neyroud et al., 1997
ND	NDP	Berger et al., 1992; Chen et al., 1992
OSMEDA/STL3	COL11A2	Vikkula et al., 1995
OSMEDB/STL3	COL11A2	Vikkula et al., 1995
PDS	SLC26A4	Everett et al., 1997
PRLTS1	HSD17B4	Pierce et al., 2010
PRLTS3/DFNB81	CLPP	Jenkinson et al., 2013
STL1	COL2A1	Ahmad et al., 1991
TCS1	TCOF1	Treacher Collins Syndrome Collaborative Group, 1996
USH1B	MYO7A	Weil et al., 1995
USH1C	USH1C	Verpy et al., 2000
USH1D	CDH23	Bolz et al., 2001
USH1F	PCDH15	Ahmed et al., 2001; Alagramam et al., 2001
USH1G	USH1G/SANS	Weil et al., 2003
USH2A	USH2A	Eudy et al., 1998

Locus (OMIM)	Gene (OMIM)	Key Gene References (PubMed)
USH2C	ADGRV1/VLGR1/GPR98	Weston et al., 2004
USH2D	WHRN	Ebermann et al., 2007
USH3A	CLRN1	Joensuu et al., 2001
WS1	PAX3	Tassabehji et al., 1992
WS2A	MITF	Tassabehji et al., 1994
WS3	PAX3	Zlotogora et al., 1995
WS4C	SOX10	Pingault et al., 1998
	CHD7	Vissers et al., 2004
BOR2	SIX5	Hoskins et al., 2007; Krug et al., 2011
DFNA2B	GJB3	Xia et al., 1998
DFNB98	TSPEAR	Delmaghani et al., 2012; Bowles et al., 2021
unassigned	GJA1	Liu et al., 2001
unassigned	MYO1C	Zadro et al., 2009
unassigned	TMTC2	Runge et al., 2016
unassigned	CEMIP	Abe et al., 2003
unassigned	USH1G	Shearer et al., 2013
AUNA1	DIAPH3	Schoen et al., 2010
DFNA40	CRYM	Abe et al., 2003
DFNA44	CCDC50	Modamio-Høybjør et al., 2007
DFNA51	TJP2	Walsh et al., 2010
DFNA56	TNC	Zhao et al., 2013
DFNA64	DIABLO/SMAC	Cheng et al., 2011
DFNA65	TBC1D24	Azaiez et al., 2014; Zhang et al., 2014
DFNA66	CD164	Nyegaard et al., 2015
DFNA69	KITLG	Zazo Seco et al., 2015
DFNA70	MCM2	Gao et al., 2015
DFNA71	DMXL2	Chen et al., 2017
DFNA72	SLC44A4	Ma et al., 2017
DFNA81	ELMOD3	Li et al., 2018
DFNB107	WBP2	Buniello et al., 2016
DFNB108	ROR1	Diaz-Horta et al., 2016
DFNB18A	USH1C	Verpy et al., 2000
DFNB23	PCDH15	Ahmed et al., 2003
DFNB32/105	CDC14A	Delmaghani et al., 2016; Imtiaz et al., 2018
DFNB44	ADCY1	Santos-Cortez et al., 2014
DFNB49/112	BDP1	Girotto et al., 2013
DFNB61	SLC26A5	Liu et al., 2003
DFNB66	DCDC2	Grati et al., 2015
DFNB88	ELMOD3	Jaworek et al., 2013
DFNB89	KARS1	Santos-Cortez et al., 2013

Locus (OMIM)	Gene (OMIM)	Key Gene References (PubMed)
DFNB97	MET	Mujtaba et al., 2015
DFNB99	TMEM132E	Li et al., 2015
DFNX6	COL4A6	Rost et al., 2014
PRLTS2	HARS2	Pierce et al., 2010
STL4	COL9A1	Van Camp et al., 2006
STL5	COL9A2	Baker et al., 2011
unassigned	ESPN	Donaudy et al., 2006
WS2D	SNAI2	Sánchez-Martin et al., 2002
WS4A	EDNRB	Attié et al., 1995
WS4B	EDN3	Edery et al., 1996
DFNA13	COL11A2	McGuirt et al., 1999
DFNA41	P2RX2	Yan et al., 2013
DFNA4A	MYH14	Donaudy et al., 2004
DFNA4B	CEACAM16	Zheng et al., 2011
DFNA50	MIR96	Mencía et al., 2009
DFNA67	OSBPL2	Xing et al., 2015; Thoenes et al., 2015
DFNA68	HOMER2	Azaiez et al., 2015
DFNB101	GRXCR2	Imtiaz et al., 2014
DFNB102	EPS8	Behlouli et al., 2014
DFNB104	RIPOR2/FAM65B	Diaz-Horta et al., 2014
DFNB106	EPS8L2	Dahmani et al., 2015
DFNB31	WHRN	Mburu et al., 2003
DFNB39	HGF	Schultz et al., 2009
DFNB53	COL11A2	Chen et al., 2005
DFNB76	SYNE4	Horn et al., 2013
DFNB91	SERPINB6	Sirmaci et al., 2010
JLNS2	KCNE1	Tyson et al., 1997; Schulze-Bahr et al., 1997
STL6	COL9A3	Faletra et al., 2014
WS4A	EDNRB	Attié et al., 1995
WS4B	EDN3	Edery et al., 1996
AUNA2	ATP11A	Chepurwar et al., 2023
AUNA3	TMEM43	Jang et al., 2021
AUNB1	OTOF	Varga et al., 2003
DFNA21	RIPOR2/FAM65B	de Bruijn et al., 2020
DFNA23	SIX1	Mosrati et al., 2011
DFNA27	REST	Nakano et al., 2018
DFNA34	NLRP3	Nakanishi et al., 2017
DFNA37	COL11A1	Booth et al., 2019
DFNA39	DSPP	Xiao et al., 2001
DFNA3A	GJB2	Kelsell et al., 1997
DFNA3B	GJB6	Grifa et al., 1999

Locus (OMIM)	Gene (OMIM)	Key Gene References (PubMed)
DFNA7	LMX1A	Wesdorp et al., 2018
DFNA73	PTPRQ	Eisenberger et al., 2018
DFNA74	PDE1C	Wang et al., 2018
DFNA75	TRRAP	Xia et al., 2019
DFNA76	PLS1	Schrauwen et al., 2019
DFNA77	ABCC1	Li et al., 2019
DFNA78	SLC12A2	Mutai et al., 2020
DFNA79	SCD5	Lu et al., 2020
DFNA80	GREB1L	Schrauwen et al., 2018
DFNA82	ATP2B2	Smits et al., 2019
DFNA83	MAP1B	Cui et al., 2020
DFNA84	ATP11A	Pater et al., 2022
DFNA85	USP48	Bassani et al., 2021
DFNA86	THOC1	Zhang et al., 2020
DFNA87	PI4KB	Su et al., 2020
DFNA88	EPHA10	Huang et al., 2023
DFNA89	ATOH1	Brownstein et al., 2020
DFNA90	MYO3A	Grati et al., 2016
DFNB100	PPIP5K2	Yousaf et al., 2018
DFNB103	CLIC5	Seco et al., 2015
DFNB109	ESRP1	Rohacek et al., 2017
DFNB110	COCH	JanssensdeVarebeke et al., 2018
DFNB114	GRAP	Li et al., 2019
DFNB115	SPNS2	Ingham et al., 2019
DFNB116	CLDN9	Sineni et al., 2019
DFNB117	CLRN2	Vona et al., 2021
DFNB118	GDF6	Bademci et al., 2020
DFNB119	AFG2B	Richard et al., 2021
DFNB120	MINAR2	Bademci et al., 2022
DFNB121	GPR156	Greene et al., 2023
DFNB122	TMTC4	Li et al., 2023
DFNB123	STX4	Schrauwen et al., 2023
DFNB2	MYO7A	Liu et al., 1997; Weil et al., 1997
DFNB26	GAB1	Yousaf et al., 2018
DFNB37	MYO6	Ahmed et al., 2003
DFNB60	SLC22A4	Ben Said et al., 2016
DFNB70	PNPT1	von Ameln et al., 2012
DFNB82	GPSM2	Walsh et al., 2010
DFNX7	GPRASP2	Xing et al., 2017
OTSC11	FOXL1	Abdelfatah et al., 2022
PRLTS5	TWNK	Morino et al., 2014
PRLTS6	ERAL1	Chatzispyrou et al., 2017
STL2	COL11A1	Richards et al., 1996

Locus (OMIM)	Gene (OMIM)	Key Gene References (PubMed)
TCS2	POLR1D	Dauwerse et al., 2011
TCS3	POLR1C	Dauwerse et al., 2011
TCS4	POLR1B	Sanchez et al., 2020
unassigned	IFNLR1	Gao et al., 2018
unassigned	NCOA3	Salazar-Silva et al., 2021
unassigned	LRP5	Xia et al., 2017
unassigned	GAS2	Chen et al., 2021
unassigned	GOSR2	Aburayyan et al., 2023
unassigned	PKHD1L1	Redfield et al., 2024
unassigned	SERPINF1	Ziff et al., 2016; Valgaeren et al., 2019
unassigned	MEPE	Schrauwen et al., 2019
unassigned	SMARCA4	Drabkin et al., 2023
unassigned	FOXI1	Yang et al., 2007
unassigned	KCNJ10	Yang et al., 2009
unassigned	PEX6	Tucker et al., 2020
WS2E	SOX10	Bondurand et al., 2007
WS2F	KITLG	Ogawa et al., 2017
WS3	PAX3	Zlotogora et al., 1995
	SEMA3E	Lalani et al., 2004
DFNA48	MYO1A	Eisenberger et al., 2014
DFNB1B	GJB6	Wilch et al., 2010; Abou Tayoun et al., 2016
USH3B	HARS1	Puffenberger et al., 2012
DFNA25	SLC17A8	Ruel et al., 2008
DFNA28	GRHL2	Peters et al., 2002
DFNB111	MPZL2	Wesdorp et al., 2018
DFNB113	CEACAM16	Booth et al., 2018
DFNB30	MYO3A	Walsh et al., 2002
DFNB68	S1PR2	Santos-Cortez et al., 2016
PRLTS4	LARS2	Pierce et al., 2013
DFNM1/DFNB26M	METTL13	Yousaf et al., 2018
DFNM2	TRMU	Guan et al., 2006

Data obtained from [74].

Publications

Schlingmann, K.P., et al., Germline De Novo Mutations in ATP1A1 Cause Renal Hypomagnesemia, Refractory Seizures, and Intellectual Disability. Am J Hum Genet, 2018. 103(5): p. 808-816.

Gurtler, F., et al., Cellular Pathophysiology of Mutant Voltage-Dependent Ca2+ Channel CACNA1H in Primary Aldosteronism. Endocrinology, 2020. 161(10).

Drexler, K., et al., Cancer-associated cells release citrate to support tumour metastatic progression. Life Sci Alliance, 2021. 4(6).

Jordan, K., et al., Potential Involvement of Extracellular Citrate in Brain Tumor Progression. Curr Mol Med, 2022. 22(6): p. 506-513.

Issler, N., et al., A Founder Mutation in EHD1 Presents with Tubular Proteinuria and Deafness. J Am Soc Nephrol, 2022. 33(4): p. 732-745.